



**Politecnico
di Torino**



**MUSEO
NAZIONALE
DELL'AUTOMOBILE**

Thesis Dissertation
Master Degree in Automotive Engineering

Analysis and Reproduction of the Injector of Bordino's Steam Carriage Through Additive Manufacturing Technologies

Integration of Reverse Engineering and Additive Manufacturing for the Preservation of Industrial Heritage

By

Leonardo Boscarolo

Supervisor(s):

Prof.ssa Eleonora Atzeni

Prof. Alessandro Salmi

Advisor(s):

Dott.ssa Chiara Armigliato

Ing. Davide Lorenzone

Politecnico di Torino

21st July 2025

Declaration

I hereby declare that the contents and organization of this dissertation constitute my own original work and does not compromise in any way the rights of third parties, including those relating to the security of personal data.

Leonardo Boscarolo

21st July 2025

*I would like to dedicate this thesis to
my grandfather Armando,
whom I never had the chance to meet,
but whose pride I can deeply feel.*

Acknowledgements

Reaching the conclusion of my academic course, I would like to acknowledge and thank all those who, in different ways, have contributed to the realization of this thesis and to my personal and professional growth.

In the first place, I would like to sincerely thank my supervisors, Prof.ssa Eleonora Atzeni and Prof. Alessandro Salmi, for their availability, their interest in this project, the guidance and the advice they provided me, and for the freedom they gave me to explore and develop my ideas independently. I am also grateful to the lab technicians - Emanuele, Giovanni and Matteo - for their insightful suggestions and explanations.

A special thanks goes to the *Museo Nazionale dell'Automobile*, in particular to Chiara Armigliato, Davide Lorenzone and Beatrice Zucchelli. This thesis would have not been possible without their generous collaboration and the privilege they granted me to closely study such a unique historical device. Their feedback and support have been truly indispensable.

To all my old friends and the new ones: the former have always stood by me, even if I was away from home; the latter made me feel at home in a new city. Thank you for all the support, for cheering me on and always believing in me.

To my family, who have always been a source of strength and an example to follow, for the love they gave me, the trust, and liberty to choose my own path. Thank you for your inexhaustible patience and constant support you have given me all these years.

My deepest gratitude goes to Camilla, my life partner, with whom I have had the luck to share my journey for many years. I could never be thankful enough for everything you have been, and continue to be, for me.

Abstract

The preservation of antique vehicles represents a great challenge, an intersection of multiple disciplines among cultural heritage and mechanical engineering. A significant early example of the automotive history in Italy is the steam powered carriage designed by the Italian Army officer Virginio Bordino in 1854, conserved today at the *Museo Nazionale dell'Automobile (MAUTO)* in Turin. In anticipation of the museum's centenary, a ten-year restoration effort subdivided in two main parts was initiated: the conservative restoration of the original carriage and the production of a functional 1:1 replica for educational and demonstrative purposes. This thesis focuses on the reproduction of the steam-water injector, one of the most technically interesting and brilliant components of the vehicle, representing probably one of the earliest implementations of this device in a road vehicle.

The steam-water injector is a complex thermo-dynamical device that uses steam coming from the boiler to pump water from tanks back into it, without the use of mechanical moving parts and external energy. Its operation is the result of a complicated transfer of heat, mass and momentum between steam and water within a series of two convergent nozzle and a divergent one, producing a final pressure increase of the entrained water that enables the boiler feed. This apparatus was historically misunderstood, primarily due to the prevailing caloric theory of heat, yet it played a pivotal role in the evolution of thermodynamics and the eventual acceptance of the First Law of Thermodynamics.

Due to the complete lack of original technical documentation and the attention to the structural integrity of historical samples, Reverse Engineering (RE) techniques were exploited to reconstruct the geometry of the Bordino

injector. The external geometry was directly obtained via a Structured Light Scan (SLS) of the injector. A Computed Tomography (CT) was attempted on the original injector, but due to the extensive attenuation of X-rays by the metallic material, it failed. The innovative solution presented in this thesis is the internal reconstruction of a late 19-th century steam injector, conceptually similar to the Bordino one, whose components are then re-design to be fitted inside the acquired external original shape. Digital post-processing and CAD modeling were involved to enable the reconstruction of all internal and external features. In order to aid the redesign activity and the geometry tuning, an analytical model of the steam-water injector was implemented in *MATLAB* to provide performance evaluation.

To physically reproduce the component, Additive Manufacturing (AM) was selected as the suitable fabrication method, owing to its ability of realizing intricate internal geometric features and its advantage of avoiding the need of additional tools. Selective Laser Sintering (SLS) was selected to produce a final polymeric prototype of the injector, for demonstrative purposes. The injector was redesigned considering Design for Additive Manufacturing (DfAM) principles, taking into account both the possible advantages and the intrinsic limitations of the AM processes.

This work demonstrates the capabilities of the integration of RE and AM techniques in the reconstruction of complex historical devices, providing a replicable framework for future adoptions in the field of industrial heritage conservation and restoration. In addition, it contributes to the latest academic discussion over the integration of 21st-century engineering tools in the interpretation and preservation of antique machines and mechanisms.

Contents

List of Figures	ix
List of Tables	xiv
Nomenclature	xv
1 Introduction	1
2 Historical context	3
2.1 Virginio Bordino's Steam Engine Carriage	3
2.1.1 Steam powered vehicles evolution	3
2.1.2 History and characteristics of the vehicle	6
2.2 Henri Giffard and the Steam Injector	11
3 Literature review	25
3.1 State of the Art of the Steam-water Injector	25
3.1.1 Main research trends	25
3.1.2 Injector models	39
3.2 State of the Art of Additive Manufacturing and Reverse Engineering for the Reconstruction of Spare-parts	43
3.2.1 Fundamentals of AM	44
3.2.2 Fundamentals of RE	49

Contents

3.2.3	Integration of AM and RE in remanufacturing	54
3.2.4	Advantages, drawbacks, limitations of AM	58
4	Method	63
4.1	Steam-water Injector Modeling	63
4.2	Steam Carriage Technical Requirements and Specifications . .	71
4.3	Reverse engineering Process	73
4.3.1	Computed Tomography	73
4.3.2	Structured Light Scanning	75
4.3.3	Softwares for Reconstruction	76
5	Results	81
5.1	Available Injectors Analysis	81
5.1.1	H&B Sirius-"One-Movement"-1890 Injector	81
5.1.2	Bordino Injector	89
5.2	Redesigned Injector	92
5.3	Final Prototype	101
6	Conclusion	106
	References	108
	Appendix A H&B Sirius-"One-Movement"-1890 Injector	120
A.1	Technical drawings	121
A.2	Commercials	124
A.3	Photographs	131
A.4	Tomography scans	136
	Appendix B Injector Model MATLAB code	140

List of Figures

2.1	Cugnot steam powered tricycle [1]	4
2.2	London Steam Carriage [2]	4
2.3	Virginio Bordino's steam carriage [3]	6
2.4	Bordino steam carriage inside the <i>Stadio Comunale</i> [4]	9
2.5	Bordino steam carriage displayed in a symbolic scene, at the <i>Museo Nazionale dell'Automobile</i> [5]	10
2.6	Giffard's steam dirigible during the flight in 1852 [6]	15
2.7	First Giffard injector [7]	16
2.8	Blast pipe functioning schematic [8]	17
2.9	Upgraded Giffard injector with reference letters	20
2.10	The "Penberthy" automatic injector [9]	23
2.11	The Wm. Sellers & Co. 1865 automatic injector [10]	24
3.1	Typical steam-water injector pressure profile	27
3.2	Examples of steam-water injectors nozzle arrangement [11]	28
3.3	Additional features of steam-water injectors [11]	29
3.4	Mollier diagram of the ideal steam-water injector [12]	30
3.5	Dependence of entrainment ratio to throat areas ratio [13]	34
3.6	Condensation shock shifting proportionally to back-pressure valve opening ratio [14]	35

List of Figures

3.7	Frames showcasing the onset of stalling in a steam-centered injector [15] (the two-phase section of the flow are transparent, so they are the dark ones in the images)	35
3.8	Pressure distribution as function of back-pressure valve opening ratio [16]	36
3.9	Operational region and inoperative conditions for a water-centered injector [17]	37
3.10	Main global model types [11]	41
3.11	Annual revenue for segment in the collectible cars market [18]	44
3.12	Classification of AM processes [19], images from [20]	45
3.13	Cost comparison between CM and AM components, in 2018 [21]	47
3.14	Status of major AM technologies, in 2018 [21]	48
3.15	Example of iterative DfAM design workflow [22]	49
3.16	Traditional and RE manufacturing workflows [23]	50
3.17	RE classification [23]	51
3.18	3D model reconstruction process from an input mesh [24]	53
3.19	RE tolerance issue of error superposition [23]	55
3.20	Example of RE and AM integration for the reproduction of Ruston Hornsby Motor Car steering box component [25]	57
3.21	Example of RE and AM integration for the restoration of Elvis Presley's BMW 507 Roadster [25]	57
3.22	Example of RE and AM integration for the reconstruction of a Steyr 220 Roadster carburetor body [26]	57
3.23	Example of RE and AM integration for the reproduction of a car volume button [27]	59
3.24	Photogrammetry of an engine sump [28]	59
4.1	Model of the injector	64

List of Figures

4.2	Iterative model computation flowchart	70
4.3	Machine and software used for the CT scan	74
4.4	Pictures taken during the preparation of the CT scan of the H&B Sirius 1890 injector	75
4.5	Structured Light Scanning operation pictures	77
4.6	Picture of software reconstruction	80
5.1	Pictures of H&B Sirius "One-Movement" steam injector . . .	82
5.2	H&B Sirius 3D model section view with components labels . .	85
5.3	Alpha variation sensitivity of Sirius injector at 5 bar	87
5.4	Pressure variation sensitivity of Sirius injector at 50% α . . .	88
5.5	Pictures of Bordino steam injector	91
5.6	Bordino injector mounted on the boiler	92
5.7	Final redesigned injector	93
5.8	Final redesigned injector with component labels - <i>front section</i>	94
5.9	Final redesigned injector - <i>detail</i>	95
5.10	Final redesigned injector - <i>25° section</i>	95
5.11	Alpha variation sensitivity of final redesigned injector at 5 bar	98
5.12	Pressure variation sensitivity of final redesigned injector at 50% α	99
5.13	Operational area and performance maps of final redesigned injector at 50% α	100
5.14	Exploded view of the final injector. Exploded view of the final injector. 1. <i>Upper body</i> 2. <i>Middle body</i> 3. <i>Lower body</i> 4. <i>Spindle</i> 5. <i>Steam nozzle</i> 6. <i>Upper stuffing box</i> 7. <i>Indicator</i> 8. <i>Handle</i> 9. <i>Handle nut</i> 10. <i>Lower stuffing box</i> 11. <i>Overflow valve</i> 12. <i>Overflow spring</i> 13. <i>Overflow spring stop</i> 14. <i>Graphite stuffing</i> 15. <i>Positioning screw</i>	100
5.15	EOS Formiga P110 Velocis	102

List of Figures

5.16	Printing process of the polymer prototype	102
5.17	Post-processing of the polymer prototype	104
5.18	Final polymer prototype with sections opened	105
A.1	Undated technical drawing. [29]	121
A.2	1898 technical drawing. [29]	122
A.3	1930 technical drawing. [9]	123
A.4	1892 commercial. [30]	124
A.5	1893 commercial. [30]	125
A.6	1895 commercial. [30]	126
A.7	1896 commercial. [30]	127
A.8	1898 commercial. [30]	128
A.9	1958 brochure (<i>front</i>). [29]	129
A.10	1958 brochure (<i>back</i>). [29]	130
A.11	Range of extension of the steam nozzle	131
A.12	Diffuser outlet	131
A.13	Exploded view of the removable parts of the injector . 1. Lower body 2. Upper body 3. Spindle 4. Steam nozzle 5. Upper stuffing box 6. Lower stuffing box 7. Upper stuffing box nut 8. Overflow valve 9. Overflow spring 10. Overflow nut 11. Positioning screw 12. Lower regulating wheel positioner 13. Regulating wheel 14. Upper regulating wheel positioner 15. Regulating wheel nut 16. Flange screws 17. Flange nuts . . .	132
A.14	Steam nozzle	133
A.15	Square thread of steam nozzle. <i>Double start feature</i>	133
A.16	Spindle	133
A.17	Spindle detail	133
A.18	Square thread of the spindle. <i>Double start feature</i>	134

List of Figures

A.19 Overflow valve	134
A.20 Overflow gap	134
A.21 Upper stuffing box. <i>The white spiral is the stuffing.</i>	135
A.22 Mixing chamber inlet	135
A.23 Combining nozzle	136
A.24 Lower stuffing box	136
A.25 Lower body	137
A.26 Overflow valve	138
A.27 Overflow valve detail	138
A.28 Spindle and steam nozzle	139
A.29 Steam nozzle and combining tube	139

List of Tables

2.1	Summary of the characteristics of the Bordino steam carriage .	11
3.1	Summary of Existing Models of Steam-Water Injectors	42
3.2	Features comparison between commercial RE tools [31] . . .	54
5.1	Dimensions in mm of the available Sirius injector sections, as per model of Figure 4.1	86
5.2	Maximum performance of the Sirius injector at each pressure level in the operating range	89
5.3	Dimensions in mm of the final redesigned injector sections, as per model of Figure 4.1	96
5.4	Maximum performance of the final redesigned injector at each pressure level in the operating range	97

Nomenclature

Roman Symbols

α	Percentage of opening of steam nozzle-spindle
β	Momentum correction factor
ΔP	Pressure differential between inlet and outlet of the injector
\dot{m}	Mass flow rate
η	Efficiency
Γ	Lifting-pressure coefficient - Pressure gain ratio
ω	Entrainment ratio - Flowrate ratio - Jet coefficient
ρ	Density
ξ	Pressure loss coefficient
A	Area
AI	Artificial Intelligence
AM	Additive Manufacturing
ANN	Artificial Neural Network
BJT	Binder Jetting
C_p	Pressure recovery coefficient
CM	Conventional Manufacturing

Nomenclature

<i>CMM</i>	Coordinate Measuring Machine
<i>CR – P</i>	Close-Range Photogrammetry
<i>CT</i>	Computed Tomography
<i>DED</i>	Direct Energy Deposition
<i>DfAM</i>	Design for Additive Manufacturing
<i>GA</i>	Genetic Algorithm
<i>GD&T</i>	Geometric Dimensioning & Tolerancing
<i>H&B</i>	Holden & Brooke
<i>h</i>	Enthalpy
<i>HIP</i>	Hot Isostatic Pressing
<i>KBS</i>	Knowledge-Based System
<i>MEX</i>	Material Extrusion
<i>MJT</i>	Material Jetting
<i>NC</i>	Numerical Control
<i>P</i>	Pressure
<i>PBF</i>	Powder Bed Fusion
<i>R</i>	Compression ratio
<i>RC</i>	Rapid Casting
<i>RE</i>	Reverse Engineering
<i>RP</i>	Rapid Prototyping
<i>RT</i>	Rapid Tooling
<i>s</i>	Entropy
<i>SC</i>	Stereo Scanning

Nomenclature

<i>SLS</i>	Selective Laser Sintering
<i>SLS</i>	Structured Light Scanning
<i>T</i>	Temperature
<i>TIG</i>	Tungsten Inert Gas (welding)
<i>TO</i>	Topology Optimization
<i>u</i>	Speed
<i>VPP</i>	Vat Polymerization
<i>w</i>	Weight coefficient
<i>X</i>	Vapor quality

Chapter 1

Introduction

The preservation of industrial and engineering heritage is not solely an act of cultural conservation, but also a testament to the remarkable visionaries whose ingenuity pioneered the advancements in completely new engineering and physics fields. This is particularly true in the case of the two men who are central to this thesis: Virginio Bordino and Henri Giffard. Their contributions paved the way to the long trajectory towards modern mobility. In the case of Giffard, it could be even said that, in a sense, he challenged the very laws of physics: his invention was to such an extent innovative, that played a critical role in questioning and reshaping the established law of thermodynamics, setting the stage for the First Law of Thermodynamics.

The purpose of this thesis is the reproduction of one of the most technically complex devices mounted on the 1854 steam carriage built by Virginio Bordino, namely, the steam-water injector, also known as the Giffard injector. Albeit it is most seemingly a later addition to the carriage, since the injector was only invented in 1858, it still remains one of the first implementations in a road transport context. Bordino's steam carriage is the result of his experimentation with the potential application of steam engines in vehicles destined to the public roads. It is now part of the collection conserved at the *Museo Nazionale dell'Automobile (MAUTO)* in Turin, as an example of the pioneering role of Bordino in the incipient phase of automotive engineering. In preparation for the *MAUTO*'s centennial anniversary in 2033, a ten-year restoration was started.

Introduction

One of the aim of this initiative is to build a functioning replica of the carriage; the present work is thus inserted into this ambitious project, as it focuses on the reproduction of one of its components.

The thesis is organized to guide the reader through the entire re-engineering process, starting from a historical contextualization and theoretical background of the injector, through the modeling strategies and the experimental procedures and finally the realization of a polymeric prototype. An extensive literature review is provided to indicate the state of the art in the steam-water injector modeling and its working principles understanding, and in the role of the integration of AM and RE in the restoration of classic cars. The methodology chapter describes the scanning, modeling and simulation activities performed. Eventually, the final results are presented, together with an accurate performance characterization of the redesigned injector.

The primary scope of this work is to demonstrate the feasibility and accuracy of modern digital workflows for the conservation of mechanical systems. Moreover, it is aimed to stimulate interest towards such marvelous 19th-century inventions - such as the steam carriage and the injector - that should continue to hold engineering relevance and merit continued study, despite having been developed more than 150 years ago.

Chapter 2

Historical context

2.1 Virginio Bordino's Steam Engine Carriage

2.1.1 Steam powered vehicles evolution

It is unanimously agreed that the world's first automobile was built by the French inventor and engineer Joseph-Nicolas Cugnot (1725-1804) in 1769, known as the *Fardier à vapeur* (Figure 2.1), a four-ton steam powered tricycle [32]. While serving in the military, Cugnot conceived a number of mechanical innovations and later decided to construct two steam-propelled vehicles, the first in 1769 and the second in 1770. The project was soon abandoned since these turned out to be unreliable, unstable, and dangerous, hindered also by a poor performing boiler, even for the standards of the time. Famously, the second prototype was involved in possibly the first ever recorded automobile accident, when in 1771 it accidentally knocked down a wall in Paris, since Cugnot had underestimated the braking force needed to stop such a heavy vehicle [33].

Nevertheless, the steam engine was destined to be used in future pioneering attempts, mainly at the heart of the Industrial Revolution: Great Britain. An example is the work of the British inventor Richard Trevithick (1771-1833), who conceived multiple steam-powered inventions, such as the first high-pressure steam engine and the first working railway steam locomotive. It is worth to mention the "Puffing Devil", a full size steam road locomotive built in 1801,

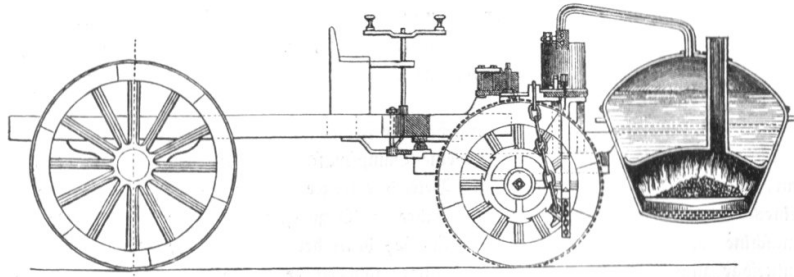


Fig. 2.1 Cugnot steam powered tricycle [1]

and the "London Steam Carriage" of 1803, a more refined vehicle with a horizontal boiler and a rear-wheel drive system, which though failed to attract commercial interest [34].

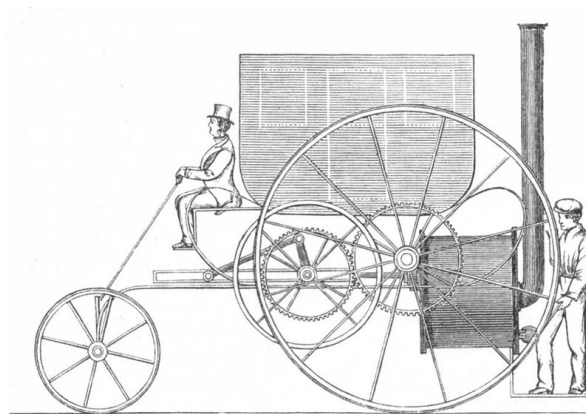


Fig. 2.2 London Steam Carriage [2]

These early efforts were followed by other significant innovations throughout the first decades of the nineteenth century. British engineer Goldsworthy Gurney (1793-1875) contributed to the development of steam engines, by being credited with the invention of the blast pipe. In France, inventors such as Onesiphore Pecqueur (1792-1852) focused on gear-based drivetrains and the early concepts of differential axles, which would become fundamental in automotive engineering [35]. Remarkably, in 1829 George Stephenson's *Rocket* locomotive won the *Rainhill Trials*, a competition born to test his argument that locomotives equipped with a steam-engine would have the best motive power to work in the then nearly completed Liverpool and Manchester Railway (L&MR), instead of using stationary steam engines to power the trains by

2.1 Virginio Bordino's Steam Engine Carriage

means of cables. Of the ten subscribed locomotives, only five were able to compete in the race and Stephenson's Rocket was the only one to complete the course [36].

Italy, by contrast, was a later adopter of these new technologies. It was not until 1836 that the first patent for a steam powered vehicle was granted in the Kingdom of the Two Sicilies [37]. In the same year, in the Kingdom of Sardinia, Captain Virginio Bordino (1804-1879), an artillery officer and engineer of the Savoy Army, had just returned from a state-sponsored mission commissioned to study steam technology in England [38]. His first prototype was built in 1836 and has since been lost, but curiously, the engineering drawings that had survived reveal that the boiler design of that vehicle was inspired by that of British Colonel Francis Maceroni (1788-1846). He will then build a second prototype in 1854 - shown in Figure 2.3 -, which is the one conserved at the *Museo Nazionale dell'Automobile*, known as *MAUTO*. This vehicle is an early example of retrofitting, in which a horse-driven carriage was adapted to make room for a steam engine system. Bordino indeed modified and structurally strengthened the body to accommodate the necessary devices such as the two-cylinder engine, the water pumps, and the rear mounted boiler. This machine is recognizable as one of the first effective automobiles built in Italy. It can also be pointed out that this machine is an early example of a common automotive trend: the hybridization passage for which a new technology is first tested by exploiting existing structures, such as the example of the return of electric investments in the 1990s, in which engineers first tested the new electric designs by transforming ICE-based cars into electric one.



Fig. 2.3 Virginio Bordino's steam carriage [3]

2.1.2 History and characteristics of the vehicle

Virginio Bordino, already at the start of his career, had gained recognition in northern Italy for his impressive engineering achievements, such as the restoration of the *Santuario di Vicoforte* and the elevation of the columns of the *Chiesa della Gran Madre di Dio* in Turin. These projects earned him widespread notoriety, even more due to his young age, and established his reputation as a well-rounded engineer, with a strong knowledge of mechanics. In light of these, the *Accademia Militare* made the decision to send him to England to study the advancements in mechanical engineering and steam propulsion. The following quote describes this designation, as officially reported in the account by Parrini [38]:

2.1 Virginio Bordino's Steam Engine Carriage

Original:

“Questa civica amministrazione, scrivevano al giovine ufficiale il marchese Benso di Cavour e l'avv. Villa, Sindaci di Torino, il primo di aprile 1833, siccome fu la prima ad ammirare i singolari saggi del suo ingegno sul calcolo delle forze motrici, allorchè si inalzarono le colonne del peristilio della chiesa oltre Po, così ama anche di esser la prima a rallegrarsi con V.S. illustrissima del favorevole attestato che gliene viene in oggi compartito dalla Maestà Sua, coll'indirizzarla negli esteri stati per raccogliere i nuovi ritrovati della meccanica onde cimentati colle perfette sue cognizioni in tal scienza possa un giorno farne profittare questo Stato.”

Translation:

“This municipal administration, wrote to the young officer the Marquis Benso di Cavour and the lawyer Villa, Mayors of Turin, on the first of April 1833, since it was the first to admire the remarkable demonstrations of your brilliance in the calculus of motive forces, when were raised the columns of the peristyle of the church beyond the Po, thus it also wishes to be the first to congratulate to Your Most Illustrious Lordship of the favorable certificate that upon you has today been conferred by His Majesty, as in assigning you to foreign states to gather the latest discoveries in mechanics so as tested against your perfect knowledge of such science they may one day be of profit to this State.”

In the same historical account, it is explained that Bordino was the first Italian engineer to seriously address the problem of steam propulsion on ordinary roads. He experimented two prototypes: a three-wheeled calèche and a Dumont-style four-wheeled carriage. According to the sources, by 1865 both vehicles weren't anymore used, as in that year Bordino lost his only daughter, for whose amusement he built the Dumont carriage. Following this tragic loss, neither Bordino neither anyone else attempted to operate the vehicles again. Moreover, it is also documented that, on the 6th of July 1859, Virginio Bordino submitted a request for a six-years monopoly on the development of two types of steam vehicles: one intended for use on public roads and another for private application [39].

Subsequently, Bordino's wife chose to sell one of the prototypes and donate the other to the *Museo Industriale di Torino*. Given the historical relevance of

Historical context

the first prototype, the museum initially requested the donation of the three-wheeled calèche. However, after conducting research through various sources, it was discovered that this carriage had undergone multiple modifications and thus it wasn't anymore possible to be presented as manufactured in 1836. As a result, the museum opted to acquire the later Dumont prototype, since it was in excellent condition, much better than the earlier one. This vehicle was operated only for a few test rides in Turin before being painted in July 1865. By that time, however, Bordino's daughter was already ill in her bed. In addition, the 1854 carriage was a better manufactured prototype and a more advanced engineering solution, as it incorporated the improvements derived from the thirty years accumulated experience of Bordino. Unfortunately, due to deteriorated state of the earlier calèche prototype, a decision was later made to demolish it and sell the remaining as scrap material. When the vehicle was officially stored in the *Museo*, the vice-director remarked as follows:

Original:

“[la vettura] si terrà esposta al pubblico insieme alle collezioni di meccanica, e servirà di esemplare storico per attestare l'applicazione fatta da un intelligente ed erudito alto funzionario italiano, della forza del vapore alla locomozione delle vetture sulle strade ordinarie.”

Translation:

“[the machine] will be kept exhibited to the public along the mechanical collections, and it will serve as a historical example to attest the application made by an intelligent and erudite high-ranking Italian official, of steam force for the propulsion of vehicles on ordinary roads.”

Records indicate that the 1854 Dumont-style carriage, while being preserved in the *Museo Industriale*, underwent a "put back in order" restoration process. In 1906, ownership of the vehicle was transferred to the *Politecnico di Torino*, known at the time also as the *Regio Istituto di Ingegneria di Torino*. It is also indicated that, prior to 1933, the carriage was again restored by the automobile company *FIAT*. Following its exhibition during the 1933 *Retrospectiva dell'automobile* fair, Carlo Biscaretti di Ruffia (1879-1959), the founder of what would later become the current *Museo Nazionale dell'Automobile*, became very interested in this steam vehicle and initiated the dealing process to acquire it for the newly established institution. The vehicle will be officially transferred in 1936, after which the carriage underwent another restoration.

2.1 Virginio Bordino's Steam Engine Carriage

For a brief period, between 1939 and 1959, the vehicle was exhibited at the *Stadio Mussolini di Torino*, also known as the *Stadio Comunale* (Figure 2.4). It was afterwards relocated to its current location within the newly opened museum premises on *Corso Unità d'Italia*, which opened to the public in 1960.



Fig. 2.4 Bordino steam carriage inside the *Stadio Comunale* [4]

During the museum's major rearrangement between 2007 and 2011, the vehicle was relocated inside and moved to an upper floor, at the very start of the guided tour of the museum. The carriage is here displayed within a highly symbolic scene, in which two horses are depicted dissolving into a cloud of steam, an allegorical representation of the epochal transition from horse-driven propulsion to steam-powered transportation, of which this carriage represents a pioneering example (Figure 2.5). Beginning in 2014, the *Fondazione CCR "La Venaria Reale"* initiated an extensive diagnostic and conservation campaign. In 2023, the *Museo Nazionale dell'Automobile* decided to begin the ten-year restoration of this piece of history, which is in anticipation of the museum's centenary in 2033. The restoration process is subdivided into two paths: the original carriage is restored in a conservative manner and returned to its orig-

Historical context

inal state (e.g., the red painting was discovered not to be the original color, which was instead the royal Savoy blue), while a 1:1 functioning replica is built for educational and demonstrative purposes, to allow the public to witness how this incredible machine worked [5].

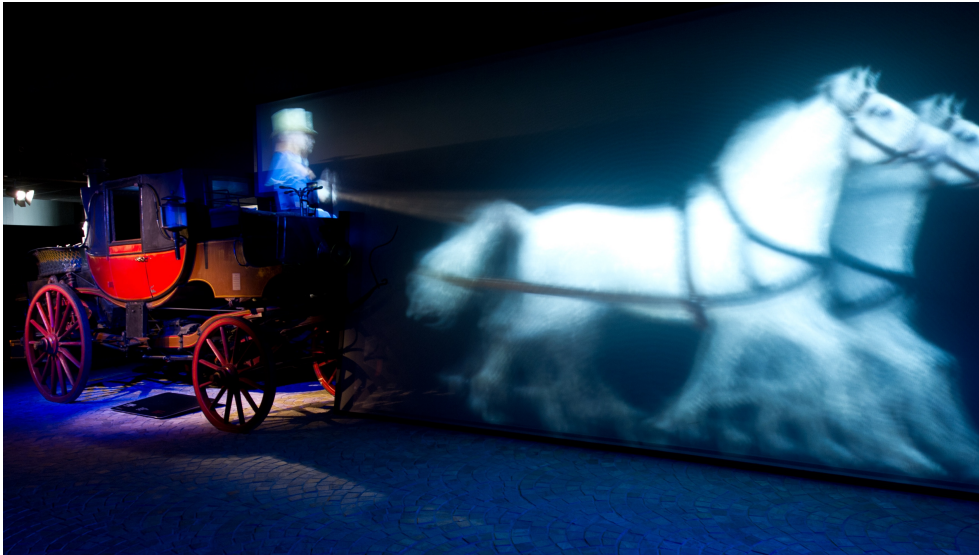


Fig. 2.5 Bordino steam carriage displayed in a symbolic scene, at the *Museo Nazionale dell'Automobile* [5]

In conclusion, a summary of the main characteristic of the Bordino steam carriage is provided in Table 2.1. Additionally, it is recommended to watch the animated video produced by *MAUTO*, which offers a comprehensive visual reconstruction of the steam carriage in operation [40].

2.2 Henri Giffard and the Steam Injector

Table 2.1 Summary of the characteristics of the Bordino steam carriage

<i>1854 Bordino Steam Carriage</i>	
Type	Landau/Dumont
Year	1854
Wheels	4 total (2 driving)
Boiler tubes	38
Cylinders	2 double-acting
Bore and stroke	250x450 mm
Water tanks	4
Fuel	Carbon coke
Passengers	11 (14 with a tender)
Range	2 hours
Boiler maximum pressure	5 bar
Maximum speed	6 km/h

Source: "La trazione a vapore sulle strade ordinarie, 1875" [41]

2.2 Henri Giffard and the Steam Injector

The present section is mostly based on the considerations of Kranakis (1982) included in the book: *The French Connection: Giffard's Injector and the Nature of Heat* [42].

In 1858, to the Parisian inventor and engineer Henri Giffard (1825-1882) was granted the patent for the steam-water injector, a mechanically simple device able to draw water into steam boilers using the same steam produced by them. Few inventions have been so influential, ground-breaking, and paradoxical viewed as the injector. Even though Joule and Helmholtz already developed the First Law of Thermodynamics between 1843 and 1849, along with its corollary concerning the mechanical equivalent of heat, this theory was not universally known and accepted; instead, the caloric heat theory was dominant: heat was basically conceived as a fluid which permeates matter and which possesses the property of self-repellency, whereas the matter particles had the opposite internal power of self-attraction. Following this thesis, the

Historical context

phase transition of water into steam, as a result of the introduction of heat, was explained as an immission of caloric particles for which, after a critical threshold of quantity is achieved, the attraction of the water molecules is subdued by the dominant force of repellency of the heat ones. In addition, heat was seen as completely independent from the mechanical energy of a system, therefore, in steam engines the only working power considered was that of pressure. Consequently, the injector could not be satisfactorily explained by the caloric theory, seeming in a way almost as a device defying the laws of physics: a jet of steam, drawn in from the boiler at a specific pressure, passes through a device in which no external work is introduced, without moving parts, and returns into the same boiler eventually condensed to a higher pressure than before, even doubled, while also drawing in water from tanks that could be even 4-5 meters below the injector. The consideration of pressure as the sole motive power for the steam injector was therefore not enough, without considering the influence of heat.

An illustrative fact is that still in 1908 the inner principles of the injector were not completely clear by all the engineering community, so that the renowned physicist Henri Poincaré (1854-1912) in that year published a milestone book called *Thermodynamique* [43], in which an original analysis demonstrated that the paradox could be finally explained thanks to the laws of thermodynamics. Ultimately, the injector can be viewed as the disruptive device that obliged engineers and physicist to question the established theory of heat and ponder new ones, serving as a catalyst for the development of modern thermodynamics.

Despite the confusion that the injector brought up, its efficient functioning and the advantages of its use for steam boilers were undeniable, so that in 1899 it is said that "there is scarcely a locomotive in the world that is not equipped with one or two injectors" and that many young engineers at that time didn't even ever seen one of the old mechanical pumps. The injector has indeed the importance of having resolved the longstanding problem of the boilers feed water supply: with the proper operation it was virtually unbreakable and being without moving parts it was free from wear, unlike the classic pumps that were

2.2 Henri Giffard and the Steam Injector

highly subjected to failures and needed frequent maintenance [44].

It is interesting to cite the words of an engineer that described the introduction of the injector in England by Sharp, Stewart & Co. firm of Manchester:

"In the autumn of 1859 when our representative in Paris sent over to me a No. 4 Injector as a curiosity and engineering anomaly, he told me simply what it did, but gave no instructions for fixing or working. At about the same time the Paris representative of Messrs. Robert Stephenson & Co., Newcastle, sent over to them a similar Injector. I set to work at once, and by good luck coupled up the correct pipes to their proper flanges, but was a great deal bothered what to do with the overflow flange. After a few nights' work I got my Injector fixed and got up steam, and to some extent began clumsily experimenting as the pressure rose to 60 pounds, the full working pressure of the boiler. I had the Injector fixed over a tank fed by a ball tap and closed by the boiler. I turned steam on and was staggered by the rush of water into the tank from the overflow pipe, and thought something was wrong. However, I continued to turn the steam spindle, and the escape from the overflow sensibly diminished until I could turn no further. In the mean time the ball tap started running furiously into the tank, showing me that water was going somewhere and I knew it could go nowhere else but into the boiler. I then began to operate with the four thread screw at the side, and found that it adjusted the water supply, and succeeded in getting the overflow "dry." I then opened the peep-holes opposite the space between the combining and the receiving nozzles, and saw the white stream passing from one to the other on its way to the boiler. I then ceased operations, and had a pipe of tobacco, and let some water out of the blow-off cock; then I tied a piece of spun yarn round the glass water gauge to prepare for another start, and shortly after, the senior partner came round for a stroll and found me operating. I stopped it, started it, and regulated it so much to his satisfaction that within one week the monopoly of its manufacture in England was secured

Historical context

by the firm. Unfortunately for Stephenson & Co., they coupled their sample Injector up incorrectly, and it would not work." [44, pp. 4–5]

The inventor of the injector, Henri Giffard, was a rather remarkable man passionate about aviation, despite the fact that he wasn't actually a graduated engineer: he was never enrolled at the *École centrale*, the principal complex of engineering schools based in Paris, which also included the *École polytechnique*. Instead, he worked for some time as a locomotive engineer and, fascinated by them, he was asking his friends who studied at the *École* to pass down their notes. Charles De Comberousse (1826-1897), a mathematician professor at the engineering school, indicated that:

"Giffard, acquainted with students at his school, borrowed their notebooks, studied their projects, took the same courses independently, and became, without a diploma, an engineer at the same time as them and even before them." [45]

This does not imply that Giffard underestimated the importance of knowledge and use of theory. Instead, he actually was one of the first pioneer of the transition that was occurring in the engineering world: passing from a "cut and try" approach to a more methodological and scientific one, taking advantage of the theories available at the time. He indeed conceived a complete theoretical framework of its injector already in 1850. But that year, since he hold mainly interest in aviation, he was working on a more important project: the development of the first steam powered dirigible, which he would then finally build and successfully fly in 1852. He therefore didn't have the time and financial resources to commit to the steam injector, for which he will then return to focus in 1858, building a first working prototype thanks to his long lasting partnership with Henri-Pierre Flaud (1817-1874) shop, an important Parisian mechanical engineer [46].

It is interesting to point out the conceptual techniques that Giffard exploited both for its aerial studies and the injector ones, typical traits of the elegant and deductive style of French science: the borrowing from other fields of

2.2 Henri Giffard and the Steam Injector

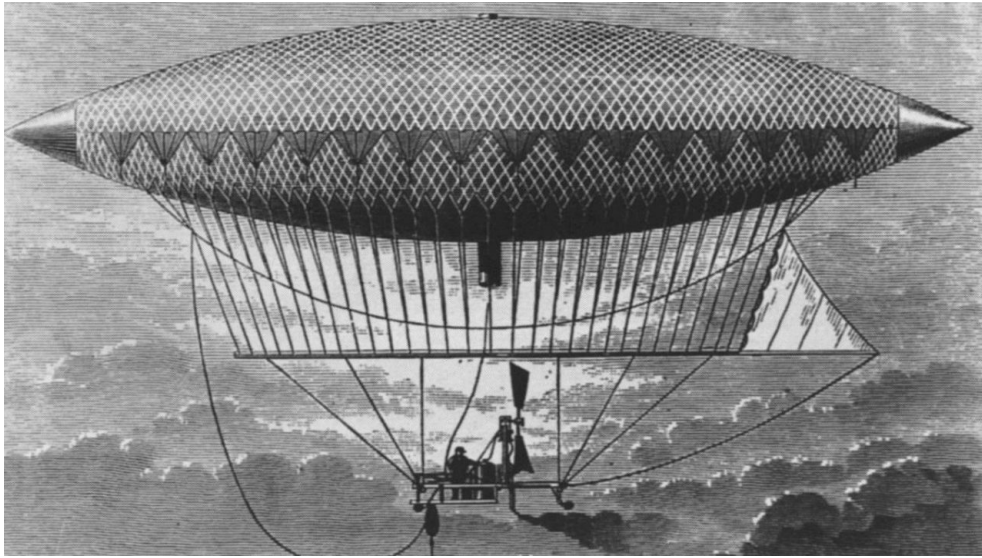


Fig. 2.6 Giffard's steam dirigible during the flight in 1852 [6]

physics to fill the gaps of immature ones and the method of studying system at microscopic scale to predict their macroscopic behavior. For example, since at the time there wasn't almost any aerodynamic knowledge, Giffard designed the dirigible in Figure 2.6 considering first how a body immersed in a fluid affects microscopically the particles surrounding it. The consequence was that he correctly deduced that the perturbation introduced by the body into the air was limited to a short distance, he therefore decided to implement the known laws of hydraulics into the design process, considering the volume of fluid displaced as if through a conduit. Though limited, since not always directly applicable, the theory used by Giffard nonetheless enabled him to design the aerostat with an aerodynamic shape. As a matter of fact, he already understood the limitations of his predictions, thus made many experiments to expand and confirm his initial hypothesis.

The method used to develop the first injector, shown in Figure 2.7, involved again an analysis of the technological problem which resulted into a system of basic laws that could approximately explain the phenomena of the device and guide the design and validation process. The idea of the injector was born to solve a problem regarding his aerial steam-powered navigation efforts: the before-mentioned unreliability, weight, bulkiness and high power request of

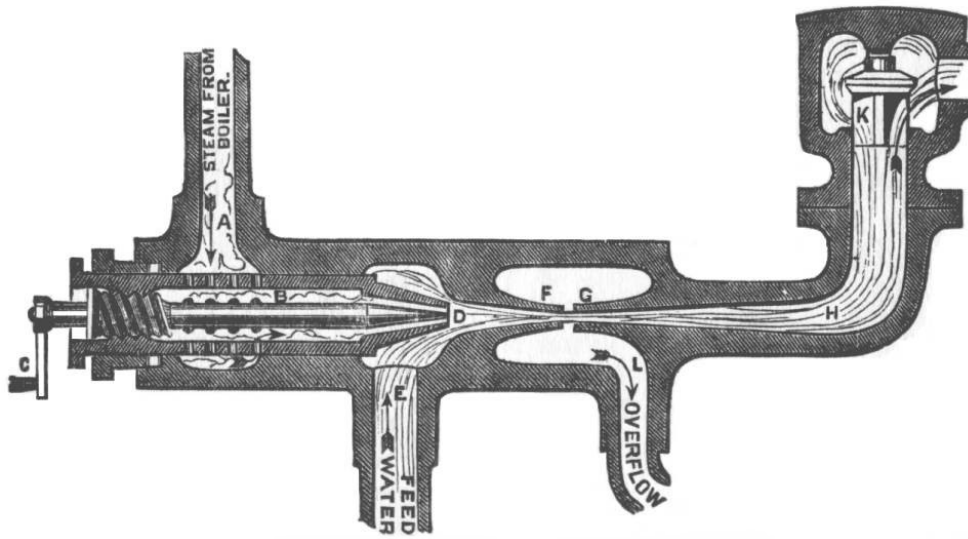


Fig. 2.7 First Giffard injector [7]

common water pumps. To solve the problem, he investigated the possibility of building a device with lower mass and no moving parts to completely eliminate the frictions that the steam engine needs to compensate. Once more, the principle was obtained from the hydraulic field: the principle of induced currents, which is now familiar as Bernoulli's theorem. Before Bernoulli, the principle was already investigated by Giovanni Venturi (1746-1822) in 1797, following his studies of fluid behavior and the invention of the Venturi tube. Although he already comprehended the importance of this principle, he could not give a precise theoretical explanation of it. Nevertheless, it was empirically clear to him and his contemporary that a fluid which is accelerated has the ability to accelerate other surrounding fluids (a natural phenomenon is the wind produced in the proximity of waterfalls). Nowadays we can rigorously explain the principle by means of Bernoulli's theorem, which states that, since ideally energy is conserved, a fluid which accelerates diminishes its pressure. Therefore, a differential pressure is generated relative to a neighboring fluid at higher pressure, causing the latter to accelerate toward the former. It is probable that Giffard was acquainted with an earlier application of the principle of induced currents: the blast pipe.

2.2 Henri Giffard and the Steam Injector

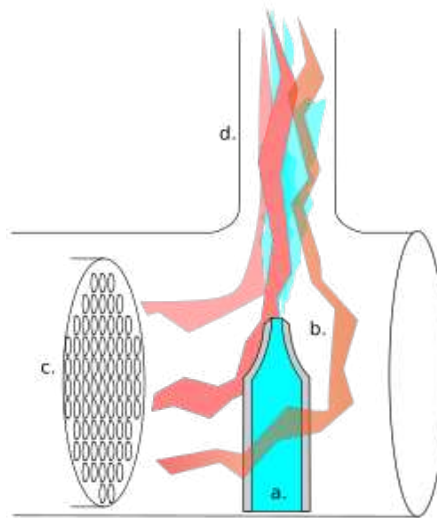


Fig. 2.8 Blast pipe functioning schematic [8]

This device, shown in Figure 2.8, was commonly used to increase the air draft in locomotives and consecutively increase the rate of combustion in the furnace. Its principle was rather simple: a convergent nozzle facing upward and collocated at the base of the smokestack was used to spray an accelerated stream of steam up this tube, thus accelerating the exhaust gases and creating a pressure drop behind; this results in an acceleration also of the gases entering the smokestack from the furnace, therefore increasing the draft. It was used as an alternative or in conjunction with the height-adjustable smoke chimneys for this purpose. Surely the knowledge of this process was known to Giffard, thus hinting him of a way to attract other fluids by means of other accelerated ones. In a way, the combination of nozzles in the injector can remember the one of blast pipe and smokestack. It is no coincidence that Giffard called the combining tube of his injector "*la cheminée*", which translates to chimney in French.

Contrary to most mechanics and engineers who only comprehended the effects of the blast of steam, however, Giffard had such a training to further inspect the physics behind the working principle of the blast pipe. Thanks to already mentioned French scientific approach and his mechanics knowledge, he microscopically foresaw that the impact between steam and the gases could be analogous to an inelastic collision. He therefore hypothesized that the power

Historical context

of steam lays in its momentum transfer capability rather than its pressure. He indeed stated:

"...the molecules of steam [are] comparable to a series of small, heated billiard balls...which, after their exit from the nozzle in which they acquired their velocity, and at whatever distance from that nozzle, come to collide with another series of billiard balls, or musket balls, cooler and larger or heavier, which are the liquid molecules with which they share their heat and momentum, proceeding from thereon with a common velocity." [47, translated]

Incredibly enough, as this statement demonstrates, Giffard also predicted that the principle of induced currents could be a mechanism for heat exchange, even though it was not a direct consequence. His knowledge of this principle was critical since momentum transfer and heat exchange were not obvious features of the blast pipe, neither they had been paramount for its development, instead they were central for the operation of the injector. It is only thanks to these intuitions that Giffard figured out the feasibility of the injector. Prior to proceeding, it is now necessary to give a complete outline of how the operation mechanism of the injector.

The most basic and intuitive explanation of the operation of the injector is by imagining a boiler with two convergent nozzles: one exhausting steam and the other water. As pressurized water passes through the nozzle, its velocity increases from zero while proportionally its pressure drops, in accordance with Bernoulli's principle. When water comes in contact with the ambient air, it will have dropped to atmospheric pressure, while acquiring a noticeable speed (let us call this speed V). The same happens considering the steam nozzle, which increases steam exit velocity. But the mechanism is different, and here comes into play the problem of the caloric theory: due to the first law of thermodynamics, steam possesses significantly more internal energy, or heat energy, which is function of its temperature, in comparison to water (as a reference, the internal energy of water at 5 bar is $U_W = 639.68 \frac{kJ}{kg}$ while for steam is equal to $U_S = 2561.2 \frac{kJ}{kg}$, an increase of 300% [48]). As steam flows through the nozzle, in addition to pressure, also heat energy is converted into

2.2 Henri Giffard and the Steam Injector

kinetic one. Moreover, we can add that steam follows the laws of compressible flow, while water the incompressible ones, thus together with pressure also its temperature and density decrease. The final result is that steam gains a speed which is many times greater than water, which it can be now assumed equal to $20V$. If we return to focus on the water nozzle, and now we suppose that the flow could be reversed so that water could enter from the atmosphere to the boiler, we can predict that at the end of the introduction the water will have zero velocity and pressure equal to the boiler one. Furthermore, if we consider to give water an initial speed of V , the water could actually be directed into the boiler thanks to an divergent nozzle, commonly named as diffuser, for which the kinetic energy is transformed into pressure one, to win the boiler pressure. If we then suppose that even a fraction of the steam flow's high speed can be transferred to the water stream by their collision, it becomes evident that the entering pressure of water can exceed the boiler one. That is at the simplest what enables the injector to use steam to amplify even ten times the water pressure, and it was the explanation that was generally given at the start of the last century, in books such as the seminal "Practice and Theory of the Injector" by Strickland Kneass [10]. Nowadays, further research gained deeper insight on how pressure rise is produced by the mixing of water and steam; however, that required technological devices and knowledge that weren't available at the time. So it should be noted that this is not the complete explanation, since it lacks completely the mentioning of the condensation shock effect, although still partially true. The full operation of the injector is explained in Section 3.1.

It is now possible to understand the operation of the most basic form of injector and what are the components that comprise one. Consider Figure 2.9. Upon opening of the steam cock, steam coming from the boiler enters the device by the flanged connection A , flowing thus through the steam ram a' in which many little holes a'' are produced. Steam is regulated thanks to the spindle s , maneuvered by the hand wheel F , which adjust the annular area of passage through the convergent nozzle a and which needs to be drawn back usually one turn from a tight contact with the nozzle a to start it. The rapid discharge of steam into the combining tube b , after displacing the entrained air in the suction pipe B , establish a low pressure region in which water, at atmospheric pressure inside the tanks, is sucked by. After all air is

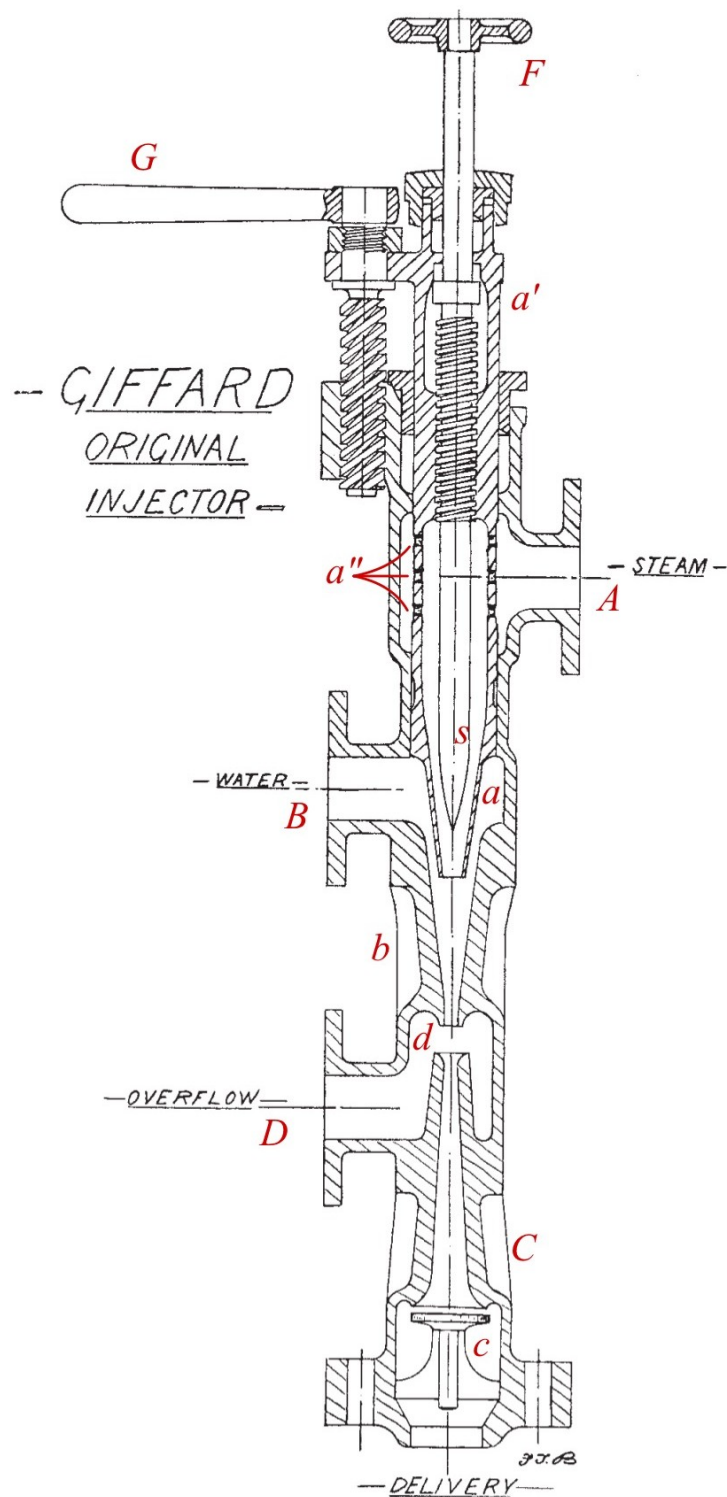


Fig. 2.9 Upgraded Giffard injector with reference letters

2.2 Henri Giffard and the Steam Injector

exhausted, the spindle is drawn fully back and thus the increased discharge of steam imparts to the intaken water sufficient speed to cross the overflow space d without spillage, to than gain as much as possible pressure through the discharging nozzle C , opening the no-return safety valve c which prevents water from the boiler to return inside the injector. At start, after the air is exhausted, during the time in which the correct relation between the annular area of the nozzle and the larger end of the combining tube is not satisfied, or when the pressure isn't enough to overcome the resistance of the boiler's valve, the fluids are able to evacuate the injector by means of the overflow pipe D , which is generally in direct contact with ambient air. When the injector is operating properly, it is said that runs "dry" since no water is spilled out from the overflow. Overflow usually happens for two reasons: if the supply of water is not enough to completely condensate steam through the combining tube (since steam is a compressible fluid, pressure, speed and density are dependent one another: if steam isn't completely condensed, its density remains far lower than that of water, it follows that the steam flow retains most of the speed and that it isn't converted into pressure, hence reducing the mixture's total pressure, which most probable is not enough to overcome the boiler's pressure) or if the amount of water is too high to be affected and pressurized by the steam impact. It is clear that to work, the injector needs a precise range of ratio between the mass flow of steam and water. It is for this reason that, compared to the very first design of Figure 2.7, Giffard introduced the adjustment of the water area by the lever G , which gives an axial movement to the steam ram a and permits to regulate the annular water flow area [49].

To summarize, the injector is made by two nozzles and one diffuser which combined perform different functions. The steam nozzle aim is to convert heat and pressure of steam into kinetic energy. In the combining tube, Bernoulli's theorem enables the pressure drop of steam to draw in water and to effectuate a heat, mass and momentum transfer between the two. Finally, the diffuser transforms part of the kinetic energy gained by the water into pressure. Clearly, although founded on the same principle, the injector is a quite more sophisticated device compared to the blast pipe.

Historical context

It isn't necessary to provide a lengthy explanation of every aspect of Giffard's theory, for more details it is suggested to read Giffard's self-written book [47] or to read pages 19 to 21 of Kranakis's dissertation [42]. However, it is interesting to point out that although not accurate, Giffard's theoretical procedure enabled him to build a rational framework in which he could predict what were the actual parameters affecting the injector's operation. To address an example of its limitations, the speed of steam at the nozzle outlet was calculated by Giffard using Torricelli's theorem, even if it wasn't applicable due to the compressibility of steam. Despite all the limits, his theory nevertheless let Giffard understand that it was needed to regulate the flow of water into the mixing tube in correlation to the amount of steam inlet, even though it was impossible to him to accurately determine this ratio.

Giffard actually developed the framework in a short period of time, but to transform it into a workable device it took far longer time. He himself didn't actually completely succeeded in this task. Only after years of modifications and testing from the engineering community the injector really became a mature, reliable and efficient device. Some upgrades related to the ability of the injector to self-restart without any manual input from the operator in case of sudden and short-time interruptions of the water feed - as for locomobiles, this could occur in case of bumps or holes in the terrain - usually by means of overflow valves, movable sealing washers and auxiliary overflow arrangements; these components had the scope of avoid the entrainment of air, dangerous for the boilers, and of maintaining for the short interruption the depression produced by the expanding steam, which would then automatically draw the water feed in. In the original injector, during water feed break, the high pressure steam, without any water with which condensate, would blow back inside the supply pipe: the operator would need then to reduce the amount of steam regulating the spindle until the water jet issuing could be reinstated.

One of the most famous solution to this problem was the one of the "Penberthy" automatic injector, depicted in Figure 2.10. Here the restarting feature is enable thanks to both an overflow valve *N*, resting on the seat *P*, and a sliding washer *T* which, as steam condensation during mixing with water further develops the low pressure zone in the combining tube *Y*, raises up and

2.2 Henri Giffard and the Steam Injector

seals the cylindrical overflow chamber. During feed stops, the washer opens and lets free discharge of steam to the overflow through it [50, 10].

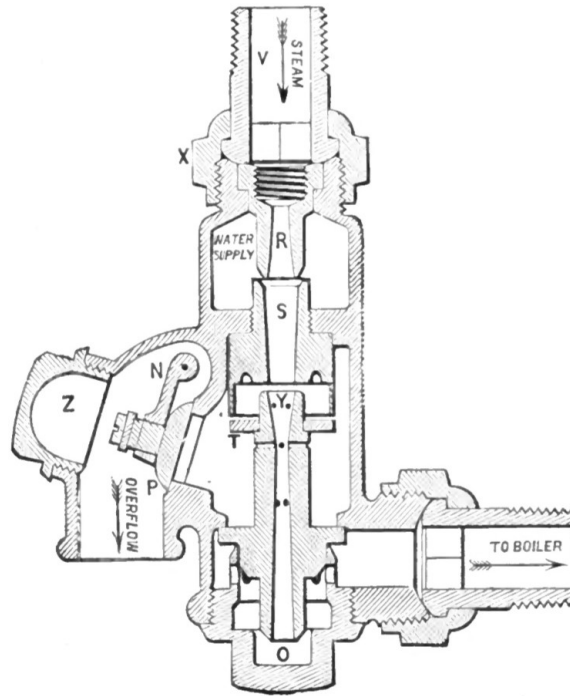


Fig. 2.10 The "Penberthy" automatic injector [9]

Another great technological advancement was the introduction of automatic systems with further reduced amount of skill required to the operator. As mentioned before, to correctly work, the injector of Figure 2.9 required the manual setting of both the spindle to regulate the steam flow and the steam nozzle ram to regulate the water feed. Many engineers reduced the regulation to just the steam one by implementing a sliding set of tubes that would automatically calibrate the proportion of water to the steam introduced. The first example is the one produced by the Wm. Sellers & Co. in 1865, exposed in Figure 2.11. The combining tube *b* and delivery tube *c* are united together and packed by the stuffing boxes *g* and *h* positioned at the outlet of the injector. Between *b* and *c* the opening *d* enables the flow of mixture to communicate with the closed overflow chamber *D*. This enabled to establish a balance of pressure between the closed chamber *D* and the chamber *b'*: as the amount of steam condensed is varied, the local pressure in *D* is consequently varied and this produce a differential pressure that to be equilibrated would shift

Historical context

the position altogether of the tubes, thus effectively regulating the chamber b' volume and the annular entrainment area of water from the supply pipe B [10]. As a result, this class of automated injectors did not require an overflow discharge mechanism, as this risk is inherently eliminated.

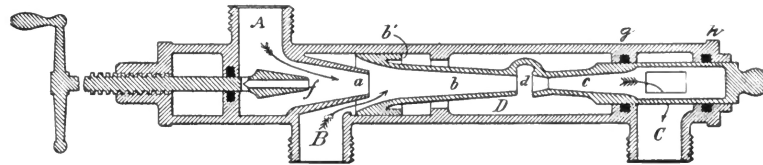


Fig. 2.11 The Wm. Sellers & Co. 1865 automatic injector [10]

Particularly worth mentioning, is an improvement owed to the Austrian engineer Schau, who discovered in 1869 the effect of postponing a divergent section to the common only convergent steam nozzle, as the one named a in Figure 2.11, thus developing a primordial De-Laval nozzle. This opened the introduction in the market of a series of supersonic steam nozzle injectors, which would over time become mainstream. Actually, the discovery isn't due to any supersonic consideration, indeed the De-Laval nozzle is a much later invention, but emerged from a set of experiment performed with different designs of steam nozzle outlets: the convergent-divergent one was found to be the one producing the best steam discharging shape. Some local pressure measurements and speed calculations were actually performed and some hints indicated the possibility of choking the flow at the nozzle throat, however it wasn't completely understood why [10, pp.53-65].

To conclude, since it is difficult to gather information about such an antique device, here are suggested sources available in literature which one could use to gain more insight about the theory and practice of the injectors [10, 43, 47, 51–54], or to delve into the working and schematics of common injector designs [9, 10, 50, 54–56]. Moreover, to gain a comprehensive understanding on how steam-powered system worked, their components and the operation, two magistral books are recommended [57, 58].

Chapter 3

Literature review

3.1 State of the Art of the Steam-water Injector

3.1.1 Main research trends

In this section a summary of the most interesting findings in literature concerning the steam-water injector is presented. Scholars have been historically referring to it with various names: *injector*, *ejector*, *jet pump*, *thermo-compressor* and *condensuctor*. In light of the redesign purpose central to this thesis, particular attention is dedicated to identifying a suitable model to support the design process.

Since its invention in 1858, the steam-water injector has been a crucial component in most steam-powered vehicles and stationary boilers. However, starting around the 1920s-1930s, the steam engine was progressively abandoned and its importance significantly declined, so that the research effort about it virtually ceased. It wasn't until the mid-50s of last century that some scholars began investigating other possible purposes of the steam-water injector, extraneous to the original one. Since then, potential applications regarded the injector mainly as a reliable passive safety system for nuclear power plants [11, 12, 59–65], or as a high performing heat exchanger [14, 65–67] - for example, for city districts heating - or as ejector in refrigeration systems [68] - obviously in this case the fluids used are refrigerant ones and not water - and

supercritical Rankine cycles [63, 69].

As anticipated in Chapter 2, a complete understanding of the complex thermo-fluid-dynamics principles occurring inside the steam-water injector has not been available for decades: it was thought that the main principle allowing the injector to drastically raise the water pressure was just the momentum transfer occurring between the steam flow and the water drawn in. The observation that the resulting water flow into the boiler has high pressure but low speed was thus all attributed to the effect of the diffuser. It is now ascertained that the actual pressure raising phenomenon is the manifestation of a condensation shock in the mixing nozzle or in the diffuser - the actual position is still debated, as it was found that the inlet and back-pressure conditions can greatly affect where it occurs [14–16, 70–73] -.

As steam flows into the mixing tube and mixes with water it transfers to the latter heat, momentum, and mass through interfacial shear flow: the apparent consequence is that it condenses. Therefore, the steam flow, already at low pressure due to the action of the steam nozzle, increases even more the depression level due to the significant volume shrinkage. This has the effect of drastically increase the water flow - an aspect actually already understood since the beginning - but also another subtle outcome: at some distance in the mixing nozzle the pressure becomes so low that it becomes lower than water's vapor pressure, so that the water part of the mixture instantly boils, thus effectively inducing the cavitation phenomenon. The bubbles just created are then crushed by the surrounding water, which fills up the cavity formed behind, driven by its kinetic energy. Viewed from a mechanical point of view, the bubble collapse has the same effect of a "mechanical amplifier", conveying the kinetic energy into a more concentrated fluid volume: the work done by this energy equates the work done by the pressure field, thus increasing the final pressure. The summary presented in Section 2.2 can be therefore be completed by specifying that, while the steam nozzle converts steam heat into kinetic energy, the mixing nozzle converts most of this energy into pressure through the onset of a condensation shock. It should be pointed out that since not all the kinetic energy of the mixture of condensed steam and water is transformed into pressure by the condensation shock phenomenon, a diffuser is anyway needed

3.1 State of the Art of the Steam-water Injector

to extend to the maximum the pressure augmentation. Anand has extensively phenomenologically studied and mathematically modeled the condensation shock [59] in his PhD thesis. In Figure 3.1 it is possible to observe that the steepest pressure gain happens in the mixing nozzle, while the diffuser has a lower impact.

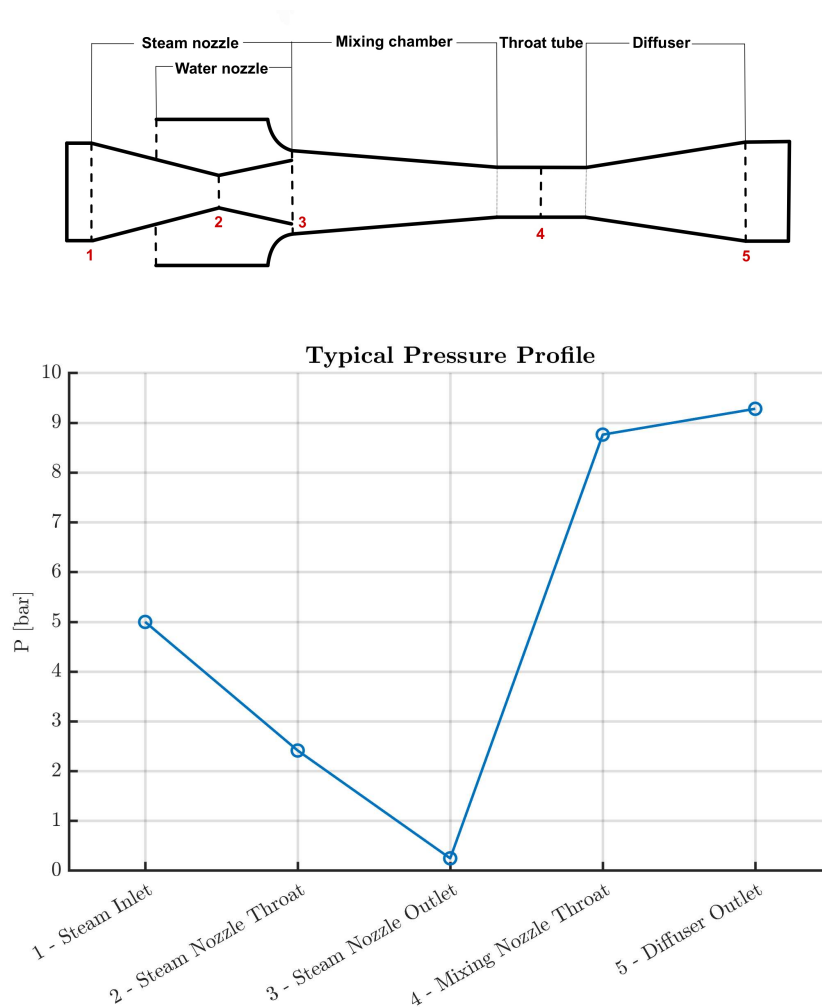


Fig. 3.1 Typical steam-water injector pressure profile

All antique injectors were designed with a central steam nozzle and an enveloping annular inlet of water. However, over the years, several academics analyzed a version of the injector where the central jet is liquid, surrounded by an annular steam flow. Although it was found that the overall difference between the two - regarding the average properties of the outlet liquid

Literature review

stream, such as pressure, temperature and speed - is quite limited, the internal mechanism of pressure raising and flow structure differ substantially [15]. Nevertheless, the central steam nozzle design is often considered easier to design and ultimately more convenient, since it minimizes the dimension of the steam nozzle and avoids direct contact between the steam discharging flow and the walls in the mixing tube, to reduce viscous dissipations and heat transfer to the injector body [12]. In 2015, Takeya et al. have made an incredible effort in reviewing all the available steam-water injector designs in literature, displayed here in Figure 3.2. In addition, some injector designs investigated supplementary features such as a constant area throat tube just after the mixing nozzle (Figure 3.3a) or an overflow port, which, as explained in Section 2.2, is useful during startup and to discharge the excess of steam (Figure 3.3b).

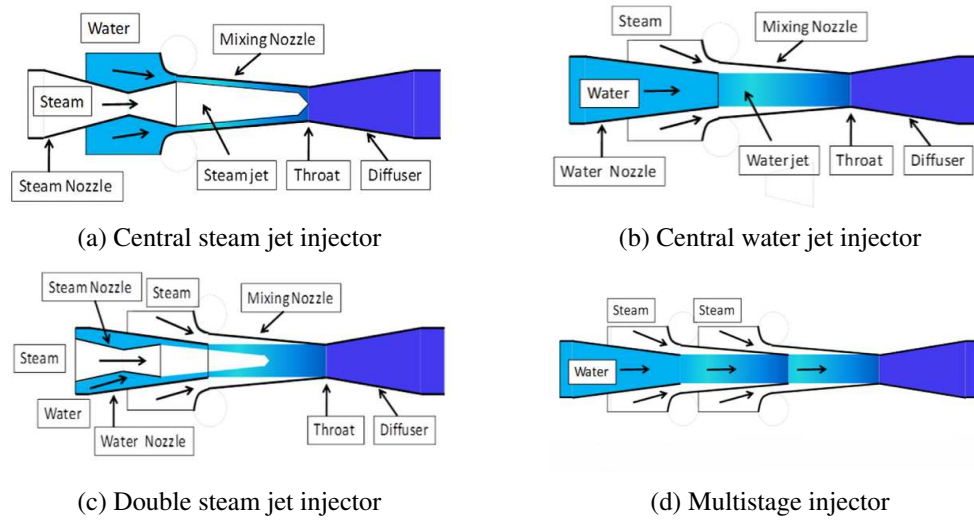


Fig. 3.2 Examples of steam-water injectors nozzle arrangement [11]

Independently from the arrangement of the nozzles, the ideal process of the steam-water injector follows the Mollier diagram in Figure 3.4. Usually, for simplicity, it is assumed that steam enters the steam nozzle in saturated condition at a pressure P_{G_o} ; undergoes an adiabatic expansion in the convergent-divergent nozzle to the point a , lowering both quality and pressure to P_{G_a} , therefore at steam nozzle outlet is generally found steam but also liquid droplets; through the mixing nozzle steam completely condenses, reaching point e in the proximity of the mixing throat, hence here only liquid is present;

3.1 State of the Art of the Steam-water Injector

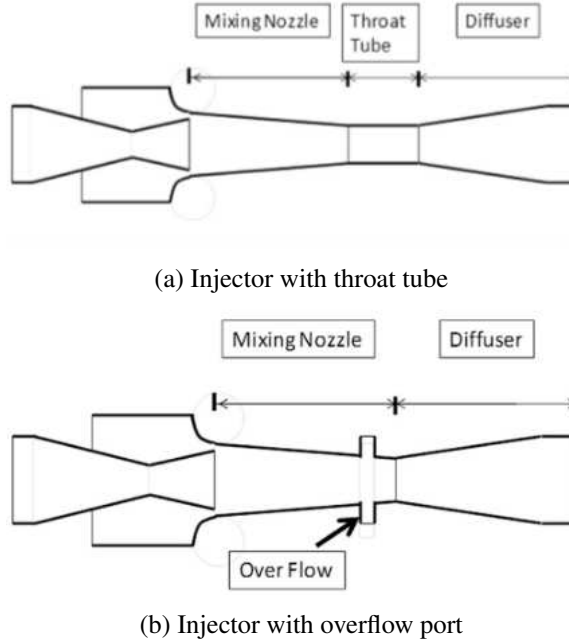


Fig. 3.3 Additional features of steam-water injectors [11]

finally, the diffuser transforms the remaining kinetic energy into pressure, thus increasing it to P_{o_e} at the point o_e .

An injector performance can be directly and easily evaluated either by the discharge pressure level $P_{w,out}$ or the water mass flowrate $\dot{m}_{w,out}$ at the diffuser outlet. Nevertheless, over the years, other parameters were developed to better describe the operation of the steam-water injector. They are mainly dimensionless parameters which focus each on one ability of the injector: the entrainment ratio, the compression ratio and the pressure gain ratio.

The entrainment ratio ω is used to quantify the ability of the injector to drawn in the suction flow compared to the motive flow. Most papers use Equation 3.1a, since it directly express the amount of water that a unit of steam mass can pump. However, some use the inverse Equation 3.1b [68, 73–76].

$$\omega = \frac{m_w}{m_s} \quad (3.1a)$$

$$\omega = \frac{m_s}{m_w} \quad (3.1b)$$

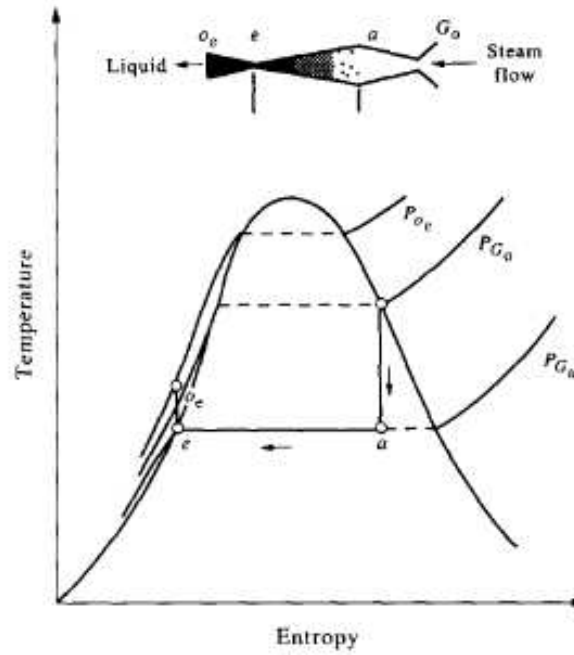


Fig. 3.4 Mollier diagram of the ideal steam-water injector [12]

The pressure raising capability of the injector is instead assessed thanks to the dimensionless parameter R . This ratio highlights how much the injector is able to increase the pressure of the inlet flow of water.

$$R = \frac{P_{w,out}}{P_{w,in}} \quad (3.2)$$

Finally, the last performance indicator is the pressure gain ratio Γ , which is the ratio between the water pressure at the diffuser outlet and the pressure of steam at inlet, thus it needs to be greater than unity if the injector needs to work as a pump.

$$\Gamma = \frac{P_{w,out}}{P_s} \quad (3.3)$$

For most use cases these parameters are enough to characterize the injector operation and many research groups found that they are dependent one another, usually inversely proportional. Some other parameters seldom used are the exergy efficiency and the equivalent heat transfer coefficient.

3.1 State of the Art of the Steam-water Injector

One of the oldest scholar paper about the steam-water injector was produced by Kaye et al. [77] and is dated 1956. Unfortunately it is either unpublished or for private communication, it is therefore not publicly available. However, a review of the paper is present in other works of collaborators. Firstly, it is interesting to underline the fact that they refer to the injector as the *condensuctor*, a name recurring in that time period but not anymore used, highlighting the ability of the device to suck in water thanks to the condensation phenomenon. The research was inserted in the attempt to propose the injector as a back-pressure reduction device to increase the efficiency of the propulsive system of some deep-water torpedoes. The preliminary work consisted in an analytical attempt to demonstrate that a constant-pressure condensation could result in a higher pressure gain than a constant-area one. The main purpose however was to evaluate the effect of the presence of a part of non-condensable gas such as CO_2 in the primary flow. The ratio range of gas content of interest was up to 20% of the total steam flow. The result was that there was little difference seen in the pressure gain when the non-condensable ratio was less than 5%. This subject was however later studied by Gouse and Leigh, reaching a similar conclusion [78], but extending the allowable percentage in the range of 20% to 50%.

Globally, the recent academic effort mostly relates to the investigation of the mixing flow structure, characterization of the performance, the position and occurrence of the condensation shock, the direct contact condensation mechanism, the heat transfer capabilities and the operational range definition. Minor topics are multi-dimensional CFD simulations and new design improvements. For the most part, the water-centered injector is the one more studied compared to the steam-centered or the other complex ones.

An interesting take on the design of the injector is the study of Yan et al. [66], which analyzed the effect of swirling vanes both into the steam nozzle and in the water nozzle. The research group conducted various experiments at different operating conditions and also performed an exergy efficiency analysis. The conclusion is that the water swirl vanes actually greatly improve the entrainment ratio and overall exergy efficiency of the injector, in addition to higher outlet water temperature. On the other hand, the steam vanes had the

opposite effect. Anyway, swirling vanes weren't further studied. Although intriguing, it has been decided to not include them in this thesis's final injector design.

The steam-water injector can be also used as a heat exchanger or for waste heat recovery. In 2009 Trela et al. [79] determined the average heat transfer coefficient from experimental data of an injector and concluded that it can achieve values as high as $700 \frac{kW}{m^2K}$, which is about 100 times greater than the ones of shell-and-tube heat exchangers. Zhang et al. [74] remarked that most conventional power machines are not able to utilize the waste heat produced. For this reason, an injector can be used to recover most of the heat thanks to the direct contact heat transfer which happens in the mixing nozzle, unlike other conventional surface heat exchangers. Abe and Shibayama [14] computed the heat transfer coefficients and Nusselt coefficient of a water-centered injector employing a control volume model and compared the results obtained from Dittus-Boelter equations for forced-convection heat exchangers and the Nusselt equations for film condensation heat transfer. The discovery was that the coefficients of the injector were at least an order of magnitude greater compared to both the other two. Miwa et al. [80] employed the temperature measurements of an experiment to calculate the average heat transfer coefficient of their injector system, neglecting the heat losses to the environment. It was again established the capabilities of this device, which resulted in a system heat transfer coefficient in the order of $10^5 \frac{W}{m^2K}$. Moreover, it was found that the heat transfer is proportional to the inlet steam pressure, but independent on the water flow rate. In 2021, Kwidziński [67] experimented four different steam-centered injector and determined the average heat transfer coefficient for each one. The resulted range was from 200 to $800 \frac{kW}{m^2K}$. Moreover, it is suggested that this values are consequence of the highly developed interface surface in the mixing nozzle and the large temperature and speed velocity gradients between steam and water at the inlet of the chamber.

The condensation shock and mixing process characterization is by far the biggest research trend in the field. In the second half of the 20th century, Gouse and Leigh, Grolmes and Anand [59, 60, 78] investigated primarily the jet breakup process and atomization. If the first assumed no perceivable jet

3.1 State of the Art of the Steam-water Injector

breakup in the mixing process, due to the limited information available, the other two scholars filled the gap and concluded that it doesn't just actually occur in the injector, but it even has a major role in the condensation process. Initially, scholars tended to assume complete condensation of the flow at the mixing chamber throat, such as Cattadori et al. [12] and Narabayashi et al. [63]. However, in 2001 Malibashev [70] visually observed many planar transparent models of the injector, conveniently enclosed by two quartz-glass walls. This possibility enabled him to notice that at the diffuser inlet the flow was indeed most transparent, thus indicating the predominance of water phase, but with separate steam bubbles still present. This indicated that it was possible to obtain incomplete condensation at the end of the mixing chamber. In addition, the size of the throat was found to be critical, since the condensation shock location was dependent on it, and it could be moved upstream or downstream the throat by varying the back-pressure level. Actually, when the condensation shifted upstream the throat, the injector stopped working. One additional interesting finding is that a too short mixing chamber length can effectively hinder the mixing process. The dependence of the mixing process, and in the end of the discharge pressure, to the mixing throat size was also observed by Kwidziński [71]: without deterioration of flow stability, it was found that a discharge pressure rise of 20% was achievable by reducing the throat section to a value comparable to the one of the steam nozzle throat. Ma et al. in 2017 [13] discovered a similar dependency to this ratio by the entrainment ratio, as displayed in Figure 3.5, where A_4 is the steam nozzle throat area and A_7 the one of the mixing chamber throat.

Abe and Shibayama [14] too observed that in their investigated injector the condensation shock occurred in the regions of the throat tube or the diffuser therefore they also concluded that, contrary to other findings, steam doesn't completely condensed in the mixing nozzle. Moreover, by varying the opening ratio of the back-pressure valve, they were able to move the position of the shock wave initiation (Figure 3.6). When this point took place at the throat, the injector stopped working. In 2015, Kwidziński [15] performed multiple experiments in which pressure and temperature measurement were taken at multiple locations along the injector, with the aim of advancing the understanding of the complex flow mixing structure. It confirmed the supercritical

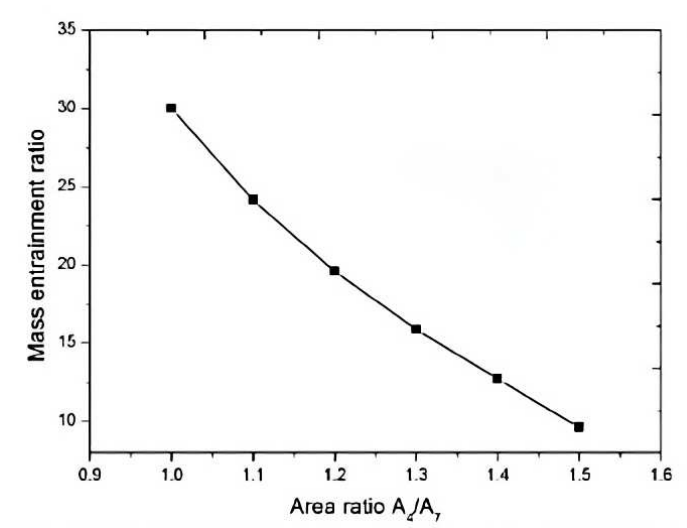


Fig. 3.5 Dependence of entrainment ratio to throat areas ratio [13]

character of the flow in the mixing chamber, since pressure fluctuations could be measured downstream the condensation shock-wave, but not upstream. He even managed to capture with a high-speed camera the onset of the stall condition in a steam-centered injector, shown in Figure 3.7, initiated by a ramped raise of back-pressure level. It should be noted how greatly the condensation reduce when the injector is stalled. Another important conclusion was that the structure of the condensation shock-wave is independent from its amplitude and location.

Kamata et al. [16], in their effort to better clarify how the flow structure develops within the diffuser, observed that the maximum discharge pressure was achievable right as the condensation wave approaches the mixing nozzle throat; any further movement upstream causes the injector to stall. In Figure 3.8 are displayed both the upstream longitudinal shift of the condensation shock and the pressure raising steep increase for very low back-pressure valve opening ratios.

An important contribution was given by Miwa et al. in 2018 [17] to characterize the inoperative conditions and the operational range of a water-centered injector, mainly as a function of inlet steam pressure and inlet water mass flow. Four different causes were found:

3.1 State of the Art of the Steam-water Injector

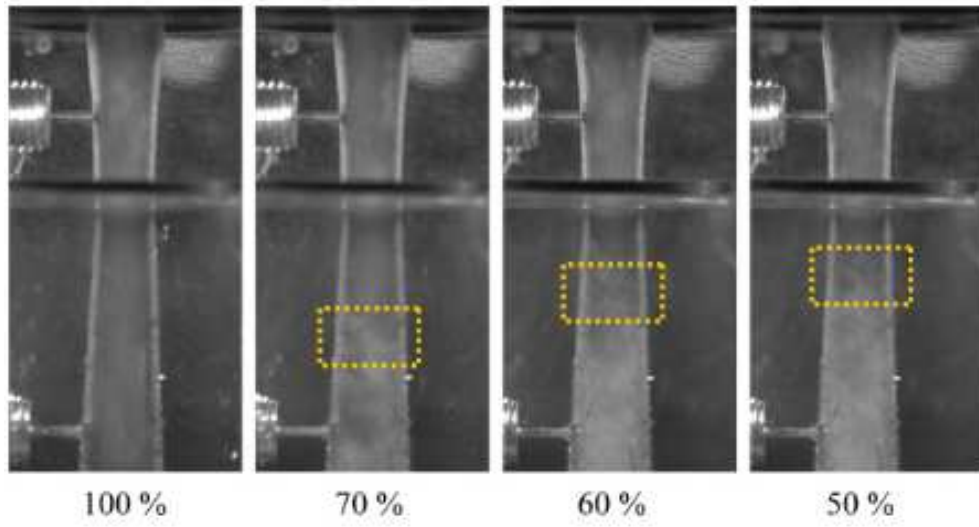


Fig. 3.6 Condensation shock shifting proportionally to back-pressure valve opening ratio [14]

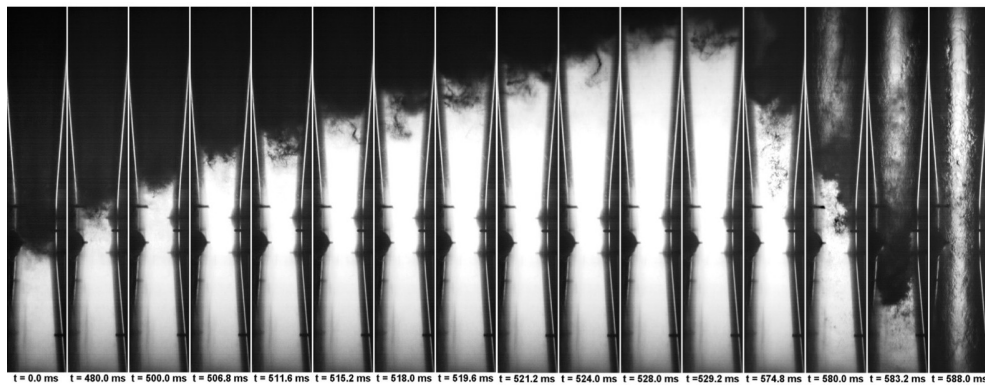


Fig. 3.7 Frames showcasing the onset of stalling in a steam-centered injector [15] (the two-phase section of the flow are transparent, so they are the dark ones in the images)

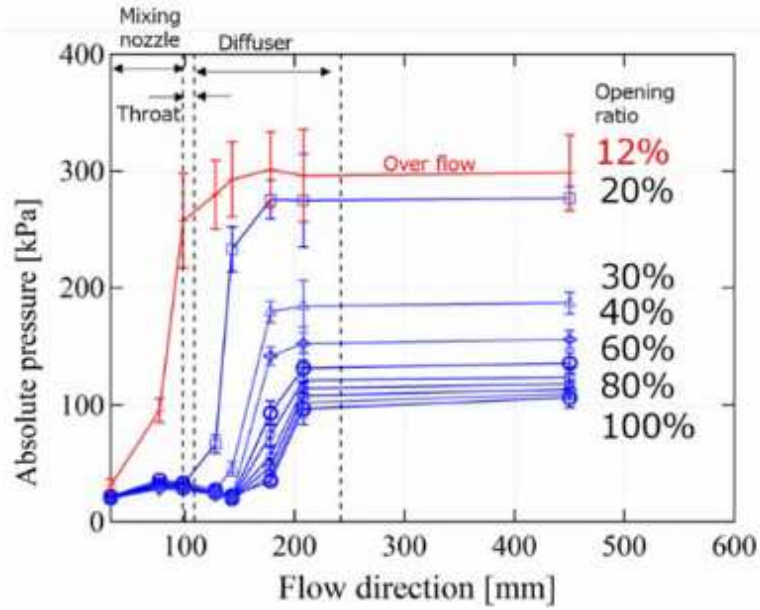


Fig. 3.8 Pressure distribution as function of back-pressure valve opening ratio [16]

1. **Outlet water mass flow fluctuations:** for low steam pressures and inlet water mass flow rates.
2. **Steam discharge depression generation ceasing:** for low steam pressures and moderately high water flow rates.
3. **Failure at maintaining maximum discharge pressure:** for high inlet steam pressures but low water flow rates.
4. **Fluctuations of the inlet water pressure:** for high inlet steam pressures and low water flow mass rates.

It was then possible to circumscribe an operational region of the injector, presented in Figure 3.9, where are also indicated the areas of each inoperative case.

Lastly, it is worth mentioning one of the latest research effort in literature. In 2025, Wang et al, [76], worked to develop a generalized model to compute the pressure at which mixing occurs in the combining nozzle. In earlier studies, scholars divided in two groups: those who assumed that mixing pressure was constant and equal to the one at the outlet of both steam and water nozzle

3.1 State of the Art of the Steam-water Injector

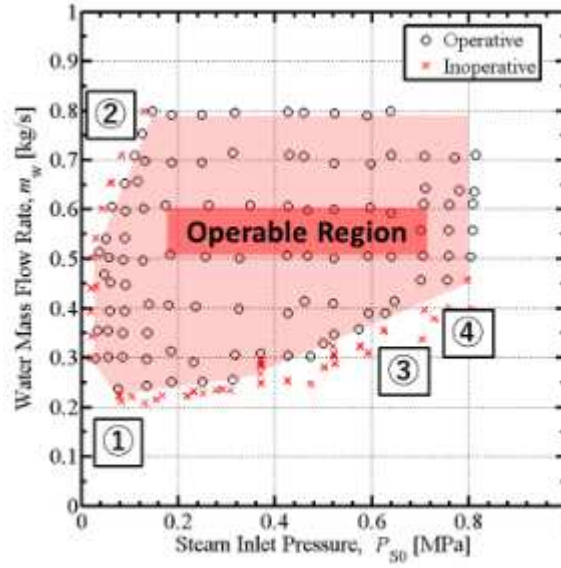


Fig. 3.9 Operational region and inoperative conditions for a water-centered injector [17]

($P_{s,mix} = P_{w,mix}$) and those who contended that the mixing pressure equalization of steam and water could happen only after a certain distance into the mixing chamber, therefore assuming unequal pressure of water and steam at their respective nozzle outlets ($P_{s,mix} \neq P_{w,mix}$). Thanks to a semi-theoretical and semi-empirical mixing chamber model and a one dimensional injector model, they managed to clarify that mixing pressure has a great impact in the prediction of discharge pressure and overall axial pressure profile inside the injector. In addition, in the experiment performed to validate the model, a pressure difference is actually found between steam and water at the outlets sections; this difference decreases along the length of the mixing chamber and turns zero near the throat.

The phenomenon of condensation shock and its characteristics remain a topic still open to debate and it is definitely recognized its weight in evaluating the operation of an injector. For the purposes of this thesis, the most pertinent aspect of the debate is the one related to the inoperative conditions and behaviors of the injector; the one designed should exhibit similar behavior to the ones investigated in literature and similar inoperative conditions.

To conclude, in this paragraph are exposed supplementary key insights that should be taken into account in the design of the injector. Cattadori et al. [12] observed that when entrainment ratio is too low, steam doesn't fully condense in the combining tube. Furthermore, they reported that the maximum discharge pressure is inversely proportional to entrainment ratio. These characteristic should be considered during the design process, in order to aim at a compromise between exiting water mass flow and pressure augmentation of it. Kwidziński [71] recognizes the benefit of adding a throat tube between the mixing nozzle and diffuser. In the case of supercritical steam injectors, the condensation happens in the form of a shock wave: if this is developed in a cylindrical tunnel instead of in the divergent flare of the diffuser, than the pressure loss due to deceleration of the supersonic flow is prevented. The same author, in a 2015 study [15], thanks to a visual observed experimental campaign, determined that the speed of the flow after the condensation shock amounts to around $8\text{-}9 \frac{m}{s}$. This speed is expected to correspond also in this thesis' injector and it can be used to verify the quality of the model. The speed of the flow in the injector was also investigated by Trela et al. [79], who reported that in supersonic injectors it can reach at steam nozzle outlet velocities in the range of 500 to 1000 $\frac{m}{s}$ and as high as 450 $\frac{m}{s}$ in subsonic nozzles. Compared to Kwidziński, the outlet water flow speed was slightly higher, around 20 $\frac{m}{s}$. This evidence can suggest that different diffuser design can have a noticeable effect on the speed of the flow at the outlet. An interesting discovery is the one of Kwidziński in 2019 [81]: he managed to operate a low pressure steam-water injector at inlet steam pressures in the range of 0.62 to 1.3 bar, effectively demonstrating that this device can also work with inlet steam in depression state, although, intuitively, the overall performance is quite poor compared to high pressure injectors. Lastly, Deberne et al. [62] indicated that thermal equilibrium at the end of the mixing section can be realistically achievable if the mixing chamber length is more than seven times greater than the outlet section diameter of the diffuser. Although not essential for the injector to work, this should be considered for a more efficient design of the injector, if the size of the reverse engineered injector allows it.

3.1.2 Injector models

Most research papers related to steam-water injectors in literature accompany to experiments also the development of an analytical model focused to analytically describe the phenomenon to be examined. The model may be entirely original, or may represent extensions or improvements of existing ones. In order to support and guide the design process of this thesis, a model is deemed necessary. Therefore, particular interest was reserved to compare and evaluate the available analytical models, with the objective of selecting the most suitable for the application.

All models can be categorized following by these criteria:

1. Type of injector :
 - **Water-centered:** the central nozzle is the water one.
 - **Steam-centered:** the central nozzle is the steam one.
2. Steam nozzle [79]:
 - **Subsonic (or subcritical):** only convergent shape. Steam in this nozzle can expand in the tapered section, but its velocity can at most reach the sonic one, when the choked condition is reached at the outlet. Mach number is therefore ≤ 1 .
 - **Supersonic (or supercritical):** convergent-divergent shape. Steam in this nozzle can further expand in the divergent flare if in the throat the choking condition is reached. Mach number is thus > 1 .
3. Closure solution of the model:
 - **Theoretical:** if the model is entirely described by equations and parameters which are only related to fundamental laws of physics.
 - **Empirical:** if to close the model an empirical relation must be obtained through experiments or data fitting.
4. Modeling method [62]:

- **Local:** the flow is modeled at each section of the injector, by considering all major phenomena. This model, although more realistic, requires a full knowledge of each phenomenon and the relationship between each other, which is usually lacking.
- **Global:** also known as the control volume method, the flow in the injector is modeled by considering large control volumes conveniently placed at the critical sections comprising the device. One dimensional conservation equations are usually employed, but they often need empirical factors to take into account the irreversibilities, thus resulting less realistic.

Most of the injector studied in literature relate to the water-centered configuration, typically equipped with a supersonic steam nozzle. As to what concerns the modeling method, there is a substantial balance between global and local models. If local models are the most heterogeneous, all global ones can be categorized by one of the three typologies illustrated in Figure 3.10: models that assume no throat tube and no condensation shock; models that add a throat tube between mixing chamber and diffuser; and models that include a condensation shock region without a throat tube. With respect to the type of closure solution, an equilibrium is found between empirical and theoretical ones.

Within the scope of this thesis, although it was pointed out that adopting a water-centered model doesn't actually invalidate the final results, a steam-centered model is preferred, since this was the classical nozzle arrangement present in 19th century locomobiles. The nozzle type assumed is supersonic, since it is also the better performing one, despite the fact that it is very likely that the original Bordino injector was equipped with a subsonic one.

In addition, since the aim of the thesis is not to contribute in the research of the operation of the injector, a global model is sufficient to provide enough insight and appropriately support the design process. Finally, since no experimental data related to the injector is available, it is therefore favored a theoretical closure solution of the model, which doesn't require any device specific empirical relations. In Table 3.1 is presented a summary of the models

3.1 State of the Art of the Steam-water Injector

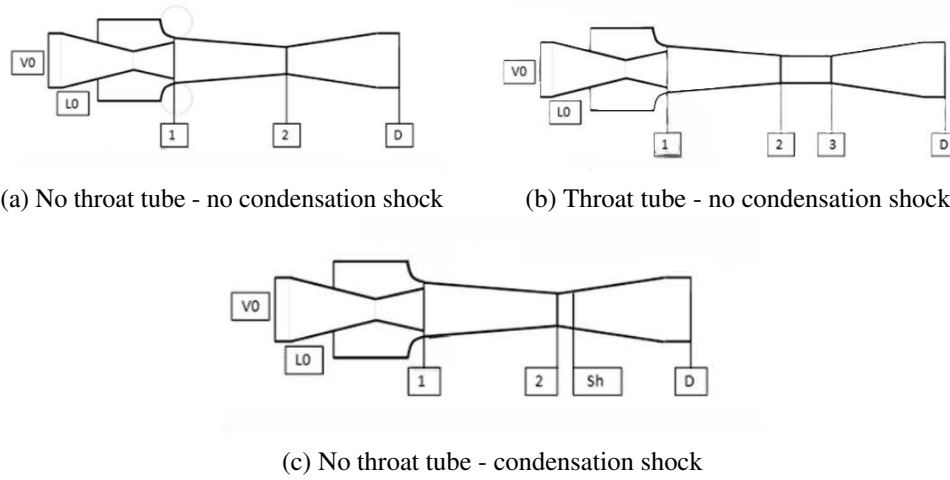


Fig. 3.10 Main global model types [11]

present in published research.

In the end, the model selected for this work is the original formulation proposed by Ma et al. (2017) [13]. One of the primary motivation is that it is one of the few models which analyzes in detail all the critical sections of the injector, included the supersonic steam nozzle. Notably, it doesn't require any empirical relations to compute pressure, speed or temperature in each section. The mixing chamber is treated as a single control volume, under assumption of complete condensation at the end of it, greatly reducing the complexity. The model achieves a good compromise between simplicity and physical fidelity, making it well-suited as a superior method to calculate the performance of an injector design and to guide the optimization of the geometric parameters. The numerical solution is obtained via an iterative calculation; both computational power and time required to run it are practical for everyday design workflows. Regarding accuracy, the authors performed a correlation with existing experiment data and reported a maximum relative error rate within 9.5%, which is considered acceptable for the level of precision required in this engineering application. A thorough description of the model and the governing equations is given in Section 4.1.

Table 3.1 Summary of Existing Models of Steam-Water Injectors

Author(s)	Year	Central Nozzle	Steam Nozzle	Solution	Method	ω	P_{mix}	Γ	R	Ref.
Grolmes	1968	Water	Supersonic	Theoretical	1D Local	$\omega = \frac{m_w}{m_s}$	$P_{s,mix} \neq P_{w,mix}$	-	-	[60]
Anand	1993	Water	Supersonic	Empirical	1D Local	-	$P_{s,mix} \neq P_{w,mix}$	-	-	[59]
Cattadori et al.	1995	Steam	Supersonic	Empirical	1D Global	$\omega = \frac{m_w}{m_s}$	$P_{s,mix} = P_{w,mix}$	-	-	[12]
Narabayashi et al.	1997	Water	Supersonic	Empirical	2D Local	-	$P_{s,mix} \neq P_{w,mix}$	-	-	[61]
Deberne et al.	1999	Water	Supersonic	Empirical	1D Global	-	$P_{s,mix} = P_{w,mix}$	-	-	[62]
Yan et al.	2005	Steam	Supersonic	Empirical	1D Local	$\omega = \frac{m_w}{m_s}$	$P_{s,mix} \neq P_{w,mix}$	$\Gamma = \frac{P_{w,outlet}}{P_s}$	-	[66]
Trela et al.	2009	Steam	Supersonic	Theoretical	1D Global	-	$P_{mix} = \frac{P_s + P_w}{2}$	-	-	[79]
Kwidziński	2010	Steam	Supersonic	Theoretical	1D Global	-	$P_{mix} = \frac{P_s^2 + P_w^2}{2}$	-	-	[71]
Zhang et al.	2012	Water	Subsonic	Empirical	1D Global	$\omega = \frac{m_s}{m_w}$	$P_{s,mix} = P_{w,mix}$	-	-	[74]
Abe and Shibayama	2014	Water	Supersonic	Theoretical	1D Global	-	$P_{s,mix} \neq P_{w,mix}$	-	-	[14]
Miwa et al.	2016	Water	Supersonic	Theoretical	1D Local	-	$P_{s,mix} \neq P_{w,mix}$	$\Gamma = \frac{P_{mix}}{P_s}$	-	[80]
Zhao et al.	2016	Ejector	Supersonic	Theoretical	1D Global	$\omega = \frac{m_s}{m_w}$	$P_{s,mix} = P_{w,mix}$	-	-	[68]
Ma et al.	2017	Steam	Supersonic	Theoretical	1D Global	$\omega = \frac{m_w}{m_s}$	$P_{s,mix} = P_{w,mix}$	-	$R = \frac{P_{w,outlet}}{P_s}$	[13]
Kwidziński	2019	Steam	Subsonic	Theoretical	1D Global	$\omega = \frac{m_w}{m_s}$	$P_{mix} = \frac{P_s + P_w}{2}$	-	-	[81]
Kwidziński	2021	Steam	Supersonic	Empirical	1D Global	-	$P_{mix} = \frac{P_s + P_w}{2}$	-	-	[67]
Miwa et al.	2021	Water	Supersonic	Empirical	1D Local	$\omega = \frac{m_s}{m_w}$	$P_{s,mix} \neq P_{w,mix}$	-	-	[75]
Ke et al.	2022	Water	Supersonic	Theoretical	1D Local	$\omega = \frac{m_s}{m_w}$	$P_{s,mix} = P_{w,mix}$	-	-	[73]
Wang et al.	2025	Water	Supersonic	Both	1D Local	$\omega = \frac{m_s}{m_w}$	$P_{s,mix} \neq P_{w,mix}$	-	$R = \frac{P_{w,outlet}}{P_s}$	[76]

3.2 State of the Art of Additive Manufacturing and Reverse Engineering for the Reconstruc- tion of Spare-parts

In the context of vehicle restoration - more broadly, in the field of spare-parts for mechanical systems - unavailability and reproducibility of components are major issues that over the decades many researchers and companies tried to address. In many cases, it is indeed often impractical to reproduce these parts by traditional manufacturing techniques due to economic, technological and logistical aspects. For this reason, Additive Manufacturing (*AM*) in conjunction with Reverse Engineering (*RE*) is receiving growing attention and importance as a possible solution.

Collectible cars - often referred to as classic cars or vintage cars - are a niche market that recently experienced an exponential growth, resulting in a global value of existing assets amounting to €800 billions in 2024 [18]. Within this market, the maintenance, restoration and spare-parts segment generates the second biggest annual revenue, as shown in Figure 3.11, demonstrating its high value and strategic importance. In the realm of classic cars, spare parts hold significant importance since they allow to maintain the operability of these goods and they directly impact their value. Moreover, these vehicles are often regarded as dynamic types of art and thus, for full appreciation, should be admired in motion and not only statically. This is a paramount aspect for *MAUTO*, which compared to many other automobiles museum, puts a lot of effort into mechanically restore the vehicles in the collection, maintaining them always functional rather than consider them only as exhibition pieces.

AM is a relatively young discipline that is revolutionizing the reproduction of spare-parts and, in combination with RE, enables companies and restorers to replicate them accurately and with high fidelity to their history, even if the original component is out of production or unavailable, or if the reproduction would be otherwise economically unfeasible. Indeed, traditionally this market primarily relied on refurbished parts sourced from wrecked vehicles, from waste of car specialists or directly from OEM inventories [82]. In addition, AM

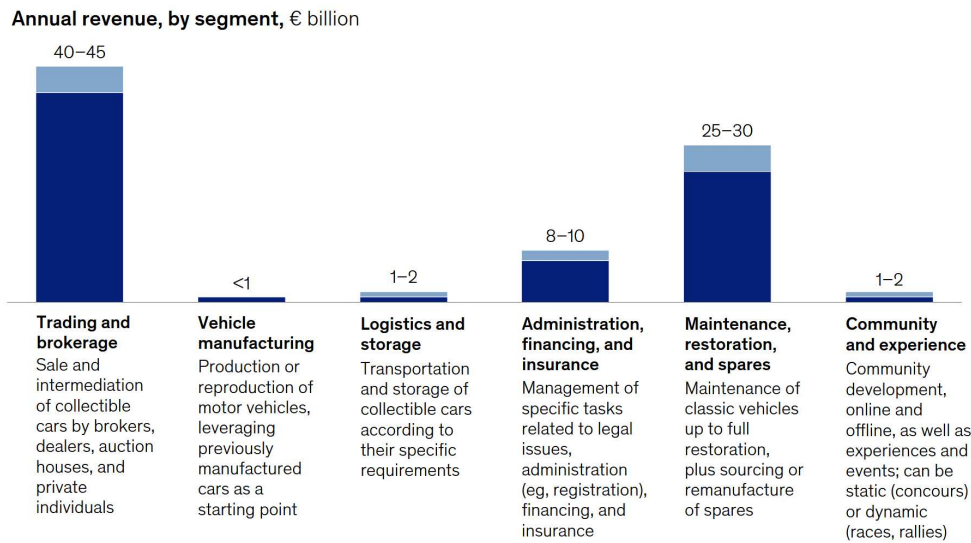


Fig. 3.11 Annual revenue for segment in the collectible cars market [18]

represents a pillar of the Industry 4.0 revolution, enabling thus the digitization and digital fabrication of these components, aiding companies in reducing costly warehouses expenses for inventory and allowing an decentralize, on-demand production [83].

3.2.1 Fundamentals of AM

Additive manufacturing, as defined by *ISO/ASTM 52900:2021(E)* [84], is the process of joining materials to make parts from 3D model data, usually layer upon layer, as opposed to subtractive manufacturing and formative manufacturing methodologies. AM originated in the 1980s with the invention of stereolithography by *3D systems* and is actually an umbrella term which encompasses a wide variety of technological processes, many of which differ substantially from each other. The classification suggested by the ISO standard is displayed in Figure 3.12; each process can be subdivided based on criteria such as the material feedstock, the material distribution, the source of bonding or fusion and the basic AM principle. In literature are present also other partially different types of classifications [83].

3.2 State of the Art of Additive Manufacturing and Reverse Engineering for the Reconstruction of Spare-parts

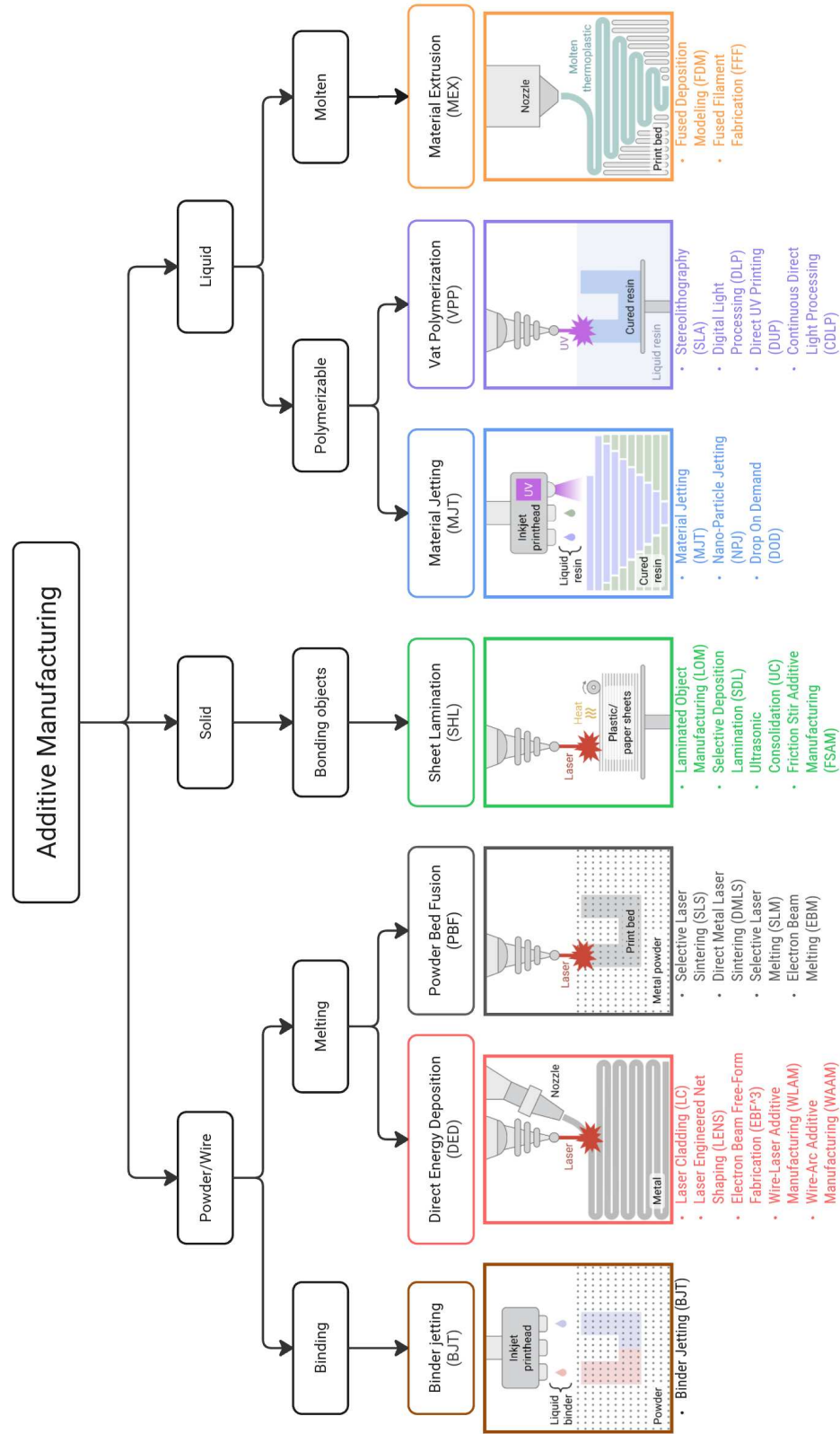


Fig. 3.12 Classification of AM processes [19], images from [20]

Literature review

All material classes are printable through at least one AM process - metals, polymers, ceramics, composites - however, compared to Conventional Manufacturing (CM), the range of available individual materials is comparably significantly lower. For instance, if for CM the number of metallic alloys available can be estimated to be around 3000 different types, the current portfolio for AM nowadays it is attested to be roughly 100.

In its early stages, AM was mainly employed as an efficient way to create tools - Rapid Tooling (RT) -, or models for casting purposes - Rapid Casting (RC) -, and finally demonstrative or functional prototypes - Rapid Prototyping (RP). Among these, RP is probably the prominent application of AM in industry. This is due to one of the greatest advantage of AM technologies: since they don't need additional tools such as casts, molds and fixtures other than the machine itself, they enable companies to perform prototype developing, testing and iteration at a dramatically increased speed and at a reduced cost compared to CM [85]. Nevertheless, lately AM is advancing briskly in all directions and most importantly towards final product manufacturing, as even metal additive manufacturing (MAM) is reaching the industrialization stage [21].

The principal processes for metallic components adopted in industry are Powder Bed Fusion (PBF), Electron Beam Melting (EBM) and Direct Energy Deposition (DED) - the last particularly suitable for the reparation of components. Despite the advantages, AM is still an expensive procedure, which is rarely justified for mass production, as illustrated in Figure 3.13. To be economically competitive, it is estimated that it would be required a reduction in costs of at least a factor of 10 [21].

However, there is an increased appeal in the use of Material Jetting (MJT) and Binder Jetting (BJT) for cost-effective high production volumes of low performance parts - Figure 3.14. Among AM processes, DED in particular stands out as an interesting flexible and versatile process, suited mainly for repairing - and in some cases even remanufacturing - of metallic components in automotive and aerospace sectors. Compared to conventional Tungsten Inert

3.2 State of the Art of Additive Manufacturing and Reverse Engineering for the Reconstruction of Spare-parts

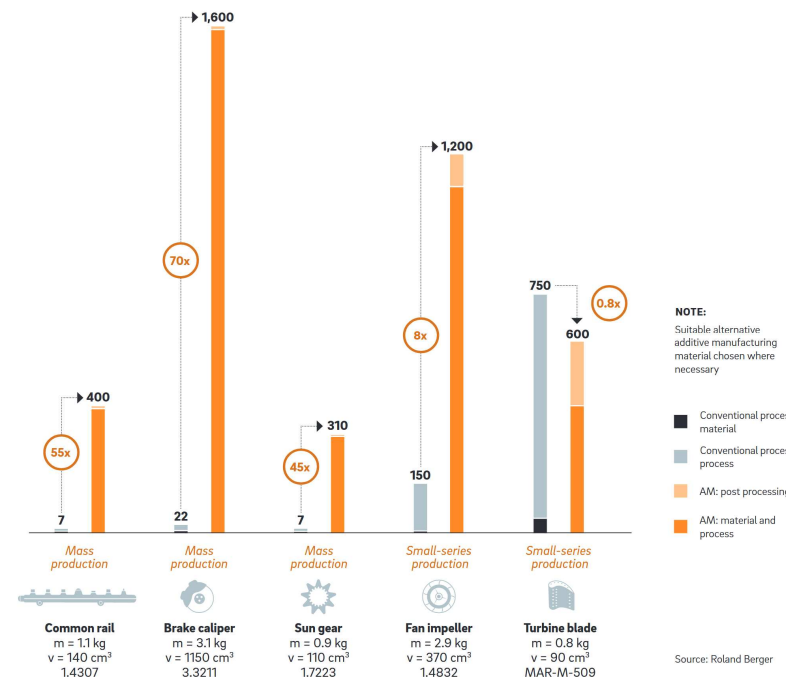


Fig. 3.13 Cost comparison between CM and AM components, in 2018 [21]

Gas welding (TIG), DED offers several advantages such as the lower heat input, the lower warpage and distortion and the superior metallurgical bonding. Whenever possible, reparation should also be the preferred choice since it is more sustainable, as a complete remanufacturing process from raw material can be even 50% more energy demanding. DED is extensively confirmed in literature to be not only cost-effective, but also time-saving; moreover, this process adds the possibility of add special features to a damaged part, so that it isn't merely repaired but also improved performance-wise [86].

To fully unlock the potential of Additive Manufacturing, DfAM - Design for Additive Manufacturing - principles should be implemented starting from the initial phases of the design process. DfAM is the complete set of tools, design guidelines and methods that leverage the design freedom that AM processes enable. These includes, for exaple, tools such as Topology Optimization (TO), to decrease to the minimum the material usage needed for the component to bear the designed loads, and the use of lattice structures to engineer internal porosity of components for lightweighting purposes or to dramatically increase

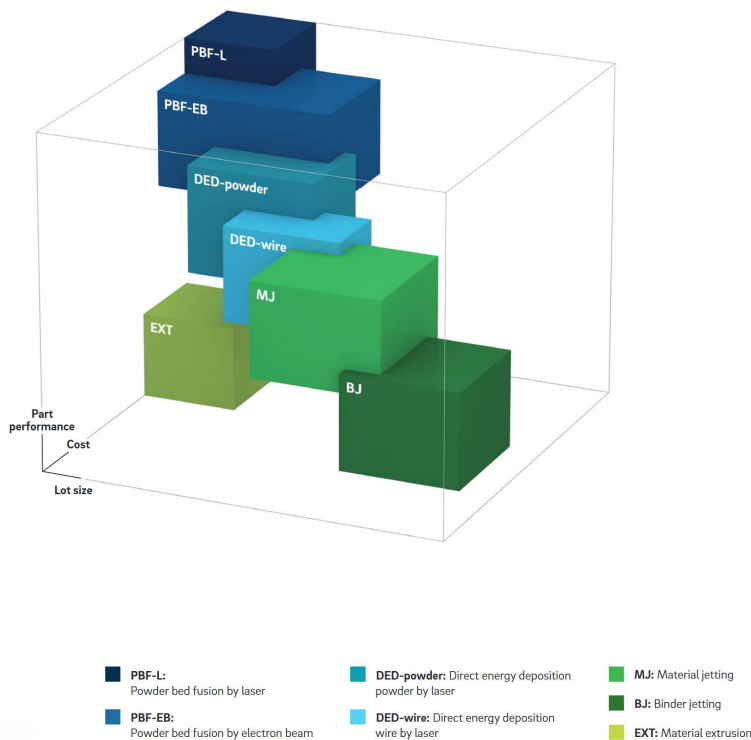


Fig. 3.14 Status of major AM technologies, in 2018 [21]

the internal surface area of systems such as heat exchangers.

Vaneker et al. created an excellent framework to acquire knowledge and insight of the available methods comprised in DfAM [87]. A general lack of this knowledge is indeed still found in industry, probably because AM has begun to be considered as a really competitive production technology, other than for prototypes and tools, only in the last decade. In general, the design of a component for AM must follow an iterative procedure such as that of Figure 3.15, requiring multiple design and evaluation loops to optimize a product or increase its manufacturability. Moreover, the broad number of different types of AM processes, each with their peculiar advantages and limitations, poses as a barrier for their adoption, standardization and knowledge transfer. AM machine settings need indeed to be meticulously calibrated material-wise and process-wise; these are generally categorized in four categories: energy related (e.g. laser power, beam speed, nozzle heating power), scan/movement related (e.g. scan strategy, beam focus size, extrusion head speed), feedstock material

3.2 State of the Art of Additive Manufacturing and Reverse Engineering for the Reconstruction of Spare-parts

related (e.g. particle size distribution, powder flowability, filament diameter) and temperature related (e.g. build plate temperature, chamber temperature, extruding nozzle temperature) [22].

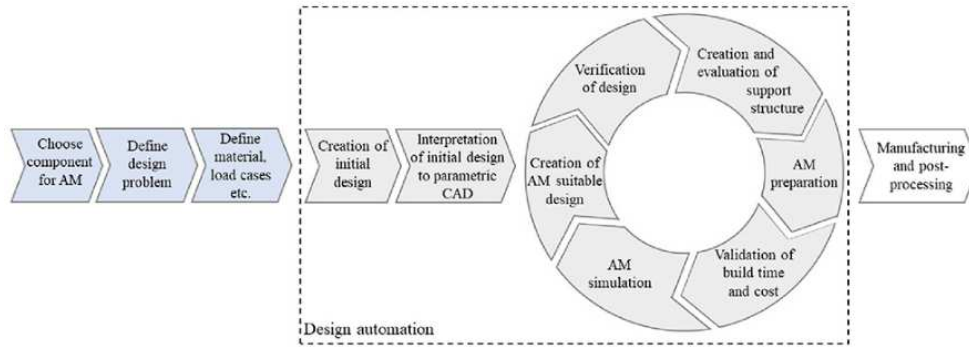


Fig. 3.15 Example of iterative DfAM design workflow [22]

To conclude, compared to conventional methods, AM suffers from the substantial lack of knowledge based engineering and DfAM repositories to share the knowledge and discoveries. This shortcoming often results in the reliance on "trial-and-error", increasing development time, cost and efficiency. A shared structured framework could enhance the quality of the design and thus accelerate the innovation.

3.2.2 Fundamentals of RE

Reverse Engineering (RE) is defined as the practice of acquiring knowledge or design information from an existing finished product to comprehend its design, architecture, geometry, components, and operating principles [23]. Compared to traditional manufacturing process, the development follows an inverted approach: starting from the existing product, a backward direction is followed to reconstruct a digital model, which is then re-designed or re-engineered and eventually manufactured, as illustrated in Figure 3.16.

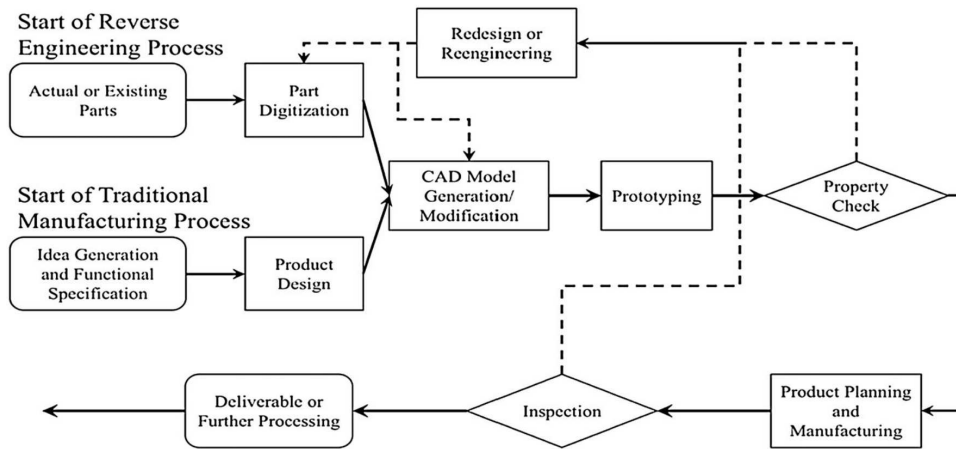


Fig. 3.16 Traditional and RE manufacturing workflows [23]

Usually, the purpose of RE can be categorized in one of the four following cases [23]:

- **Design of a new product:** to digitize a physical prototype into CAD data, such as in the example of car external design clay maquettes.
- **Modification of existing products:** to update an initial CAD design if manual modifications have been performed after prototyping.
- **Loss of product design data:** if the CAD data has been lost or corrupted and it is needed to manufacture the component.
- **Inspect the product:** to acquire actual geometrical data from the existing component and compare it with the benchmark CAD measures, to quantify the manufacturing geometrical deviation.

Traditionally, to perform the digitization, the component geometry was obtained by measuring at discrete points the surfaces with a Coordinate Measuring Machine (CMM), thus creating a "cloud of points" which is converted into parametric or surface features in CAD platforms. Nowadays however, many other alternatives are available, which are summarized in the diagram of Figure 3.17.

RE techniques can be macroscopically classified into contact and non-contact methods. Contact methods were historically the first developed and

3.2 State of the Art of Additive Manufacturing and Reverse Engineering for the Reconstruction of Spare-parts

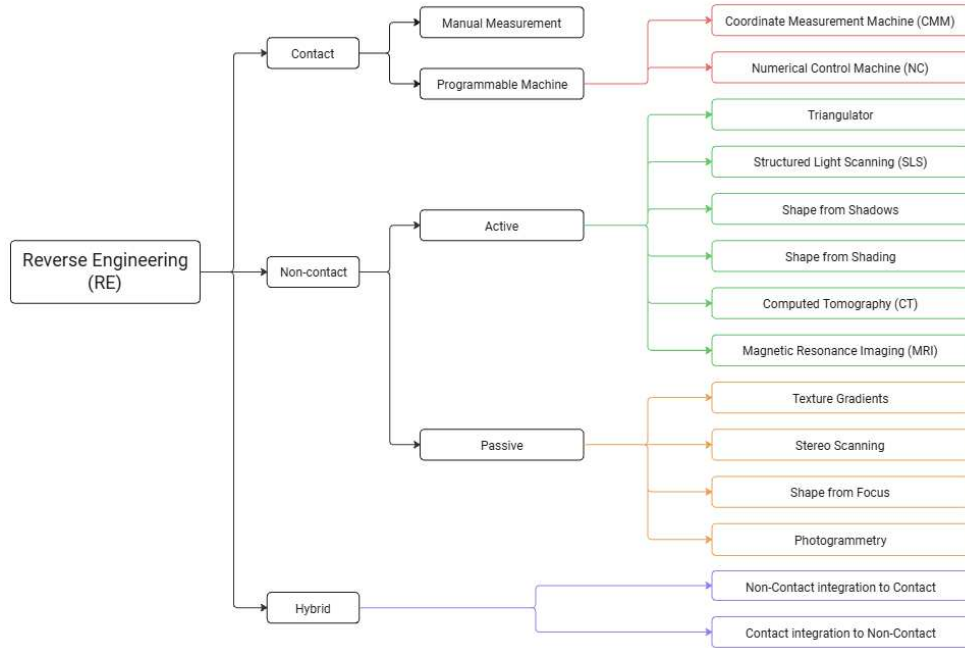


Fig. 3.17 RE classification [23]

they simply require mechanical contact between the probe of the measuring device and the surfaces to be acquired. Compared to non-contact methods, they usually tend to be more accurate and with higher surface quality; however, they require definitely higher time to complete the scanning process. The most antique forms of contact measurement are the manual ones, where experienced workers measure and identify the features of a component by means of instruments such as calipers, measuring gauges and angle finders. This methods are the simplest, but also the less accurate. Today are mostly used to confirm some geometric features scanned by other more advanced scanning processes. An interesting advancement in this field is the integration of appropriate measuring appartuses on Numerical Control (NC) machines, so that in a single machine are integrated both manufacturing and inspection tools.

As to what concerns non-contact methods, on the other hand, they commonly use mediums such as light, laser, sound and X-rays to deduce surface information without physical contact. These methods are further subdivided into active and passive systems, depending on whether a projected energy is used on the part or if the system passively captures naturally light emitted

or reflected from the object. The most notable examples of active systems are Structured Light Scanning (SLS), by which a known pattern of light is projected onto a surface and the geometric information is extrapolated by a specialized software which analyses the resulting distorted pattern, and Computed Tomography (CT), by which X-ray beams are sent from an emitter and received on the opposite side, attenuated by the different internal and external densities of the component, on a receiver. CT is the only non-destructive method which can acquire the internal structure of an object. Leading passive methods are Stereo Scanning (SC) and Photogrammetry, which both utilize cameras to acquire the 3D surface data from the object, generally requiring less expensive equipment [23].

In his Master's thesis, Colombo [88] conducted a thorough review of all the main available methods of reverse engineering, available as of 2019. In the study, many valuable recommendations are also given, such as the coating of shiny surfaces of an object with non-reflective powder, which would otherwise result unmeasurable by processes such as SLS. Moreover, the entire step-by-step process from the initial data source to the final reverse engineered part is explained for multiple cases, considering different starting points: whether is available the physical part, the 2D drawings, the 3D model and so on. The processes are also systematically compared in terms of cost of equipment, accuracy and time needed.

An insightful study is the one of Segreto et al. [89], in which two RE methods - CMM and a portable scanning system - are compared for the 3D model generation of cultural heritage objects, with the purpose of conservation, maintenance and reproduction. The topic is highly pertinent to the scope of this thesis, especially regarding the potential of the use of digitization to enable the public accessibility to a reproduction instead of the original historical object, to reduce the several risks related. Additionally, this can facilitate the restoration of the artifacts without the unwanted exhibition gaps, which can be therefore undertaken by displaying instead digital or physical reproductions.

3.2 State of the Art of Additive Manufacturing and Reverse Engineering for the Reconstruction of Spare-parts

In 2012, Wang et al. [24] proposed a framework to reconstruct the 3D model from the surface mesh of an existing body, which is subdivided in four phases: it starts from the pre-processing stage of the input mesh, followed by the segmentation into individual geometric patches. Solid or surface feature based strategies can then reconstruct the primitive shapes from the patches, which are then post-processed with modeling operations to assemble the final model. The process is visually explained in Figure 3.18.

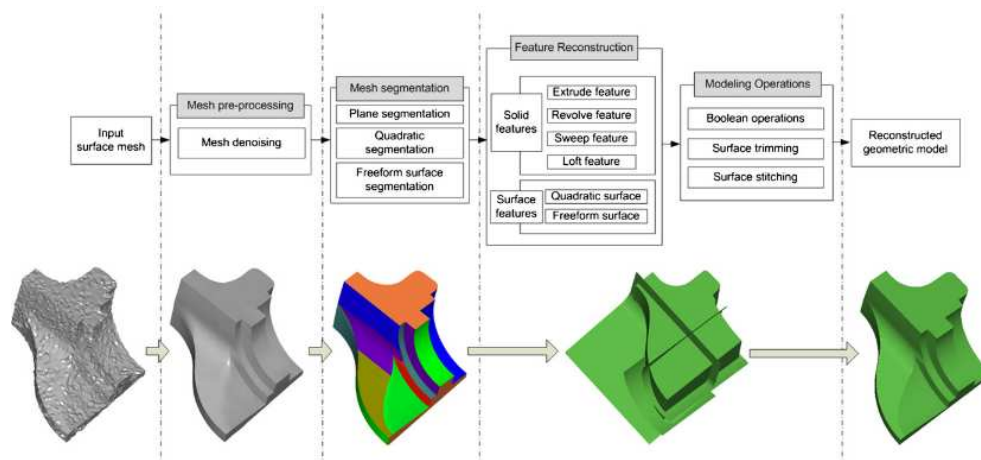


Fig. 3.18 3D model reconstruction process from an input mesh [24]

A review of additional frameworks is present in the study by Buonamici et al. [31]. Among the reconstruction methods mentioned, an interesting approach is the one based on 2D mesh cross-sections of the components. This is inspired by the traditional CAD modeling, since it mostly relies on 2D sketching which are then extruded or revolved to generate 3D shapes. This method can be very effective and straight-forward in case of axisymmetric components, where a reconstructed half cross-section can be revolved around its axis. Moreover, in this paper is included a table comparing the main RE features of multiple tools, which is here reproduced in Table 3.2.

To conclude, a frequently overlooked limit of all reverse engineering lies in the difficulty of estimating the tolerances required for the part reconstructed. This problem is even accentuated by the error superposition that each step introduces into the design. One of the earliest studies addressing this issue is the one of Kaisarlis et al. [90]. Since tolerance assignment is generally

Literature review

	DesignX ²	Polyworks	EGS ³	Inventor ¹	NX ⁴	ScanTo3D ⁵	Restyle ⁶	Fusion360 ¹
Primitive fitting	✓	✓	✓	✓	✓	✓	✓	
Parametric modeling	✓			✓	✓	✓	✓	✓
NURBS surface fit	✓	✓	✓	✓	✓	✓	✓	✓
Rev./Ext. surface fit	✓						✓	
Mesh-based sketches	✓	✓			✓	✓		✓
Geometric constraints	✓		✓	✓	✓			
Direct link to CAD	✓	✓						
Automatic filleting	✓							

¹ Autodesk ² Geomagic ³ Leios2 ⁴ Siemens ⁵ Solidworks ⁶ PTC Creo Parametric

Table 3.2 Features comparison between commercial RE tools [31]

a matter of expertise or experiment of the designers working on the part, the authors' idea is to develop a shared industry Knowledge-Based System (KBS) to automate this process. The KBS would estimate a set of tolerance candidates that could work on a scanned component, to ensure the best fit. A similar framework was later introduced by Geng and Bidanda [91]: a KBS developed based on ASME and ISO GD&T standards, taking advantage of the established practice in metrology and quality control of production systems.

Finally, Figure 3.19 illustrates the topic about tolerancing error stacking, which is unavoidably introduced in each phase of RE and reproduction. This aspect could lead to unexpected mating problem if the reproduced component should be mounted in an original assembly. The total accumulated error displayed is the sum of the contribution from each stage: the initial designed tolerance error σ , the manufacturing error σ_M , the scanning error σ_{RE} and the final reproduction error σ_{AM} . In order to ensure the compatibility of the reproduced component with the original system, it should be satisfied the following inequality: $\pm\sigma_M + \pm\sigma_{RE} + \pm\sigma_{AM} < \pm\sigma$. This underlines the rigorous tolerance management that is required in the RE and AM workflow to obtain an overall high reproduction precision.

3.2.3 Integration of AM and RE in remanufacturing

In recent years, Additive Manufacturing and Reverse Engineering are frequently employed in conjunction, comprising a powerful methodology which enables the remanufacturing of components through a comprehensive digital

3.2 State of the Art of Additive Manufacturing and Reverse Engineering for the Reconstruction of Spare-parts

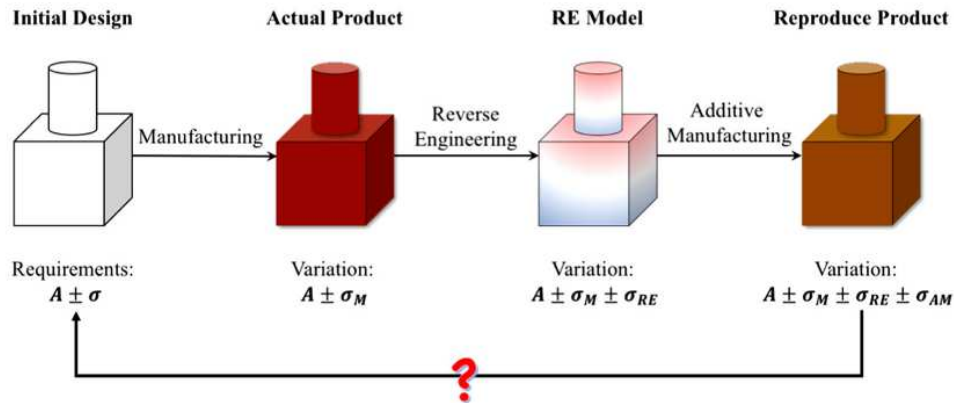


Fig. 3.19 RE tolerance issue of error superposition [23]

approach. This synergy is especially relevant in the context of heritage components for classic vehicles, which most of the time are no longer in production or lack the original drawings, technical documentation or tooling. It should be intuitive that in this case there is essential a faithful reproduction of the original spare-parts, as to not invalidate the historical integrity of a classic car, in addition to the basic mechanical concerns. Notably, one of the biggest challenge of AM - being very cost-effective for individual or small batches of production, but definitely unfeasible for mass volumes - in this context becomes a point of strength.

First of all, a key challenge faced by companies is that of determining which spare-parts are actually suitable for production via AM. To answer to this dilemma, Frandsen et al. [92] performed an extensive literature review aimed at gaining insights for the selection and eventually proposed a multiple criteria approach to identify, based on upfront determined objectives, the potential candidates. Among the most relevant technical characteristics for the suitability for AM are the dimensions, weight and material specifications of the components.

The most cited and complete review of the integration of AM and RE for classic-car restoration is the 2022 study by Dalpadulo et al. [26]. The authors provide a general overview of the digital restoration process and, based on the examples currently available in literature, derive a framework that can be classi-

Literature review

fied to two primary criteria: the material of the original part - polymeric, metal or even composite - and whether AM is used directly or indirectly. The latter mainly refers to RT or RC applications. In the publication, for each type of restoration, multiple examples are indicated. AM is found to be employed for practically every category of automotive components: from interior dashboard and consoles, to panels, fenders and bumpers of the bodywork, to structural parts such as the suspension or the wheels and even elements of the powertrain. As to what concerns the AM processes used, although all types have been applied, there is a clear predominance of polymeric MEX, probably due to the very low cost, ease-of-use and industry knowledge. The primary application of AM for metallic components is still as an intermediate step in the process, such as for casting and tooling, rather than for direct part fabrication. Furthermore, due to the conservative approach of classic car restoration, the standard is to use in AM materials as close as possible to the original ones.

Luniya and Chimata [25] in a 2021 conference paper examined this niche sector as a whole, both from the technological and economical perspective, providing additional examples of successful applications of AM and RE in restoration projects. Many challenges are although slowing down the adoption of these new technologies, mainly due to the lack of standardization, the high cost of the machines - which can be prohibitive for companies which aren't only focused on AM production - and the before-mentioned still limited available material library.

In Figures 3.20, 3.21 and 3.22 are presented three notorious example of the capability that the combination of these two recent technologies can achieve: the reconstruction of a damaged steering box for the restoration of a Ruston Hornsby Motor Car; the complete restoration of Elvis Presley's BMW 507 Roadster, in which many parts were manufactured by AM; the remanufacturing of the carburetor body of a Steyr 220 Roadster, both by following the original design (*center*) and with a reduction of 30% in time and cost by following DfAM design guidelines (*right*).

3.2 State of the Art of Additive Manufacturing and Reverse Engineering for the Reconstruction of Spare-parts



(a) Original damaged part



(b) 3D printed part

Fig. 3.20 Example of RE and AM integration for the reproduction of Ruston Hornsby Motor Car steering box component [25]



(a) Original

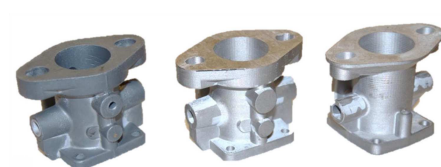


(b) Restored

Fig. 3.21 Example of RE and AM integration for the restoration of Elvis Presley's BMW 507 Roadster [25]



(a) Steyr 220 Roadster



(b) Reconstructed carburetor body

Fig. 3.22 Example of RE and AM integration for the reconstruction of a Steyr 220 Roadster carburetor body [26]

Given that the restoration of classic cars is often carried out by individuals or small-scale companies, the available financial budget is usually limited. For this reason, easy and low-cost scanning methods such as Photogrammetry are gaining increasing interest within this niche market. This technique involves an optical camera device which is used to acquire multiple snapshot of an object from different angles, which are then automatically matched and processed by a specialized software to extract geometrical data. The big advantage of this method, is that, at the most basic level, it can be performed just by an everyday smartphone and by affordable computing hardware and software. A practical application of optical scanning and AM to reproduce a plastic car volume button is presented by Paulic et al. [27]; the comparison between the original piece and the result is displayed in Figure 3.23.

In a 2020 research paper, Bacciaglia et al. [28] performed the reverse engineering of an engine sump through photogrammetry data acquired by a digital camera, cheap and easily available, visible in Figure 3.24. However, in their case, the result of the reconstruction had an error too large, which impaired the feasibility of the practical use of this technology. In contrast, significant better dimensional accuracy was achieved by Petruccioli et al. [93], who evaluated the average error of the output from Close-Range Photogrammetry (C-RP) of a Ferrari 250 Testa Rossa bonnet and a Ferrari 275 GTB front lamp housing. The average deviation from the original component was inside the $\pm 3\text{mm}$ range, which was considered acceptable, compared to the typical range of $\pm 1\text{mm}$ of handcrafted sheet metal working processes. Even if some localized maximum deviations were outside the acceptable range, those were visible enough to be easily manually corrected. Overall, photogrammetry can be an interesting solution to the reverse engineering problem of classic cars, that, although limited, can be in most cases accurate enough to be practical and broadly accessible.

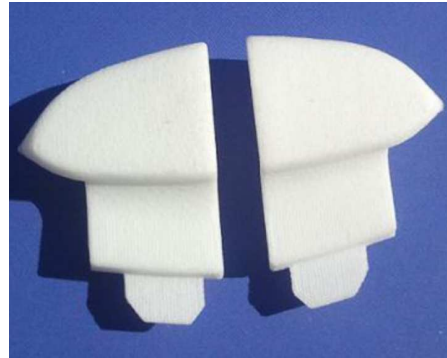
3.2.4 Advantages, drawbacks, limitations of AM

AM is increasingly being applied in the industry to increase one or more of the following three perceived value drivers: profit, risk mitigation and lead time

3.2 State of the Art of Additive Manufacturing and Reverse Engineering for the Reconstruction of Spare-parts



(a) Original plastic button

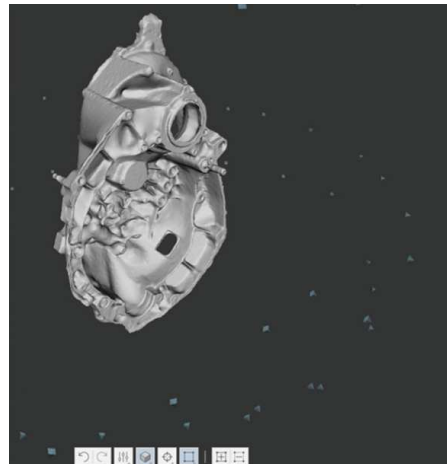


(b) 3D printed plastic button

Fig. 3.23 Example of RE and AM integration for the reproduction of a car volume button [27]



(a) Snapshot capturing with a digital camera



(b) Point cloud in Autodesk Recap Photo

Fig. 3.24 Photogrammetry of an engine sump [28]

reduction. From a monetary point of view, AM can be beneficial for small batches of production, where conventional manufacturing usually falls short due to the requirement of costly tooling and setup times. In addition, AM introduces advantages also in terms of reduced resource consumption, better inventory management, because of its digital nature, and lower transportation costs due to the possibility of on-demand, localized production [94].

The additive processes, thanks to the layer-by-layer part construction, allow to produce parts geometrically impossible or highly inefficient to be produced by traditional methods, thus enabling to extend to the maximum the performance capabilities of a component via design strategies such as lightweighting, topology optimization and lattice structures. Moreover, the integrated design possible with AM allows to reduce the number of components in a system by combining multiple functions into a single part, reducing assembling time, points of failure and system complexity [22].

Currently, the available materials in the industry are already existing ones that have been adapted or found suitable to AM; recently, a new trend is emerging: the development of materials engineered from scratch, specifically addressed for additive - examples are Al2139AM and Scalmalloy - in order to fully exploit the capabilities these new technologies offer [95].

An important aspect of today's economy is sustainability: if the power of AM is fully capitalized on, the higher energy consumption needed to produce a component in AM, definitely higher compared to CM, can be more than compensated by the life-cycle energy savings that an optimized additive product can obtain [96].

Lately, Artificial Intelligence (AI) systems have gained a lot of attention globally. AM and AI can be used together in what is commonly known as "collaborative design": hybrid algorithms such as Genetic Algorithms (GA) and Artificial Neural Networks (ANN) can be integrated in the AM workflow, combining big data and computational power to streamline generative design

3.2 State of the Art of Additive Manufacturing and Reverse Engineering for the Reconstruction of Spare-parts

processes and aid the designers into faster optimize a component [97].

Nonetheless, several other challenges still remain. A key one at this global industry adoption stage is the lack of standardization and regulatory compliance, which discourages greatly investments by companies and industrial confidence [85]. Additionally, although a powerful tool, TO is still not directly applicable: it must be combined with the common design guidelines since most of the time the output of the algorithms isn't refined enough. A prevailing approach is that of performing TO to use the output as a reference, than model and design the part using standard CAD features to imitate the shape [22].

Another challenge is that of reducing the number of post-processing operations required before obtaining a final usable component: additional steps such as milling, grinding and cutting are often needed to meet the final dimensional specifications or to reduce the internal porosity, such as with Hot Isostatic Pressing (HIP). These processes increase both the production time and cost.

Given the steep evolution of AM in recent years, there is also a growing need for accurate cost prediction models to aid companies in predicting the feasibility of an AM investment, which is still of high entity. However, the heterogeneity of processes and materials poses as a barrier to the development of a universal cost model. Kadir et al. [98] addressed this challenge through a systematic review of the available cost models, categorizing them according to their relevance for accounting, manufacturing operations and management within an organization. From a supply chain perspective, Naghshineh et al. [99] proposed a valuable set of diagnostic questions which a company can answer to strategically assess the feasibility and ponder the possible benefits achievable with the introduction of AM in its supply chain.

An often overlooked drawback of AM is the high uncertainty regarding failure rate of AM, compared to CM. This variability arises due to the long build times and the sensitivity to environmental and process variations, intrinsic of all AM processes. Peron et al. [100] quantified the standard deviation of AM failure rate to be around 48%, versus 21% of CM. The researchers found

that without taking it into account in the scenarios studied, AM was more convenient in 76% of the cases. However, when the variability is considered, the number drops to 45.1%, thus diminishing the potentiality of AM. To mitigate the problem, the authors suggested two tools to reduce the uncertainty: porosity assessment and in-situ monitoring. Sacrificial testing was also considered, but it was found to be consistently inconvenient. The demonstrated potential savings by adopting one of the two strategies in the manufacturing process was amounting to as high as €1000 per spare-part unit annually.

Despite the advancements, the high cost of the AM machines and of the materials remains a barrier in the adoption of AM for mass production. Although these are rapidly decreasing over the years, AM still is best suited for low-volume, high complexity applications [94]. Furthermore, CAE analysis of components designed for additive is often complicated by the inherent anisotropy of the manufactured components and the possible presence of complicated internal geometries. The anisotropy is usually due to the different resistance given by the adhesion of the layers along the building direction, compared to the other two directions. Most AM processes need also support structures to manage overhangs during printing, contributing to material waste and requiring additional post-processing operation to remove them. To conclude, the following are the eight major research trends in the field as identified by Frandsen et al. [92]:

1. AM technology selection
2. Supply chain considerations
3. Product design considerations
4. Production cost models
5. Environmental aspects
6. Strategic challenges
7. Manufacturing systems
8. Open-source innovation

Chapter 4

Method

4.1 Steam-water Injector Modeling

The objective of this section is to describe in depth the analytical model adopted to support the design and analysis of the injectors studied in this thesis. As previously discussed in Section 3.1, in literature are present multiple models, differing in terms of complexity, type of closure equation and assumptions. Based on the aim of this thesis, it was explained that the best fitting model is the one proposed by Ma et al. (2017), due to its balance between analytical rigor and practicality.

The following paragraphs are intended to present the structure and governing equations of the model, the underlying assumptions, and the iterative numerical strategy implemented to close the solution. The entire MATLAB code implemented is reported in Appendix B.

In Figure 4.1 is displayed the model used, comprising the numbering convention adopted for the critical sections. It should be noted that, compared to the one used in Figure 3.1, this model doesn't consider any throat tube; however, it should be repeated that the absence of this part doesn't actually modify the modeling of the injector, but rather it should only be considered as a practical addition that can improve the operation. The important sections are identified as:

Method

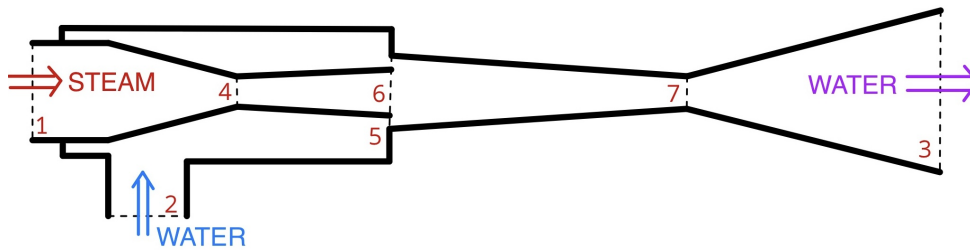


Fig. 4.1 Model of the injector

1. Inlet of steam nozzle
2. Inlet of water nozzle
3. Outlet of diffuser
4. Throat of steam nozzle
5. Outlet of water nozzle
6. Outlet of steam nozzle
7. Mixing chamber outlet

The assumptions considered in the model are the subsequent:

1. The injector is assumed to operate only in critical/supersonic flow regime, therefore, at the steam nozzle throat the flow is choked.
2. The pressure of steam and water at the interface - the inlet of the mixing chamber - is assumed to be equal.
3. The inlet steam is assumed to be at least in saturated state.
4. It is assumed that the mixture of steam and water is completely condensed at the exit of the mixing chamber.
5. The inlet speed of inlet steam and inlet water is negligible.
6. The heat transfer between the fluids and the injector walls is neglected.
7. The gravitational force is neglected.

4.1 Steam-water Injector Modeling

8. The isentropic efficiencies of the converging (η_1) and diverging (η_2) sections of the steam nozzle are given. (The values are taken from Ma et al. (2017) [13])
9. The pressure loss coefficient ξ_1 of the water nozzle is given. (The value is taken from Zhang et al. (2012) [74])
10. The momentum correction factor β for the mixing chamber is given. (The value is taken from Ma et al. (2017) [13])
11. The pressure recovery coefficient C_p is given. (The value is taken from Cattadori et al. (1995) [12])
12. The water and steam states in all sections are computationally determined using the MATLAB package *XSteam* [101], which adopts IAPWS-IF97 formulation [102].

The initial data needed is: pressure and temperature of inlet steam P_1, T_1 , pressure and temperature of inlet water P_2, T_2 and all the section areas $A_1, A_2, A_3, A_4, A_5, A_6, A_7$. Indeed, the cross-sectional areas of the injector are the sole degree of freedom available to the designer, to ensure that the injector performance meets the technical requirements.

To begin with, we should focus on what is occurring inside the steam supersonic nozzle. The governing equations are:

$$\eta_1 = \frac{h_1 - h_4}{h_1 - h_{4,is}} \quad (4.1)$$

$$h_{4,is} = f(P_4, s_1) \quad (4.2)$$

$$h_1 = h_4 + \frac{u_4^2}{2} \quad (4.3)$$

$$C_4 = f(P_4, h_4) \quad (4.4)$$

Method

The first iterative computation is the one needed to determine all the variables based on an assumed value of pressure at the steam nozzle throat P_4 . Thanks to this pressure and by computing the entropy of inlet steam, it is possible to determine the ideal isentropic enthalpy $h_{4,is}$ using Equation 4.2 - η_1 is assumed to be equal to 0.9. By rearranging Equation 4.1, h_4 should be computed. Now, an important detail should be highlighted: even though inlet steam is assumed to be superheated or at minimum saturated, it is likely that it becomes wet at the nozzle throat due to the expansion in the converging section of the nozzle. Therefore, Equation 4.4 should be implemented accordingly in correlation with the steam quality X_4 at the throat. In Appendix B is presented a possible solution at lines 97-101. Finally, using Equation 4.3, the steam speed u_4 should be computed. Since it was assumed that steam is choked at the throat, thus reaching the sonic velocity, it should be true that $u_4 = C_4$. If the relation doesn't hold, P_4 must be varied iteratively until the difference between u_4 and C_4 isn't below a predefined tolerance ($|u_4 - C_4| < tol$). Since now the pressure at the throat P_4 is established, it is possible to compute the density of the dry or wet vapor at this section:

$$\rho_4 = f(P_4, h_4) \quad (4.5)$$

It is then possible to compute the steam mass flow rate as a function of the steam nozzle throat area A_4 :

$$\dot{m}_1 = \rho_4 A_4 u_4 \quad (4.6)$$

At this stage, there is enough data to compute the remaining properties of steam flow at the throat: temperature T_4 , vapor quality X_4 and entropy s_4 .

Focusing on the divergent section of the steam nozzle, a second iterative algorithm is needed to determine a value for the outlet pressure P_6 , using the mass and energy Equations 4.7-4.11. As mentioned previously, η_2 is assumed to hold the same value as η_1 of 0.9. From Equation 4.10 it should be computed the ideal isentropic enthalpy $h_{6,is}$. This is then used in Equation 4.9 to obtain the value of h_6 . Now all the terms are known for Equation 4.8 and u_6 should then be determined. Eventually, ρ_6 is obtained from Equation 4.7 and this

4.1 Steam-water Injector Modeling

value, to conclude each iteration, should be compared to ρ'_6 , obtained from an assumed value of P_6 using Equation 4.11. The iterative computation should be terminated when the difference between ρ_6 and ρ'_6 is below a tolerance, which can either be the same as the former, either a different one ($|\rho_6 - \rho'_6| < tol$).

$$\dot{m}_1 = \rho_6 A_6 u_6 \quad (4.7)$$

$$h_6 + \frac{u_6^2}{2} = h_4 + \frac{u_4^2}{2} \quad (4.8)$$

$$\eta_2 = \frac{h_4 - h_6}{h_4 - h_{6,is}} \quad (4.9)$$

$$h_{6,is} = f(P_6, s_4) \quad (4.10)$$

$$\rho'_6 = f(P_6, h_6) \quad (4.11)$$

Also in this case, the leftover properties of steam at the steam nozzle outlet should be properly determined.

The steam flow then impacts to a water stream drawn in from the suction pipe 2 and interfacing at section 5. It is recalled that, as per Hypothesis 2, at the interface is assumed that water pressure P_5 is equal to steam pressure P_6 . In addition, the Hypothesis 6 stated that the heat transfer to the walls is neglected, thus it can be assumed that the water doesn't vary its temperature throughout the water nozzle, so that $T_5 = T_2$. Finally, the Hypothesis 5 stated that the initial water speed u_2 should be negligible, therefore is not present in Equation 4.13. Starting from Equation 4.12, the speed at the water nozzle exit u_5 should be computed, to be used then in Equation 4.13 to determine the water enthalpy h_5 . The water densities ρ_2 and ρ_5 and enthalpy h_2 are easily calculated as a function of pressure and temperature.

$$\frac{u_5^2}{2} = \xi_1 \left(\frac{P_2}{\rho_2} - \frac{P_5}{\rho_5} \right) \quad (4.12)$$

Method

$$h_5 + \frac{u_5^2}{2} = h_2 \quad (4.13)$$

It is now possible, using Equation 4.14, to determine the water mass flow ratio \dot{m}_2 :

$$\dot{m}_2 = \rho_5 A_5 u_5 \quad (4.14)$$

The mixing chamber, as discussed in Chapter 3, is the one part of the injector which holds the greatest complexity regarding modeling and there isn't yet a single approach universally agreed upon. The condensation shock wave is probably the hardest part to model realistically and there are usually multiple unknown variables. In most studies, this section is considered separately and conveniently modeled, but in some other studies this complex calculation is completely avoided by reducing the mixing chamber to a single control volume and assuming complete condensation at the exit of it, as done by Zhao et al. [68]. In this thesis model, the whole complex mixing process is simplified to just a set of mass, heat and momentum transfer equations, adopting a momentum correction factor β equal to 0.75. The third and last iterative computation is thus performed comparing the density ρ_7 obtained from Equation 4.15 from the density ρ_7' obtained from Equation 4.17 ($|\rho_7 - \rho_7'| < tol$). The two equations hold two unknown variables: the mixture speed at mixing chamber outlet u_7 , which can be computed using Equation 4.18, and the enthalpy at the same section h_7 which should be calculated using Equation 4.16.

$$\dot{m}_1 + \dot{m}_2 = \rho_7 A_7 u_7 \quad (4.15)$$

$$\dot{m}_1 h_1 + \dot{m}_2 h_2 = (\dot{m}_1 + \dot{m}_2) \left(h_7 + \frac{u_7^2}{2} \right) \quad (4.16)$$

$$\rho_7' = f(P_7, h_7) \quad (4.17)$$

4.1 Steam-water Injector Modeling

$$\beta(P_5A_5 + P_6A_6 + \dot{m}_1u_6 + \dot{m}_2u_5) = P_7A_7 + (\dot{m}_1 + \dot{m}_2)u_7 \quad (4.18)$$

To conclude, in the diffuser section of the injector the condensed water speed is converted into a static pressure increase. A simple assumption is that the density of water doesn't change between the inlet and outlet of the diffuser, thus $\rho_3 = \rho_7$. As a result, the exiting water velocity u_3 is only a function of the diffuser outlet area A_3 , as in Equation 4.19. The pressure recovery coefficient C_p , as explained in Hypothesis 11, is equal to 0.65. The head loss h_{loss} occurring in the diffuser is calculated using Equation 4.20, which is the standard hydraulic formulation for the pressure drop in a diffuser. Finally, the discharging pressure P_3 can be computed by Equation 4.21 and the outlet enthalpy h_3 by Equation 4.22.

$$\dot{m}_1 + \dot{m}_2 = \rho_3 A_3 u_3 \quad (4.19)$$

$$h_{loss} = \frac{u_7^2}{2}(1 - C_p) \quad (4.20)$$

$$\frac{u_7^2}{2} + \frac{P_7}{\rho_7} = \frac{P_3}{\rho_3} + \frac{u_3^2}{2} + h_{loss} \quad (4.21)$$

$$\dot{m}_1 h_1 + \dot{m}_2 h_2 = (\dot{m}_1 + \dot{m}_2)(h_3 + \frac{u_3^2}{2}) \quad (4.22)$$

The overall flowchart of the model solution is showed in Figure 4.2. As before-mentioned, three iterative algorithms are required in the model. These are used to find the solution of the model, starting from three assumption of pressure P_6 and densities ρ_6 and ρ_7 , in the least amount of time and iterations, to reduce the computational time. In order to do so, two numerical methods were adopted: the bisection algorithm and the regula falsi algorithm. The bisection method is probably one of the simplest and most famous, but it has the limitation of working only when the root of the problem is unique and the function is monotonic inside the range of interest. The first two functions

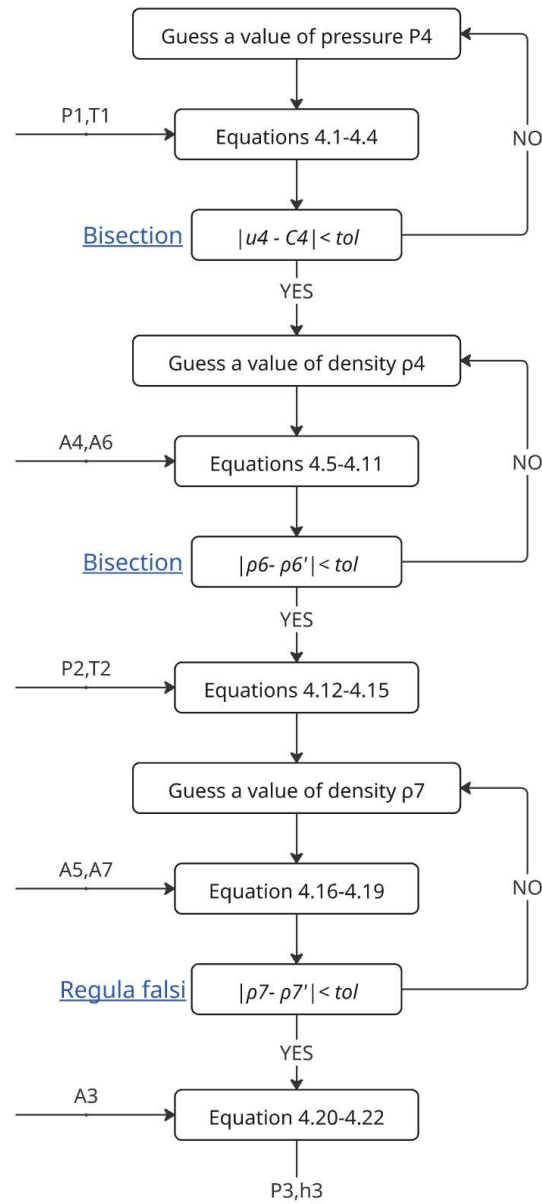


Fig. 4.2 Iterative model computation flowchart

4.2 Steam Carriage Technical Requirements and Specifications

happened to satisfy these criteria, making the bisection method applicable. On the contrary, the third function, the one related to the throat section of the mixing chamber, presented in many conditions two or more roots and the interval boundaries were often found to hold the same sign. The best alternative numeric technique in this case turned out to be the regula falsi. In addition, to prevent this method from converging to inadmissible solutions, the range of interest was limited by finding a minimum and maximum allowable pressure: outside this range either the quality was non zero, so that Hypothesis 4 wasn't satisfied, either the water density became negative, which isn't physically possible. Both algorithms are implemented in the MATLAB code in Appendix B. To conclude, for this thesis purpose, the tolerance tol of the correlation error between each variable was selected quite strict and equal to 0.001. This was the lowest value that permitted the model to run without errors and accuracy concerns. An iteration cap was also imposed, equal to just 1000, as it was clear that in just few hundreds iteration the model could already reach divergency. Whenever one of the algorithm is without solution, the working condition was deemed as unfeasible or out of the model capabilities. Compared to the standard while loop cycles, these algorithms reduce the computational time to solve the model from 1-2 minutes to less than a second.

4.2 Steam Carriage Technical Requirements and Specifications

As discussed in the previous section, the model requires an initial data set to work: the inlet pressure and temperature conditions of both water and steam. The main model parameter was considered to be the inlet steam pressure P_1 , and the inlet temperature of steam T_1 was consequently assumed to be the one at steam saturation. As to what concerns the inlet conditions of water, the inlet temperature T_2 was assumed to be always at $18^\circ C$, while the inlet pressure P_2 was calculated using the following equations:

$$h_{loss,distributed} = f \frac{L_2}{D_2} \frac{u_2^2}{2g} \quad (4.23)$$

Method

$$h_{loss,local} = 2K \frac{u_2^2}{2g} \quad (4.24)$$

$$P_2 = P_{atm} - \rho_2 g (H + h_{loss,distributed} + h_{loss,local}) \quad (4.25)$$

where f is the internal pipe rugosity (assumed equal to 0.02), L_2 and D_2 are the length and diameter of the connecting water pipe, u_2 the water speed inside the connecting pipe, H the water vertical lift and K the pressure drop coefficient for the pipe connections (assumed equal to 0.5).

In addition, the only technical requirement considered was the minimum feed water capacity necessary to ensure the proper operation of the steam carriage under maximum load conditions. This condition corresponds to the scenario in which the boiler is working at its maximum working pressure - which is 5 bar - and the steam consumption of the steam engine is at peak rate. The injector must therefore at least pump the same amount of water which is consumed as steam, to maintain a constant water level in the boiler. If excessive water is injected, the total water thermal mass is increased and hence the steam production decreased, thus reducing the efficiency of the system: more fuel would be required to increase the heat rate and, on the other hand, less power would produced by the engine due to the lower production of steam; conversely, if insufficient water is supplied, the risk is that the excess heat distorts the metal sheets constituting the boiler walls, ultimately possibly resulting in the structural failure and explosion of it. The maximum steam consumption was estimated using to the following equations:

$$V_{stroke} = \frac{\pi}{4} D_p^2 S_p \quad (4.26)$$

$$V_{max} = k V_{stroke} n_{max} N_{cyl} \quad (4.27)$$

$$Q_{s,max} = SCV_{max} \frac{60}{v_{s,max}} \quad (4.28)$$

where D_p is the diameter of the piston (equal to 250 mm), S_p is the stroke of the piston (equal to 450 mm), k is a coefficient taking into account that the engine employs double effect pistons (equal to 2), n_{max} is the assumed maximum engine speed (equal to 100 rpm), N_{cyl} is the number of cylinders (equal to 2), SC is a safety coefficient (equal to 1.5) and, finally, $v_{s,max}$ is the specific volume of saturated steam at the maximum boiler pressure. The idea is therefore to compute using Equation 4.26 the steam volume displaced per stroke by each piston, then use Equation 4.27 the total volume of steam consumed per minute, thus finally calculate with Equation 4.28 the steam consumption in L/h , increased by a safety coefficient. The final designed injector must have, given an inlet steam from the boiler at maximum working pressure, a resultant outlet water mass flow Q which satisfies $Q \geq Q_{s,max}$.

4.3 Reverse engineering Process

The reverse engineering process of the Bordino injector was conducted following three main steps:

- **Computed Tomography:** since it wasn't possible to disassemble the Bordino injector for direct inspection of its internal components, a high resolution CT scan was performed.
- **Structured Light Scanning:** to accurately acquire the external geometry of the injector, a SLS scan was carried out.
- **CAD software reconstruction:** based on the volumetric data obtained from the CT scan and the superficial geometry data acquired through SLS, the final injector was redesigned within a CAD environment.

4.3.1 Computed Tomography

All the tomographies carried out for the thesis' scope were performed on the *Phoenix v|tome|x s* CT X-ray scanner, visible in Figure 4.3a. This machine

Method

is a high-resolution system for two-dimensional X-ray inspection and for 3D tomography and metrology. This particular model is equipped with a nanofocus X-ray tube capable of reaching a maximum of 240kV and 320W [103]. The dedicated software used for the post-processing and manipulation of the resulted CT scanned data was *Hexagon VGSTUDIO MAX 5.4.0*. This program enables to perform various advanced operations such as surface determination of the voxel models, semi-automated segmentation and a full suite of alignment and measurement tools [104]. In Figure 4.3b is presented a snapshot of the three planes views (*up right, up left, down left*) and 3D reconstructed model (*down right*) used to navigate into the result of the complete tomography of one of the two injectors.

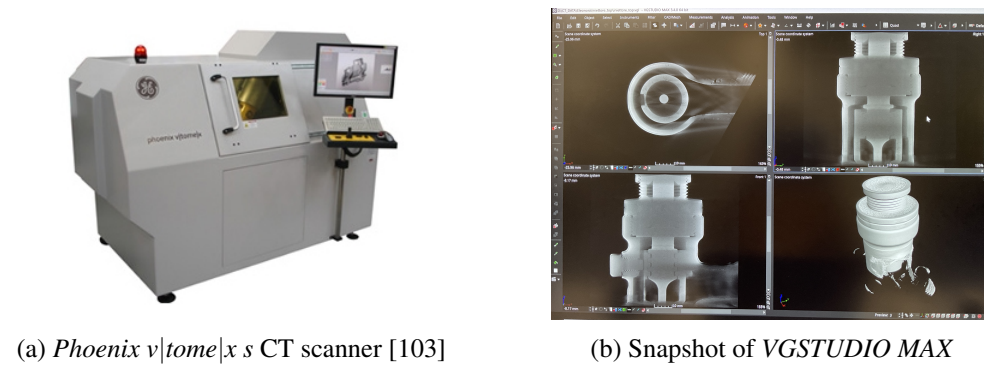


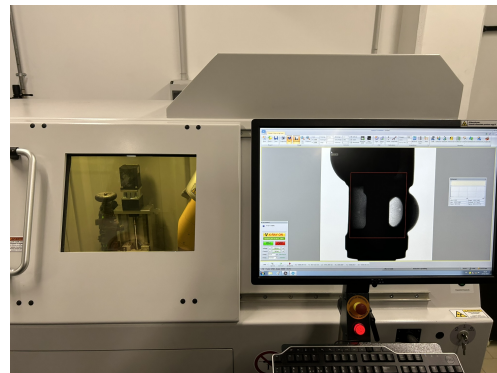
Fig. 4.3 Machine and software used for the CT scan

Unfortunately, the metallic material of the Bordino injector's casing attenuated excessively the X rays, which rendered the CT scanning of the internal geometry not good enough. One potential solution could have involved the use of an higher voltage and power CT scanner. Nevertheless, an alternative and innovative approach was adopted in this thesis. Although in the context of heritage conservation and restoration is usually preferable to preserve the complete originality of the artifact, to not jeopardize its historical authenticity, it was in this case considered acceptable to maintain in the reproduction only the external geometry of the Bordino injector. The internal structure and components were instead derived from a conceptually similar but more technically advanced injector: the Holden & Brooke (H&B) Sirius "One-Movement" 1890 injector. At this stage of the restoration of the Bordino steam carriage, we don't have unfortunately still enough information to pinpoint an exact manufacturing

year of the mounted injector. Since the steam carriage was built - or at least the construction began - in 1854, and, as specified in Chapter 2, the steam-water injector was invented in 1858, we can safely suppose that the device is a later addition. Moreover, an historical source affirms also that, starting from the year 1865, the carriage wasn't put anymore into operation [38, p. 70]. The H&B injector thus probably postdates the Bordino model by at least two decades, representing an evolution of the steam-water injector principles, but retaining most of the key components of the earlier designs.



(a) H&B 1890 in the CT scanner



(b) Preparation operations before the CT scan

Fig. 4.4 Pictures taken during the preparation of the CT scan of the H&B Sirius 1890 injector

This compromise enabled an appropriate reconstruction by taking advantage of an historically relevant substitute. In Figure 4.4 is presented, on the left, a picture of the H&B injector while being held by the chuck present in the CT scanner and, on the right, an image of the preparing operations before starting the automatic scan, such as the configuration of the voltage and current level of the X-ray emitter and the positioning into frame of the object.

4.3.2 Structured Light Scanning

In order to accurately obtain the external geometry of the Bordino injector, a Structured Light Scanning (SLS) technique was adopted. The scanner system employed was a *GOM ATOS Core 300*, depicted in Figure 4.5a, an optical 3D measuring system specifically designed for high-resolution digitization of

Method

small and medium volumes objects and comprised by a dual stereo camera setup and a blue light structured pattern projector [105].

An example of the light and dark alternating bands patterns beamed on the injector during a scanning run is shown in Figure 4.5b. As previously discussed in Section 3.2.2, shining reflective surfaces can compromise the quality of the scans. The black paint which covers the entirety of the injector was in many parts too glossy: it was thus needed to apply a non-reflective powder coating to these surfaces prior to scanning.

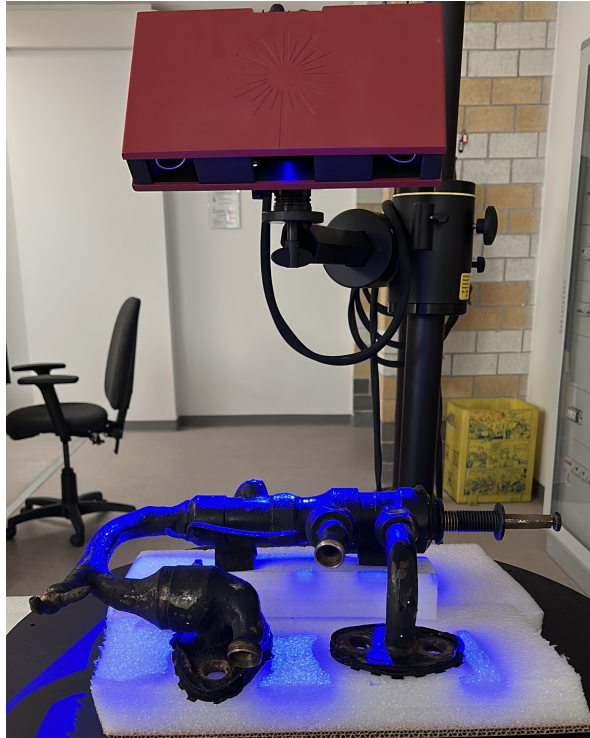
Finally, Figure 4.5c provides a detailed view of the reference markers applied on the surface of the injector. These markers are essential for spatial triangulation and are used by the scanner to calibrate the relative positions of the images captured and to match and combine adjacent scans. Indeed, to be able to proceed, at any time the scanner requires the recognition of at least 3 pre-calibrated markers. The scan acquisition and post-processing were directed using *GOM Scan 2020*, a proprietary software developed by the same manufacturer of the scanner.

This technique proved to be an exceptionally fast and accurate method for acquiring surface geometry of objects and, notably, it did not require specialized expertise to operate the scanner adequately.

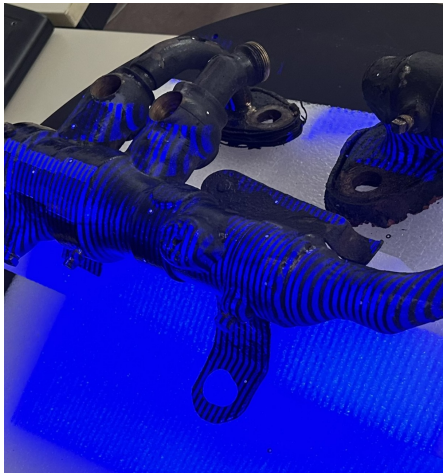
4.3.3 Softwares for Reconstruction

The final step of the reverse engineering process consisted in the post-processing of the data obtained during the two previous operations. The softwares used were *GOM Inspect 2019* for the point cloud management and mesh repairing and *Autodesk Fusion 360* for the reconstruction of the CAD model.

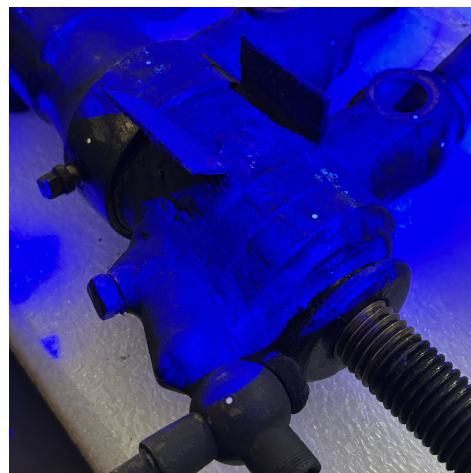
The first software, *GOM Inspect 2019*, is a 3D inspection and mesh processing suite developed by the same manufacturer of the SLS scanner, which are usually intended to be used in combination. The primary objective of the



(a) GOM ATOS Core 300



(b) Scan pattern on the injector



(c) Detail of the markers

Fig. 4.5 Structured Light Scanning operation pictures

Method

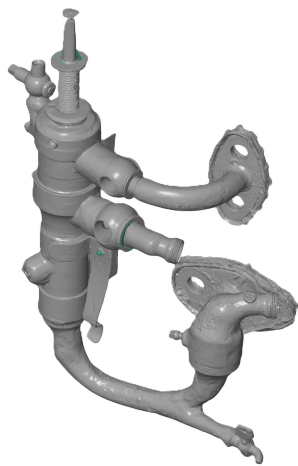
software is to inspect the dimensional accuracy and the quality of the scanned data. In this thesis' case, however, it was used to orientate the injector using the 3-2-1 alignment tool and to repair and prepare the raw mesh generated by the scanner. Given the complex shape of the Bordino injector, the raw mesh exhibited multiple open holes that the scanner wasn't able to acquire, therefore needing substantial post-processing. Ideally, it would have been preferable to conduct all the operations in one single environment, such as exploiting the available features for mesh editing in *Fusion 360*; however, the algorithms provided by *Inspect 2019* were far superior and more reliable than the non-specialized one in *Fusion 360*. The final processed and watertight mesh model of the Bordino injector is presented in Figure 4.6a.

The repaired scan was subsequently imported in *Autodesk Fusion 360* and used as reference for the 3D modeling phase (Figure 4.6b). Precisely, a remeshing operation was required in the CAD environment, as the high-resolution mesh exported from *Inspect 2019* exceeded the detail necessary for the modeling task, resulting in a heavier file to handle computationally. Several of the tools mentioned in Section 3.2.2, available in *Fusion 360* and illustrated in Figure 3.18, were tested, but, given the geometric complexity of the injector, it wasn't possible to use any of the automated fitting functions. Moreover, it should be recalled that the original Bordino injector was for a great part handcrafted, without adherence to the modern standards of manufacturing: features such as surface irregularities, welding beads and local distortions are the consequence of manual operations, rather than intentional design. These have the effect of invalidating the automatic surface recognition and feature reconstruction. In addition, examples as the misalignment between the main axis of the injector and that of the two straight valve bodies are not again a design choice, but a consequence of the limited manufacturing precision at that time. All these aspect were considered unnecessary and intentionally excluded from the final model design. The modeling approach adopted was therefore that of recreating the geometry of the injector from scratch, using the scanned mesh as a visual and dimensional guide, eventually resulting in a simplified injector better suitable for the final remanufacturing. Referring to Figure 4.6c, a key tool extensively used for modeling was that of using extracted 2D mesh sketches (*orange lines*) as reference contours for sketches to be revolved (*blue shape*), to

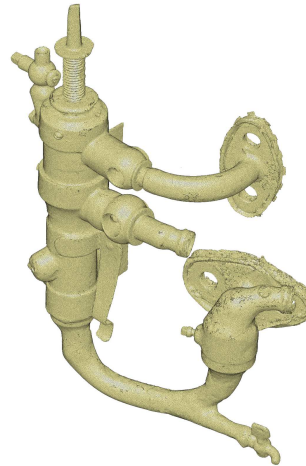
4.3 Reverse engineering Process

finally obtain the three part bodies of the injector (*gray semi-transparent mesh*).

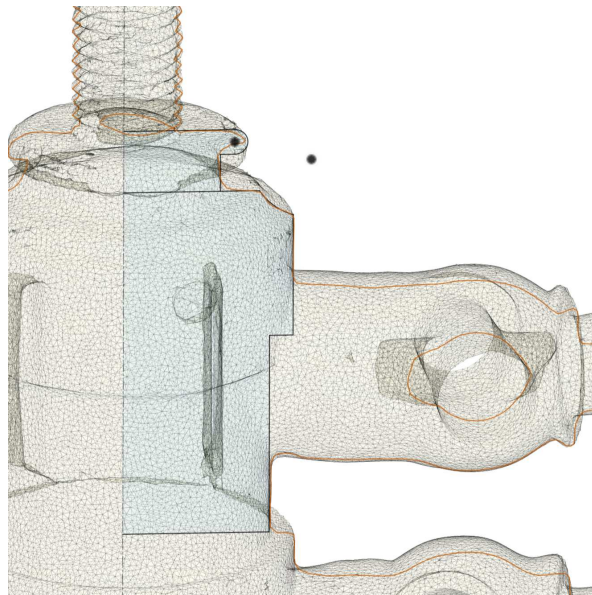
After the 3D modeling of these three bodies starting from the 3D SLS scan, the internal components comprising the CT scanned injector were redesigned to be accommodated as the internal structure of the final assembly. The redesign operation was guided by the analytical fluid-dynamic model described in Section 4.1, ensuring that the redesigned geometries satisfy the technical requirements and specification of the Bordino steam carriage. These were, in particular, the minimum feed water capacity required during the boiler operation at maximum load conditions, as well as the determination of the inlet pressure that water exhibits at the entrance of the injector, coming from the non-pressurized water tanks, as detailed in Section 4.2.



(a) Bordino in GOM Inspect 2019



(b) Bordino in Fusion 360



(c) Bordino in Fusion 360 with mesh section and sketch

Fig. 4.6 Picture of software reconstruction

Chapter 5

Results

5.1 Available Injectors Analysis

In this section is presented the analysis of the two injectors examined in this thesis: the Bordino injector, originally mounted on the Bordino steam carriage, and the Holden & Brooke Sirius-"One-Movement"-1890 injector.

5.1.1 H&B Sirius-"One-Movement"-1890 Injector

In the previous chapter, it was explained that the solution to the impossibility of inspecting the internal geometry of the Bordino injector was addressed by exploiting an available conceptually similar injector as a reference. This alternative injector was actually sourced from an antiques market, therefore with no information available beyond the fact that it was a steam-water injector. Given the compact size, it was reasonably assumed that it served originally to feed water into small tanks or boilers.

An in-depth investigation throughout various sources - including online platforms and historical books on injectors - made possible to identify the model. The injector, presented in Figure 5.1, closely resemble the model produced and designed by the British company Holden & Brooke. Originally introduced in 1890, it was referred to by multiple names: the "1890 Injector",

Results

the "Sirius Injector" and the "One-Movement Injector". The technical drawings and period advertisements found, which facilitated the determination of the model of the injector, are available in Section A.1 and Section A.2. As a matter of fact, the injector of Figure 5.1 is slightly different from the ones depicted in the drawings and the ads. Two evident features missing are the ribs on the lower body external geometry and the pointing handle. Comparing the 3D model reconstruction of Figure 5.2 and the technical drawings of Section A.1, also differences in the arrangement of the internal components can be identified. However, all versions of the model appear to share the same number of components and fundamental features. It is thus plausible that the unit available for the analysis is either a copy of another company or a simplified variant - possibly a "minor brother" - of the Sirius injector lineup, which was generally marketed for use on large-scale boilers, such as those found on railway locomotives.



Fig. 5.1 Pictures of H&B Sirius "One-Movement" steam injector

5.1 Available Injectors Analysis

Reference to the standout design feature of the injectors is found in a 1908 publication by W.A. Stanier [55]. Although the injector is not explicitly named, the description that the author provides suggests that he is referring to the model in question:

"The fixed tube type of injector if designed with the inlet area sufficiently large to take enough water at the higher pressures will work without regulation for increasing pressure up to a certain point, but it will only deliver the maximum amount of water per lb. of steam at one particular pressure. An injector therefore to work with hot feed water must be designed so that the feed is supplied to the injector under pressure if possible, and the area of the water space must be of sufficient size to take enough water at the higher pressures to condense the weight of steam passing through the steam cone, and as this varies as the steam pressure varies the injector should be adjustable. Messrs Holden and Brooke have designed an injector which ingeniously meets most of the requirements. Means are provided by which the inlet area to the combining tube and the area of the steam nozzle are simultaneously varied. The minimum area of the delivery nozzle is constant, so that a rise in the steam pressure should be met by a diminution of the steam cone orifice. As the steam pressure increases a greater weight of steam is passed, with the result that the vacuum in the combining tube falls and less water enters the annular space per lb. of steam discharged, so that this injector can be adjusted by turning the handle which for high pressures reduces the area of the steam cone and increases the area of the water passage and reverses the action for lower pressures." [55, p. 11]

Referring to Figure 5.2, which displays the complete 3D model reconstruction of the injector, it becomes clear that the rotation of the regulating wheel, fitted onto the square section of the spindle, does not result into an axial movement of the spindle: through the square-threaded mechanism, the rotation of the spindle induces instead an axial displacement of the steam nozzle. Indeed, the nozzle is constrained from rotating by a positioning screw,

Results

thus allowing only the translational movement. This combined action enables a simultaneous and inversely correlated variation of both the annular steam discharge area and the water flow annular area with a single adjustment - this is the reason for the "One-Movement" name. Therefore, this sole adjustment was specifically designed to ensure, for a given specific working steam pressure, the optimal ratio between the entrained steam and feed-water. The injector could then be operated simply by rotating the indicator, such as the one visible in Figure A.5, to the corresponding steam pressure value engraved on a circular dial. This eliminated completely the need of operator expertise or manual calibration. It is for this reason that the injector it was widely known as the one that "cannot be wrongly worked or misunderstood". Unfortunately, the dial and the indicator are not present in the injector of Figure 5.1. However, it was decided that this feature should be added in the redesigned final injector, allowing future easiness of use for any operator of the replica of the steam carriage.

The necessity of achieving the correct correlation between the rotation angle of the regulating handle and the simultaneous variation of the annular flow areas for both water and steam is the reason behind an uncommon design feature: the use of a double-start square thread between the spindle and the steam nozzle. As notable in Figures A.15 and A.18, the thread employs a double start configuration, thus allowing a lead of 10 *mm* per full rotation, while retaining the commonly used 5 *mm* pitch for square threads. It can be therefore reasonably assumed that the designers calculated the internal displacement requirements of the steam nozzle to fall within the 10 *mm* range. This allowed the injector to vary the operation of the injector across its entire functional range within just a single full turn of the handle, simplifying its usability and the design of the dial.

Another important feature of the spindle, clearly visible in Figure A.17, is in the tapered end section, which is both perforated and hollow. This was commonly done to ensure a minimum steam passage area even when the tapered needle is in full contact with its seat, thus facilitating the expulsion of air during the start-up. However, in the case of this particular injector design, this is also necessary to ensure a minimum steam passage area regardless of

5.1 Available Injectors Analysis

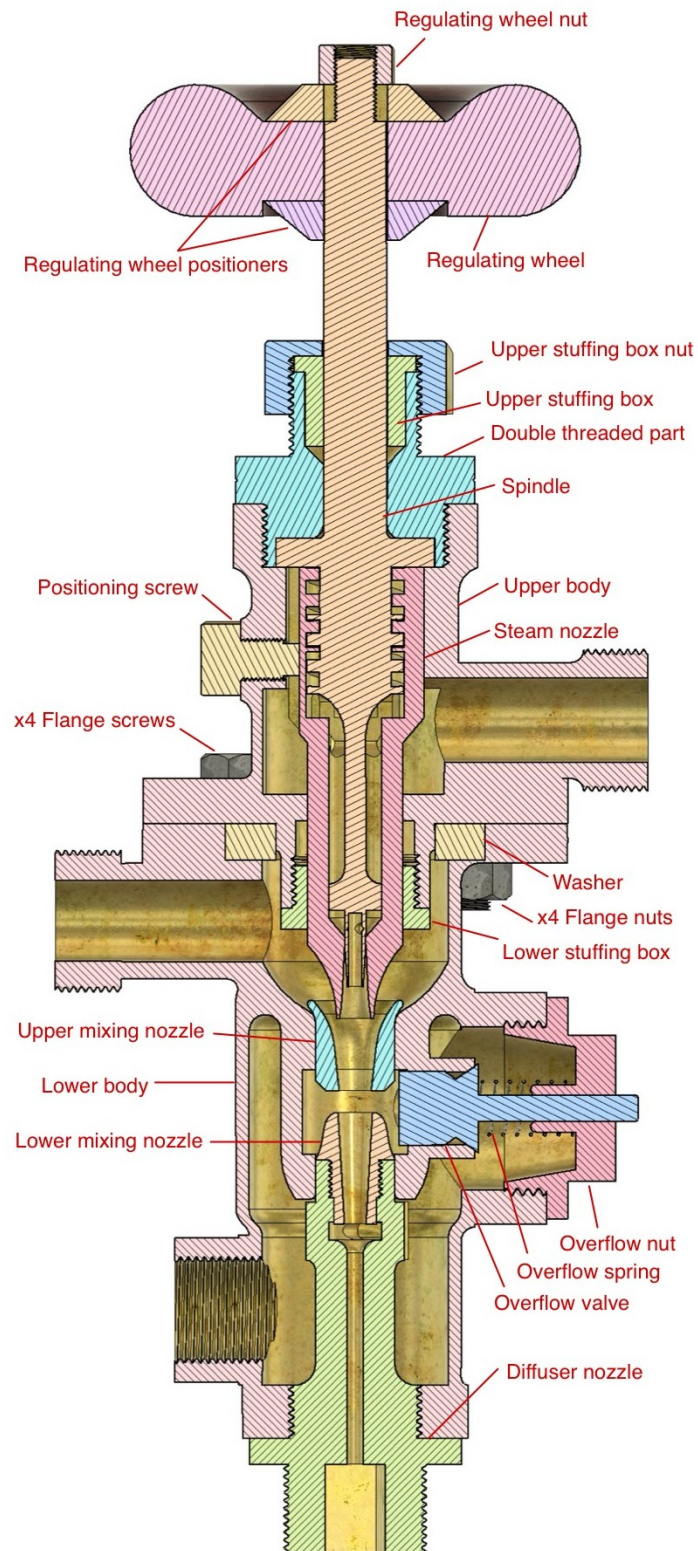


Fig. 5.2 H&B Sirius 3D model section view with components labels

Results

the nozzle position. This fixed flow area for the steam discharge is necessary for the operation and the adjustment, in the order of a few millimeters, of the annular section is enough to tune the performance of the injector throughout the whole range of pressure levels. The earlier injector designs were based on a far greater variation of the annular steam flow area, directly correlated to the axial movement of the spindle's needle.

Although reference to the water feed capacity of this injector model is provided in a 1958 brochure (Figure A.9), it is more likely related to a bigger or more advanced version of the sample available. It was therefore deemed necessary to evaluate the actual performance of the injector, employing the analytical model presented in Section 4.1. As a matter of fact, the resultant performance is comparable to the one model listed in the first row of the brochure's capacity table. However, there is a discrepancy in the nominal pipe size: while the table reports a $\frac{1}{2}$ inch pipe, the actual injector was equipped with a 1 inch one.

Figures 5.3 and 5.4 illustrate the resultant diagrams of two sensitivity test conducted on the analytical model, using the geometric data measured on the available Sirius injector and presented in Table 5.1: the first Figure presents the sensitivity test of the variation of α - defined as the percentage opening of the tapered section of the steam nozzle, corresponding to the angle of rotation of the spindle - under a constant pressure of 5 bar, which is the maximum working pressure of the carriage's boiler; the second Figure examines the pressure sensitivity of the injector in the range between 1 and 10 bar, while maintaining a fixed opening equal to $\alpha=50\%$.

Table 5.1 Dimensions in mm of the available Sirius injector sections, as per model of Figure 4.1

D1	D2	D3	D4	D5	D6	D7
14	14	11	$2.5 + 1.5(1 - \alpha)$	$\alpha \cdot 5$	6	3

To evaluate the performance of the injector, a dimensionless performance index was opportunely defined:

5.1 Available Injectors Analysis

$$PI = \frac{1}{w_{\Delta P}|\Delta P - \Delta P_{ref}| + w_{\omega}|\omega - \omega_{ref}|} \quad (5.1)$$

where $w_{\Delta P}$ and w_{ω} are the weight coefficients related to the pressure differential ΔP between outlet water and inlet steam and to the entrainment ratio ω . ΔP_{ref} and ω_{ref} are instead the reference values for the pressure differential and the entrainment ratio. As discussed in Section 3.1, the performance of the injector is inherently a matter of compromise between the entrainment ratio and the compression ratio, thus also the final outlet pressure P_3 . This inverse proportionality can be easily observable by comparing the pressure and water flow trends in both figures. In the present work, the best compromise is chosen to be at $\Delta P_{ref} = 1.5$ bar and $\omega_{ref} = 10$, while the two weights are both equal to 0.5.

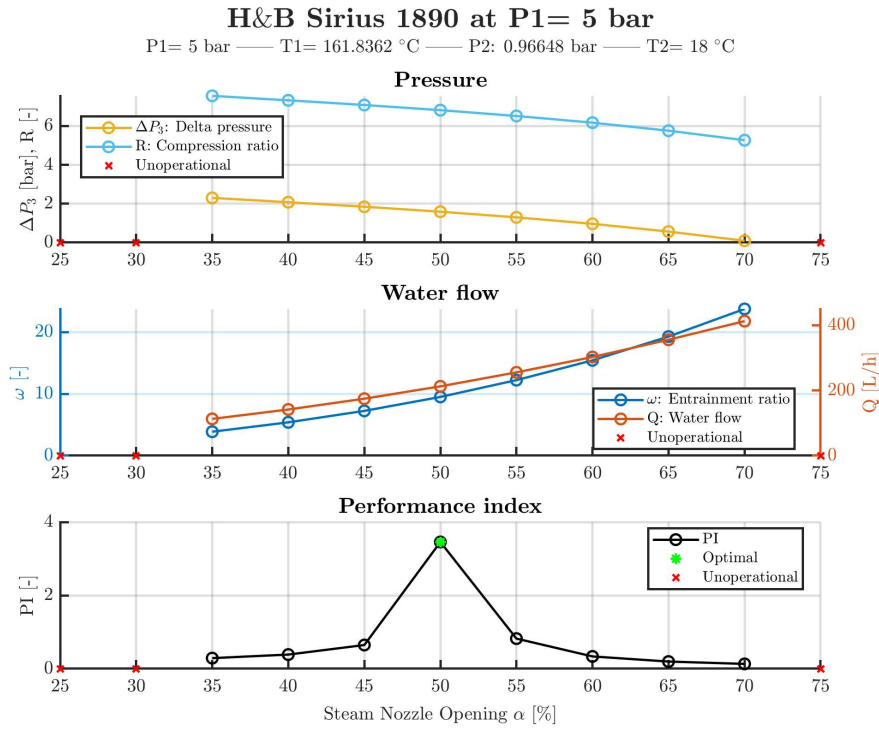


Fig. 5.3 Alpha variation sensitivity of Sirius injector at 5 bar

This tests were fundamental to understand the operational range of the Sirius injector and to evaluate the actual working of the steam-water injector.

Results

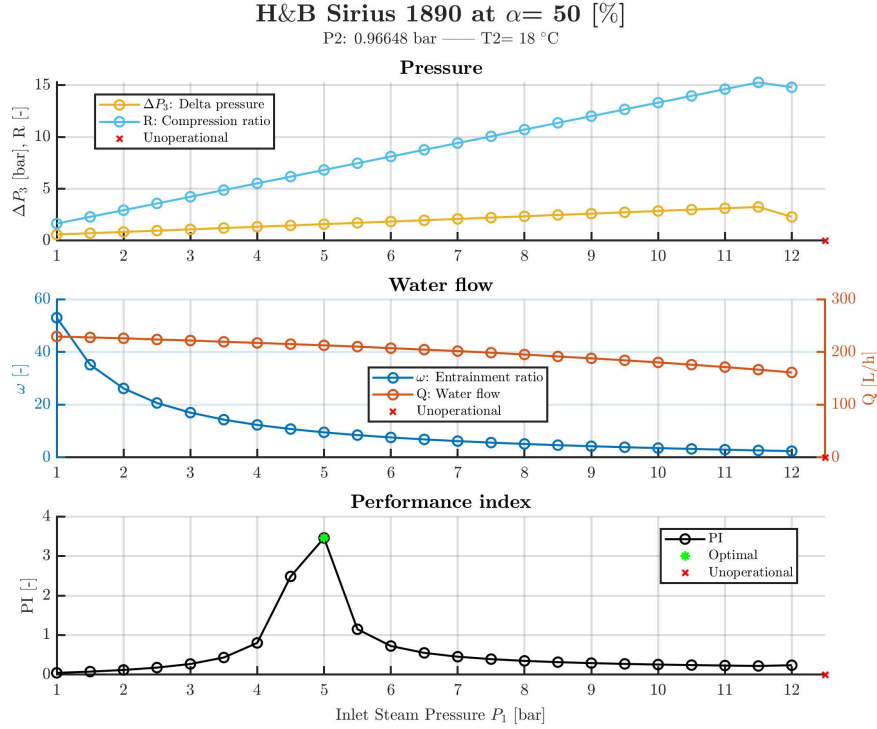


Fig. 5.4 Pressure variation sensitivity of Sirius injector at 50% α

A few notable findings, also supported by the key findings of the experiments investigated in literature, are:

- As illustrated in Figure 5.3, the x-axis represents the steam nozzle opening α , which is constrained between 25% and 75%. This range was established based on the observation that the injector does never effectively operate outside this boundary.
- The results of these tests clearly indicated that, considering the previously defined compromise, the best operation is achieved at a specific value of α . Indeed, the performance index exhibits a peak for a single opening value.
- Looking at Figure 5.4, the operational range of pressure of this injector is between 1 and 12 bar.
- Referring to Figure 5.3, it can be understood that the water flow can be modulated by adjusting the steam nozzle opening. Therefore, at

5.1 Available Injectors Analysis

constant steam pressure, increasing the nozzle opening results in a higher water feed capacity. However, this increase is limited by the associated reduction in the differential pressure between the outlet water and the boiler pressure. When this difference becomes negative, the injector is in overflow operation, thus failing to pump water into the boiler.

- By inspecting Figure 5.4, it becomes clear that any deviation of the inlet steam pressure from the optimal value associated to a given steam nozzle opening must be compensated by a corresponding adjustment of the latter.
- At the maximum operating boiler pressure of the steam carriage, this specific injector is capable of delivering a maximum water feed of 400 L/h.
- Under an inlet steam pressure of 5 bar, the performance of the injector is characterized by a maximum entrainment ratio of around 23 and a peak compression ratio of approximately 7.5.

Table 5.2 Maximum performance of the Sirius injector at each pressure level in the operating range

P1 [bar]	1	2	3	4	5	6	7	8	9	10	11	12
α_{opt} [%]	25	35	40	45	50	55	60	65	65	70	70	75
α_{min} [%]	25	25	30	30	35	35	40	40	45	45	50	50
α_{max} [%]	65	65	65	65	70	70	70	70	70	70	70	75
$\Delta P_{3,max}$ [bar]	0.7	1.2	1.6	2.1	2.3	2.4	2.8	2.7	3.0	2.7	3.1	2.8
R_{max} [-]	1.8	3.3	4.8	6.3	7.5	8.7	10.1	11.1	12.5	13.2	14.6	15.3
ω_{max} [-]	104.1	51.6	33.8	24.7	23.8	19.3	16.0	13.5	11.6	10.0	8.6	9.5
Q_{max} [$\frac{L}{h}$]	386	379	372	364	413	403	392	382	371	359	345	389

5.1.2 Bordino Injector

Unfortunately, there is very little to no information regarding the specific injector mounted on the boiler of the Bordino steam carriage. Figures 5.5a and 5.5b provide visual references of the component from the front and rear view. In particular, in Figure 5.5a are highlighted the few known features of

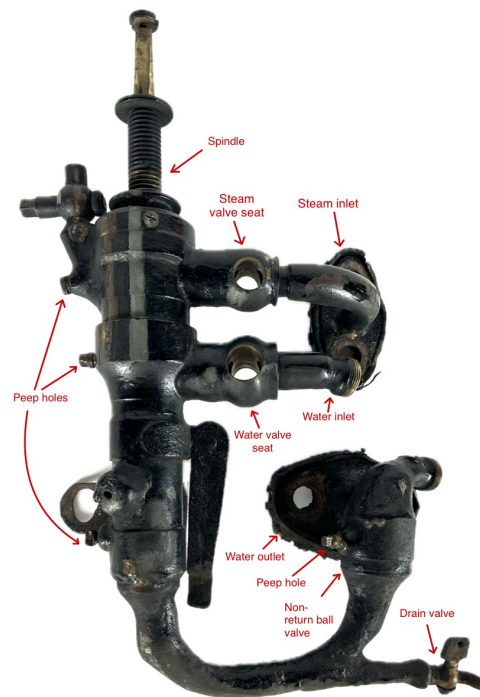
Results

this injector. The steam inlet and the water inlet are undoubtedly identified, as well as the water outlet, which includes a non-return valve just upstream the flanged connection to the boiler. The presence and position of the two flanges can provide strong evidence: the steam inlet flange is located at the top, at the boiler's steam pickup point, whereas the water outlet flange is positioned at the bottom, where the water coming from the diffuser flows directly into the boiler. What can be possibly regarded as a drain valve and a number of peep holes are visible on the sides. Moreover, at the very top of the injector, the threaded part of the spindle is present, as well as the squared seat of the regulating handle.

Although these features provide some understanding of the operation of this injector, many aspects remain open to debate. Only a CT scan could effectively define the internal geometry and operating principle of the device. An interesting observation is that the spindle actually moves vertically when rotated. This detail can suggest the absence of a water regulation mechanism such as that found in the H&B "One-Movement" injector, where the spindle rotation does not result in any axial displacement. It is therefore plausible that in this case the water flow is manually regulated either via the water valve or via a valve positioned along the feed line. Another hypothesis is the presence of an internal automated regulation system similar to that of the Sellers injector, as described in Section 2.2 and illustrated in Figure 2.11. This hypothesis is further supported by the apparent absence of an overflow pipe and valve. In addition, the presence of the drain valve could also be justified by the operation of the automatic injectors: without an overflow system, a dedicated drain is necessary to discharge during the start-up phase the excess steam. It is instead relatively clear that the injector is made out of three main bodies screwed together.

Finally, Figure 5.6 depicts the injector as it is installed on the boiler of the steam carriage. It should be noted that in this image, the regulating handle is visible on the top of the injector, and the valves are inserted in their respective seats. Furthermore, the function of the hook located on the right side of the main body is clarified: it is used to secure the lever that operates the hatch used

5.1 Available Injectors Analysis



(a) Front view



(b) Rear view

Fig. 5.5 Pictures of Bordino steam injector

Results

to feed the coal into the furnace, holding it in closed position.



Fig. 5.6 Bordino injector mounted on the boiler

5.2 Redesigned Injector

Based on all the data obtained through the reverse engineering process, the information gathered about the Sirius injector design and the corresponding performance analysis performed on it, a final injector was designed and it is depicted in Figure 5.7a. As observable, the external geometry closely resembles that of the original Bordino injector, and this resemblance can be inspected also thanks to the comparative overlay with the SLS scan shown in Figure 5.7b. On the other hand, the internal structure, illustrated in Figure 5.8, mirrors the functional layout of the Sirius injector. This is the outcome of an adaption and optimization performed in order to meet the operational requirements of the Bordino steam carriage, while also taking advantage of the perks of AM technologies.

5.2 Redesigned Injector

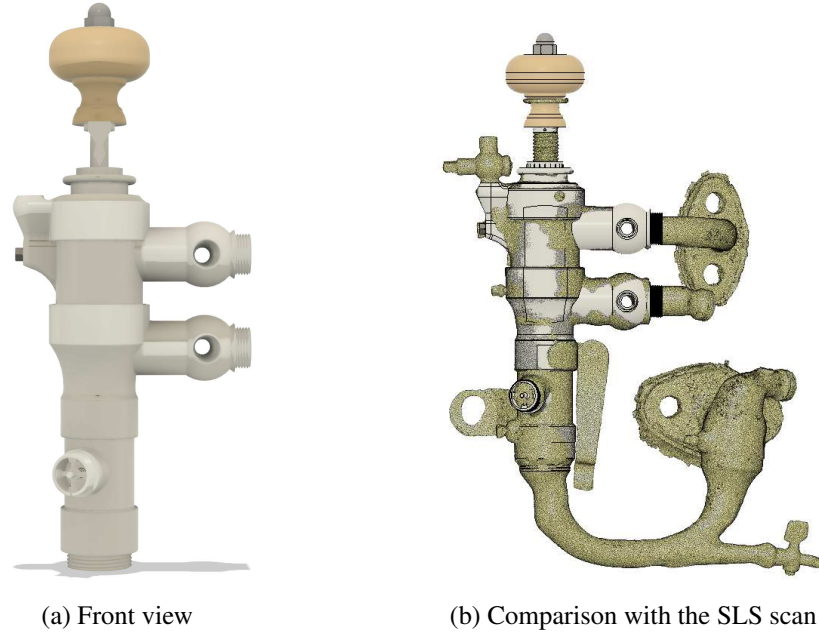


Fig. 5.7 Final redesigned injector

The external design of the original injector was preserved as faithfully as possible, with only two notable differences introduced. Firstly, the original injector lacked an overflow port; however, a 25° degree bulge was present in the lower body, which function remains uncertain. In the present design, this space was reinterpreted to accommodate the overflow assembly. Secondly, since the original injector did not feature a dial and an indicator, due to the fact that it wasn't based on the "One-movement" regulation concept, the former was added on top of the upper stuffing box and the latter was added to be fixed with a set screw on the spindle. Although not strictly needed, these additions can greatly enhance the operation and user-friendliness of the injector. The implemented dial and indicator are shown in Figure 5.9, while the sectional view of the integrated overflow port into the lower body is provided in Figure 5.10.

As it can be observed in Table 5.2, the Sirius injector exhibits a maximum feed capacity of approximately $400 \frac{L}{h}$ across the whole operational range. However, based on Equation 4.28, the steam consumption of the Bordino steam carriage is estimated to be $\sim 2100 \frac{L}{h}$, while operating at its maximum

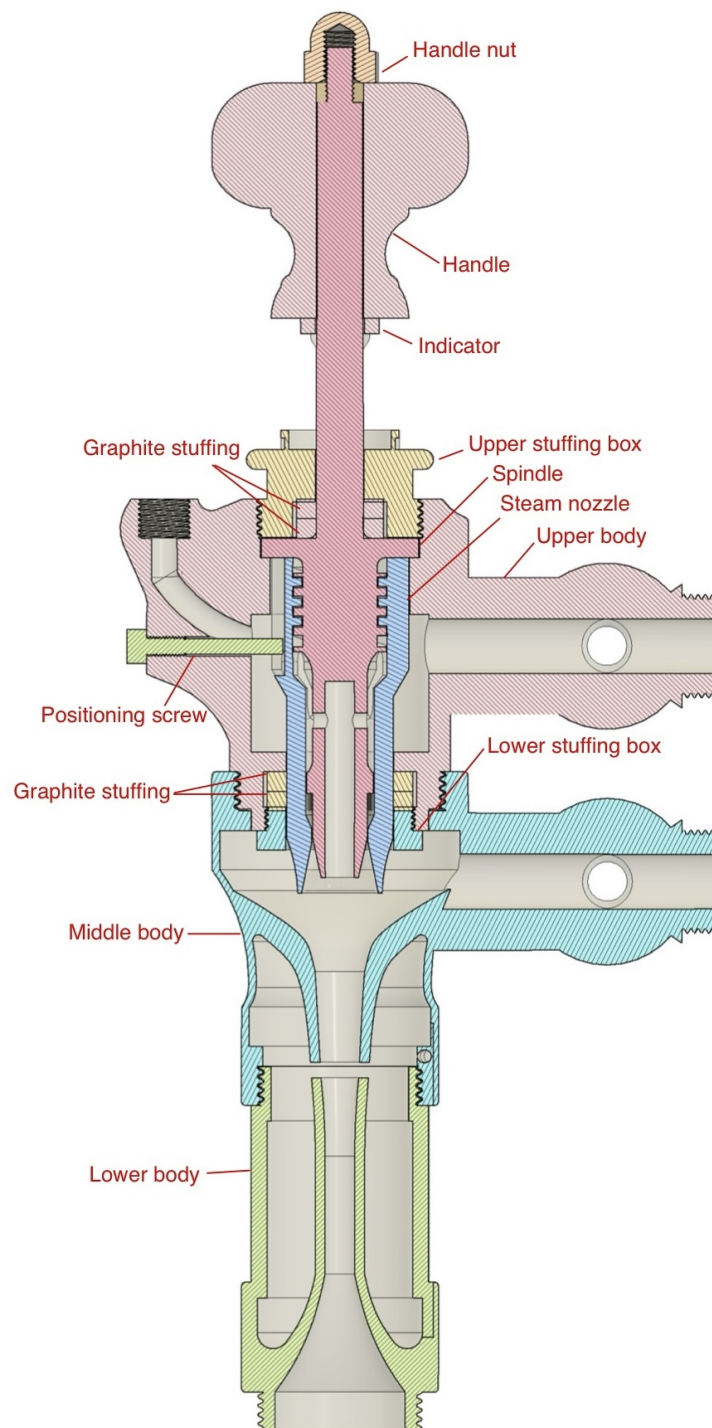


Fig. 5.8 Final redesigned injector with component labels - *front section*



Fig. 5.9 Final redesigned injector - *detail*

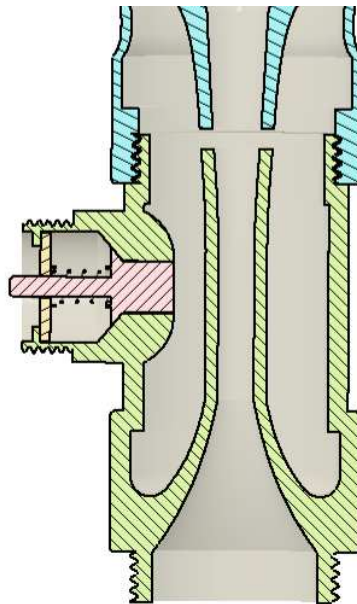


Fig. 5.10 Final redesigned injector - *25° section*

Results

working pressure of 5 *bar* and maximum engine speed of 100 *rpm*. This thus demonstrated the inadequacy of the original Sirius injector, as it is, in meeting the requirements of the carriage, thereby requiring a re-engineering process of its dimensions.

To address this, the analytical model described in Section 4.1 was again utilized to predict the performance of a scaled design and to iteratively calibrate it, in accordance to the technical demands. Given that the correct proportional relationships between the internal flow areas of the Sirius injector were already validated in Section 5.1.1 - and as emphasized in Section 3.1, these ratios are more critical than the absolute dimensions - a simple uniform scaling approach was adopted. The resulting optimal scaling factor was ascertained to be equal to 3. Notably, the final adjusted components not only ensured the functional compliance, but also resulted in good conformity to the spatial constraint given by the external shape of the original Bordino injector. This compatibility suggested that the external casing was originally designed to contain internal components of comparable scale. This should obviously be checked in the future with an opportune CT scan of the original injector. The final dimensions of the redesigned injector are reported in Table 5.3.

The maximum performance of the redesigned injector across the whole pressure range, computed with the same analytical model, is here reported in Table 5.4.

Table 5.3 Dimensions in mm of the final redesigned injector sections, as per model of Figure 4.1

D1	D2	D3	D4	D5	D6	D7
14	14	33	$7.5 + 4.5(1 - \alpha)$	$\alpha \cdot 15$	19.5	7.5

The same sensitivity analysis of the steam nozzle opening parameter α at an inlet steam pressure of 5 *bar*, previously performed on the Sirius injector in Section 5.1.1, is here replicated on the final redesigned injector. As expected, the maximum performance index is again obtained at 50% of the opening of the steam nozzle, thus validating the continuity between the original

5.2 Redesigned Injector

Table 5.4 Maximum performance of the final redesigned injector at each pressure level in the operating range

P1 [bar]	1	3	5	7	9	11	13	15
α_{opt} [%]	25	40	50	60	65	70	75	75
$\Delta P_{3,max}$ [bar]	1.5	3.7	5.6	7.7	9.1	10.2	10.9	11.5
R_{max} [-]	2.5	6.9	10.9	15.2	18.7	21.9	24.8	27.5
ω_{max} [-]	67.7	34.4	24.5	20.5	15.2	11.8	9.4	7.5
$T_{3,max}$ [°C]	71.5	121.4	142.4	189.6	192.4	193.6	219.3	227.1
Q_{max} [$\frac{L}{h}$]	2508	3404	3826	4252	4098	3930	3754	3547

and the scaled design. Moreover, at this optimal value of α , the water flow is approximately $2000 \frac{L}{h}$, thus nearly corresponding to the demanded value for the Bordino steam carriage. However, the water flow can be easily further increased by adjusting α , reaching at maximum opening around $3800 \frac{L}{h}$, effectively doubling the demand and providing a significant operational margin.

In addition, this study also included an analysis of the final water temperature at injector outlet. This parameter is useful to predict which steam nozzle opening provides the best overall thermal efficiency of the system: if water enters the boiler at a higher temperature, less heat is than required for the steam generation. Ultimately, the specific fuel consumption for the operation is thus reduced, thus increasing the thermal efficiency. As perceivable from the third graph of Figure 5.11, the outlet temperature of water decreases with the increase of α . This phenomenon can be intuitively understood by considering that, as the entrainment ratio increases proportional to the steam nozzle opening - thus more water is entrained per unit of steam -, the total feedwater heat capacity correspondingly rises. As a consequence, the heat carried and transferred by steam during mixing isn't enough to significantly increase the temperature of the larger water mass. It is thus preferable to regulate the injector to supply just enough quantity of feedwater, without greatly exceeding it, to also preserve an optimal compromise in terms of outlet water temperature.

Results

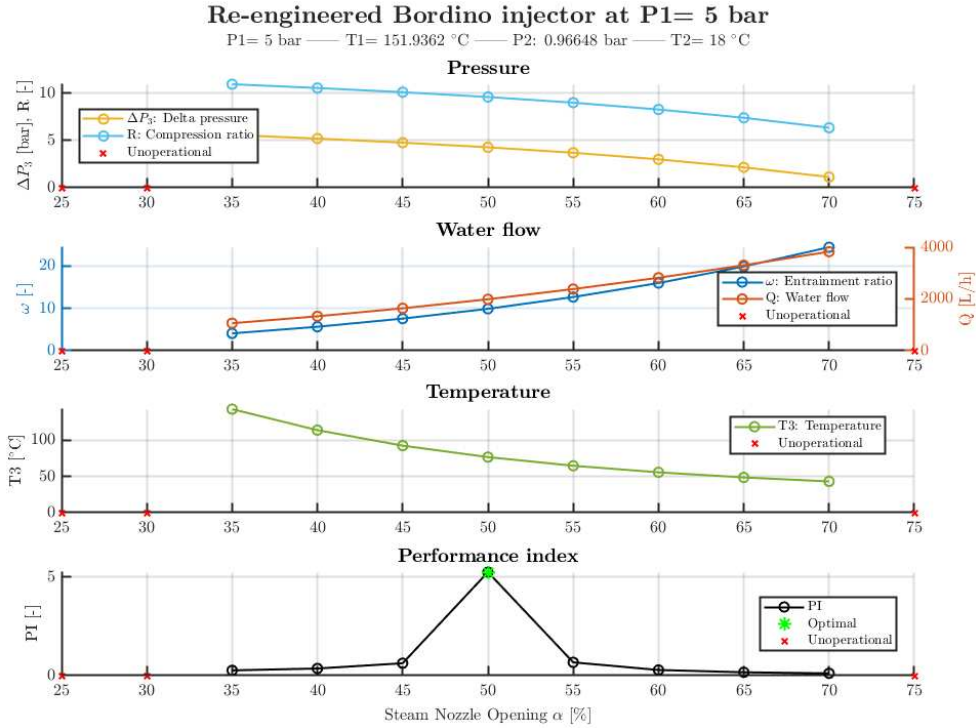


Fig. 5.11 Alpha variation sensitivity of final redesigned injector at 5 bar

Further analyses were conducted, including a pressure variation sensitivity assessment of the injector at a fixed 50% α , as shown in Figure 5.12. It can be noted that in this final injector design the maximum operational pressure is extended up to 15 bar. In addition, throughout most of the pressure range, the pressure gain ratio is approximately constant at 1.85. However, when cross-referencing this with the entrainment ratio performance map of Figure 5.13, it is evident that, for pressure over 10 bar, the entrainment ratio is insufficient. For this reason, steam pressures above this threshold were not considered in the design of the dial. It should indeed be remembered that, for locomobiles, the entrainment ratio is a more critical parameter than the compression ratio and the pressure gain ratio.

Additionally, the lower plot of Figure 5.13 provides the operational domain of the injector at $\alpha = 50\%$, as a function of the inlet steam pressure P_1 and the inlet water temperature T_2 . It is thus observed that the inlet water temperature has a considerable effect only at the boundaries of the area, while is not much

5.2 Redesigned Injector

influent between 4 and 12 *bar*.

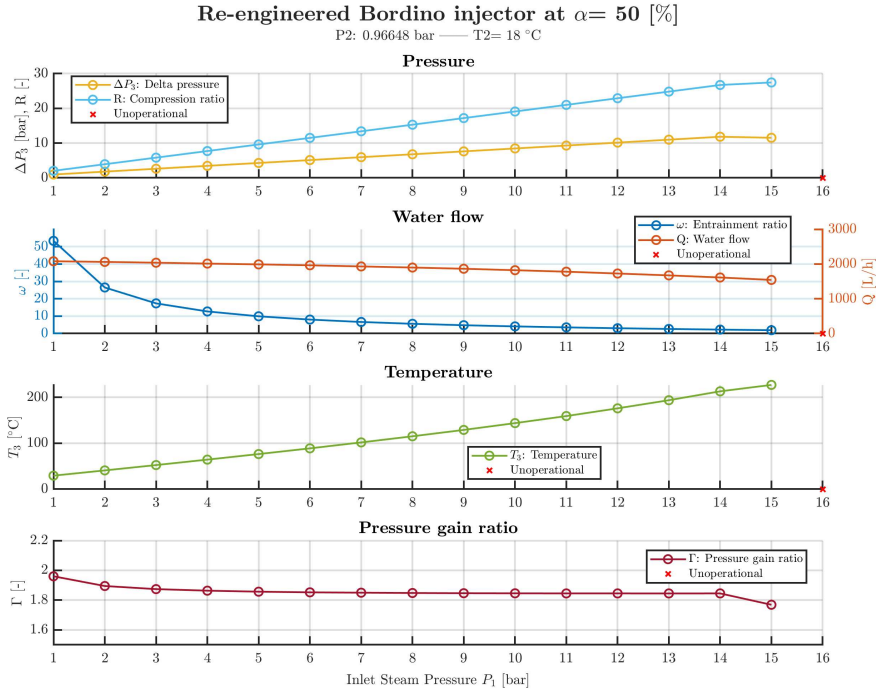


Fig. 5.12 Pressure variation sensitivity of final redesigned injector at 50% α

Finally, in Figure 5.14 is presented the exploded view of the complete redesigned injector. As discussed before, the redesign approach explicitly leveraged the potential for functional integration offered by AM, as outlined in Section 3.2.4. By comparing Figure 5.14 and Figure 5.2, it should be noted the significant reduction in the total number of components - from 28 in the original Sirius injector to 18 in the final design - without any compromise on the functionalities. This optimization was possible primarily thanks to two design decisions. First, the three main bodies of the final injector were redesigned to be assembled by threaded connections, thus eliminating the need of external bolts for the flanged joint of the Sirius configuration. Second, the multiple components forming the mixing and diffuser nozzle assemblies in the original Sirius injector were all directly integrated into the design of the middle and lower body of the new injector. Such geometric complexity and integration is solely enabled by the design freedom granted by the AM processes, and would have been probably otherwise unfeasible with conventional methods.

Results

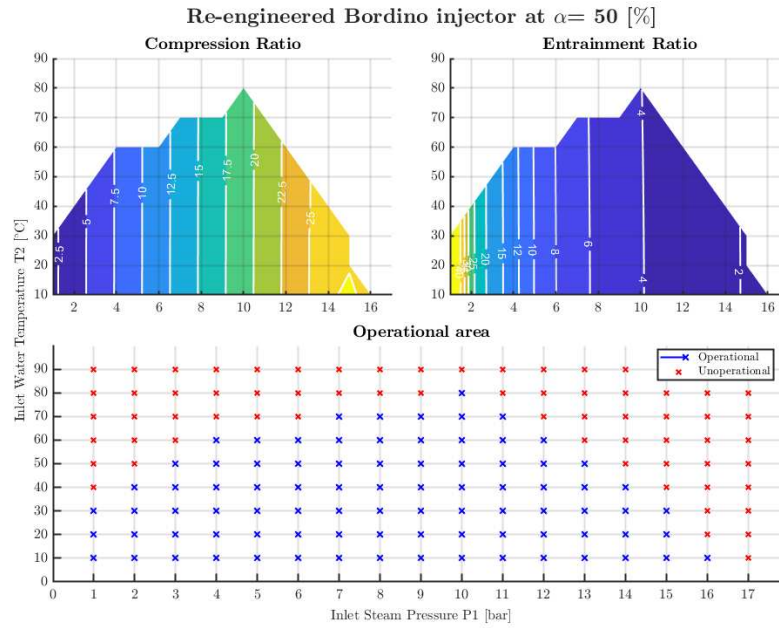


Fig. 5.13 Operational area and performance maps of final redesigned injector at 50% α

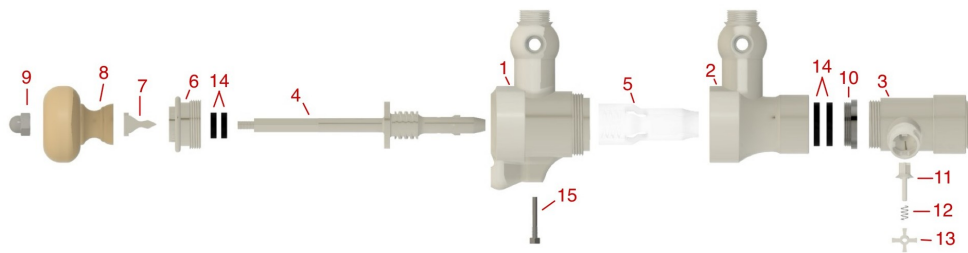


Fig. 5.14 Exploded view of the final injector. Exploded view of the final injector. 1. Upper body 2. Middle body 3. Lower body 4. Spindle 5. Steam nozzle 6. Upper stuffing box 7. Indicator 8. Handle 9. Handle nut 10. Lower stuffing box 11. Overflow valve 12. Overflow spring 13. Overflow spring stop 14. Graphite stuffing 15. Positioning screw

5.3 Final Prototype

The final phase of this thesis involved the production through AM of a demonstrative polymer prototype of the redesigned injector. The selected process was Selective Laser Sintering (SLS), chosen for its high dimensional accuracy, cost-effectiveness, maturity and reliability. In addition, this process has the great advantage of not requiring any support structure, as the powder itself has enough strength to sustain all the components during the printing process, hence reducing to the minimum the material wasted. A clearance of 0.2 mm was applied to all critical mating surfaces of the 3D model to ensure proper fit and facilitate the assembly after printing. The printing was carried out using an *EOS Formiga P110 Velocis* [106], displayed in Figure 5.15. This particular printer features a 200 x 250 x 330 mm build volume, sufficient to accommodate all the components in a single print job. The combination of the F-theta lens and the high speed scanner system enabled to complete the build in just 9 hours and 48 minutes. To create the print job file, three software were involved. First, *Materialize Magics 21.11* was used to position the components within the build volume. The slicing process was instead carried out using *EOS RP Tools*, which generated the layer-by-layer data for the fabrication. Finally, the sliced file was imported into the printer management software *EOS PSW* [107].

The material employed was the *EOS Nylon PA 2200 Performance* [108], a proprietary polyamide-12-based polymer developed by the same printer manufacturer. This material is an industry standard due to its well-balanced performance and the extensive testing performed in industrial applications. Moreover, in the *Performance* configuration, the material offers high isotropic rigidity and improved tensile strength, making it suitable for functional prototypes. The powder has an average particle size of 60 μm , thus ensuring a high resolution and excellent surface quality of the components. The SLS process is characterized by the fact that it relies on sintering: the powder is maintained at a temperature just below its sintering one - in this case approximately 169 $^{\circ}\text{C}$ - and it is fused by a laser. Notably, this laser does not require high power, but it just needs to provide enough heat to sinter the powder. A snapshot during the printing process is presented in Figure 5.16.



Fig. 5.15 EOS Formiga P110 Velocis

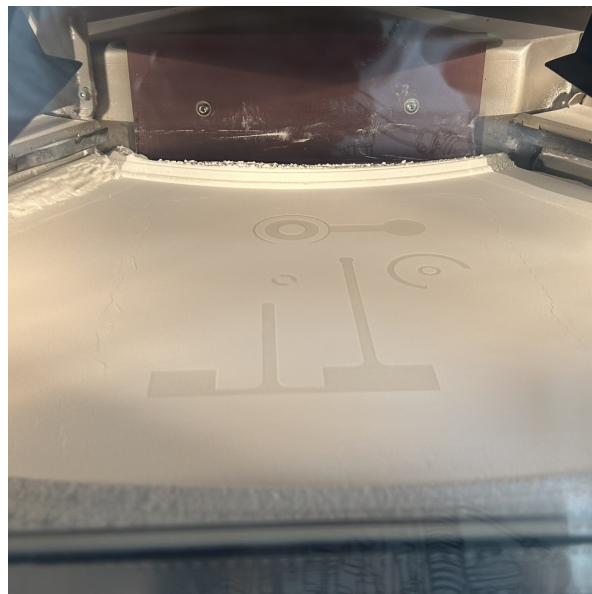


Fig. 5.16 Printing process of the polymer prototype

5.3 Final Prototype

After completion of the print job, the components need to undergo post-processing. As shown in Figure 5.17a, the printed assembly initially remains submerged in the powder volume and requires approximately 1-2 hours to cool down and be safely handled. The post-processing operation then mainly involve the removal of the components from the powder container, the coarse manual powder removal using tools such as brushes (Figure 5.17b) and the final thorough cleaning via shot peening to eliminate all the residual powder from intricate areas and cavities (Figure 5.17c).

Thanks to the 0.2 mm clearance added in the 3D model, no additional operations such as sanding, milling, re-threading and other fit adjustments were required to assemble the components. However, certain small threads were too small to be effectively printed with the precision of the SLS process. In these cases, tap drill holes were designed in place of the threads, and then manual tapping was performed after printing. Additionally, three components - the positioning screw, the lower stuffing box and the overflow spring - due to their simple geometry or commercial availability, were manufactured from metal using conventional machining techniques or directly purchased.

To conclude, in order to enhance the demonstrative characteristic of the prototype, four removable sections views were designed and produced. These sections allow direct inspection of the internal components and the operating principle of the injector. They are held in place by small 3x2 mm neodymium magnets, which are glued into dedicated seats modeled both in the injector and the sections walls. The final prototype is shown in Figure 5.18, where the opened sections reveal the key functional features, such as the axial displacement of the steam nozzle upon the rotation of the handle, and the actuation of the overflow valve in the lower body. The prototype is fully functional from a mechanical point of view and can be manually moved to simulate the operation.

Results



(a) Print job completed



(b) Manual powder removal



(c) Shot peening for powder removal

Fig. 5.17 Post-processing of the polymer prototype



Fig. 5.18 Final polymer prototype with sections opened

Chapter 6

Conclusion

The present thesis investigated the integration of modern engineering technologies in the preservation and reconstruction of historically significant mechanical components. The case study focused on the replication of the steam-water injector from Virginio Bordino's 1854 steam carriage, a pioneering example of steam-powered transport and early automotive development. The injector is selected for its functional complexity and historical value, to evaluate the capabilities and limits of AM and RE in reproducing such unique components. The main outcomes of the study are summarized as follows:

- **Historical and technical contextualization:** both the Bordino steam carriage and the Giffard injector were analyzed, focusing on their development iter, their technical characterization and the historical significance. The steam-water injector was addressed as critical in challenging the caloric theory, contributing to the advancement of modern thermodynamics. Its counterintuitive operation, poorly comprehended for nearly fifty years, was briefly illustrated. An extensive literature review revealed a recent renewed interest in the device, mainly as a passive, reliable, energy-efficient water pumping system in nuclear light-water reactors.
- **Reverse Engineering methodology:** given the non-existence of original drawings, a dual RE approach was attempted. Due to the impossibility of acquiring the internal components of the original Bordino injector, a high-resolution CT scan was performed on a conceptually analogous injector, the Holden & Brooke Sirius-"One-Movement"-1890. On the

other hand, a SLS scan was used to digitized the external geoemtry of the Bordino injector. The resulting point clouds, meshes and voxel models were post-processed and employed to model the ginal injector design.

- **Digital redesign and Additive Manufacturing fabrication:** AM was evaluated as the enabling fabrication technique, identifying SLS as the most suitable method for the polymeric prototype production. The injector was redesigned taking advantage of DfAM fundamentals, such as the integration of multiple functional parts into a single one. It was then fabricated in Nylon and easily assembled.
- **Perfomance evaluation and analytical validation:** performance analyses of both the original H&B injector and the redesigned injector were conducted via an appropriate analytical model. The evaluations confirmed the injector's pumping capabilities and aided the redesign effort. Sensitivity analyses of key parameters such as steam nozzle opening α and inlet steam pressure P_1 validated the expected performances for entrainment ratio ω , compression ratio R and water flow Q .

In conclusion, this thesis demonstrates the successful integration of RE and AM technologies in the analysis and reconstruction of a high complexity steam-era component, confirming their effectiveness not only in modern industry but also for classic car components restoration. The work contributes to the larger *MAUTO* restoration project and validates a replicable workflow for future museum activities, as well as in the wider context of classic car restoration.

Future developments includes the production of a metal prototype via AM, enabling testing on a working boiler to validate the analytical model. The ultimate aim is a fully functional injector installable on the 1:1 replica. Further optimization could be achieved via CFD simulation, despite the obstacle posed by the complex two-phase flow mixture. Finally, the proposed workflow should also be tested on the restoration of other mechanical systems in antique vehicles.

References

- [1] “Joseph Nicolas Cugnot,” Sep. 2024, page Version ID: 141260960. [Online]. Available: https://it.wikipedia.org/w/index.php?title=Joseph_Nicolas_Cugnot&oldid=141260960
- [2] “The London Steam Carriage,” Dec. 2011. [Online]. Available: <https://realsteampunk.wordpress.com/2011/12/24/the-london-steam-carriage/>
- [3] *Il museo dell’automobile Carlo Biscaretti di Ruffia di Torino - Le vetture della collezione*, ser. Collana quaderni di civiltà e cultura piemontese. Torino: Priuli e Verlucca Editori, 1998.
- [4] Fondi Storici - Centro di Documentazione MAUTO, “La carrozza Bordino all’interno dello Stadio Comunale di Torino,” 1939.
- [5] B. Zucchelli, “Il restauro della Carrozza a vapore di Virginio Bordino,” MAUTO, Torino, Nov. 2024, unpublished.
- [6] Redazione FIRSTonline, “ACCADDE OGGI - Dirigibile: nel 1852 il primo volo a motore,” Sep. 2021. [Online]. Available: <https://www.firstonline.info/accadde-oggi-dirigibile-nel-1852-il-primo-volo-a-motore/>
- [7] “Henri Giffard,” Jun. 2025, page Version ID: 1294520142. [Online]. Available: https://en.wikipedia.org/w/index.php?title=Henri_Giffard&oldid=1294520142
- [8] “Blastpipe,” Mar. 2025, page Version ID: 1278452639. [Online]. Available: <https://en.wikipedia.org/w/index.php?title=Blastpipe&oldid=1278452639>
- [9] F. Barwell, “The Steam Injector,” in *Transactions 1929-30*, ser. 174. Swindon Engineering Society, Jan. 1930, pp. 85–118, no. 174.
- [10] S. Kneass, *Practice and Theory of the Injector*, 3rd ed. New York: John Wiley & Sons, 1910. [Online]. Available: <https://archive.org/details/practicetheoryof00kneauoft/page/ii/mode/2up>

-
- [11] Y. Takeya, S. Miwa, T. Hibiki, and M. Mori, "Application of steam injector to improved safety of light water reactors," *Progress in Nuclear Energy*, vol. 78, pp. 80–100, Jan. 2015. [Online]. Available: <https://www.sciencedirect.com/science/article/pii/S0149197014002303>
- [12] G. Cattadori, L. Galbiati, L. Mazzocchi, and P. Vanini, "A single-stage high pressure steam injector for next generation reactors: Test results and analysis," *International Journal of Multiphase Flow*, vol. 21, no. 4, pp. 591–606, Aug. 1995. [Online]. Available: <https://www.sciencedirect.com/science/article/pii/030193229400086Y>
- [13] H. Ma, H. Zhao, L. Wang, Z. Yu, and X. Mao, "Modeling and investigation of a steam-water injector," *Energy Conversion and Management*, vol. 151, pp. 170–178, Nov. 2017. [Online]. Available: <https://linkinghub.elsevier.com/retrieve/pii/S0196890417307616>
- [14] Y. Abe and S. Shibayama, "Study on the characteristics of the supersonic steam injector," *Nuclear Engineering and Design*, vol. 268, pp. 191–202, Mar. 2014. [Online]. Available: <https://www.sciencedirect.com/science/article/pii/S0029549313004433>
- [15] R. Kwidziński, "Experimental investigation of condensation wave structure in steam–water injector," *International Journal of Heat and Mass Transfer*, vol. 91, pp. 594–601, Dec. 2015. [Online]. Available: <https://www.sciencedirect.com/science/article/pii/S0017931015008583>
- [16] Y. Kamata, M. Fujishiro, A. Kaneko, and Y. Abe, "Study on Flow Structure in a Supersonic Steam Injector." American Society of Mechanical Engineers Digital Collection, Jul. 2018. [Online]. Available: <https://dx-doi-org.ezproxy.biblio.polito.it/10.1115/ICONE26-82058>
- [17] S. Miwa, T. Moribe, N. Akiyama, and H. Sakashita, "Effect of the Jet Stability on Supersonic Steam Injector Operation." American Society of Mechanical Engineers Digital Collection, Jul. 2018. [Online]. Available: <https://dx-doi-org.ezproxy.biblio.polito.it/10.1115/ICONE26-82585>
- [18] M. Bertonecello, P. Hertzke, and T. Morel, "Collectible cars: From niche market to growth and innovation engine," Feb. 2025. [Online]. Available: <https://www.mckinsey.com/industries/automotive-and-assembly/our-insights/collectible-cars-from-niche-market-to-growth-and-innovation-engine>
- [19] K. Kanishka and B. Acherjee, "A systematic review of additive manufacturing-based remanufacturing techniques for component repair and restoration," *Journal of Manufacturing Processes*, vol. 89, pp. 220–283, Mar. 2023. [Online]. Available: <https://www.sciencedirect.com/science/article/pii/S152661252300052X>

References

- [20] G. Lugano, “Types of Additive Manufacturing in 3D Printing,” 2024. [Online]. Available: <https://app.biorender.com/biorender-templates/details/t-661075a3a5091ca29bb5ff3a-types-of-additive-manufacturing-in-3d-printing/?source=gallery>
- [21] B. Langefeld, M. Möhrle, C. Balzer, and P. Schildbach, “Advancements in Metal 3D Printing: Beyond Powder Bed – Additive Manufacturing on the Brink of Industrialization,” Oct. 2018. [Online]. Available: <https://www.rolandberger.com/en/Insights/Publications/Additive-manufacturing-on-the-brink-of-industrialization.html>
- [22] A. Wiberg, J. Persson, and J. Ölvander, “Design for additive manufacturing – a review of available design methods and software,” *Rapid Prototyping Journal*, vol. 25, no. 6, pp. 1080–1094, Aug. 2019, publisher: Emerald Publishing Limited. [Online]. Available: <https://www.emerald.com/insight/content/doi/10.1108/rpj-10-2018-0262/full/html>
- [23] Z. Geng and B. Bidanda, “Review of reverse engineering systems – current state of the art,” *Virtual and Physical Prototyping*, Apr. 2017, publisher: Taylor & Francis. [Online]. Available: <https://www.tandfonline.com/doi/full/10.1080/17452759.2017.1302787>
- [24] J. Wang, D. Gu, Z. Yu, C. Tan, and L. Zhou, “A framework for 3D model reconstruction in reverse engineering,” *Computers & Industrial Engineering*, vol. 63, no. 4, pp. 1189–1200, Dec. 2012. [Online]. Available: <https://www.sciencedirect.com/science/article/pii/S0360835212001842>
- [25] T. Luniya and G. Chimata, “Extending the Life of Classic Cars, the Additive Manufacturing Way,” in *Volume 2A: Advanced Manufacturing*. Virtual, Online: American Society of Mechanical Engineers, Nov. 2021. [Online]. Available: <https://asmedigitalcollection.asme.org/IMECE/proceedings/IMECE2021/85550/V02AT02A008/1132378>
- [26] E. Dalpadulo, A. Petruccioli, F. Gherardini, and F. Leali, “A Review of Automotive Spare-Part Reconstruction Based on Additive Manufacturing,” *Journal of Manufacturing and Materials Processing*, vol. 6, no. 6, 2022, place: Basel, Switzerland Publisher: MDPI AG. [Online]. Available: <https://www.proquest.com/docview/2756732698/abstract/A9A871897CAE41C3PQ/1>
- [27] M. Paulic, T. Irgolic, J. Balic, F. Cus, A. Cupar, T. Brajliah, and I. Drstvensek, “Reverse Engineering of Parts with Optical Scanning and Additive Manufacturing,” *Procedia Engineering*, vol. 69, pp. 795–803, Jan. 2014. [Online]. Available: <https://www.sciencedirect.com/science/article/pii/S1877705814003026>

- [28] A. Bacciaglia, A. Ceruti, and A. Liverani, “Photogrammetry and Additive Manufacturing Based Methodology for Decentralized Spare Part Production in Automotive Industry,” in *Intelligent Human Systems Integration 2020*. Springer, Cham, 2020, pp. 796–802, iSSN: 2194-5365. [Online]. Available: https://link.springer.com/chapter/10.1007/978-3-030-39512-4_121
- [29] “Merddin and the Injectors.” [Online]. Available: https://www.merddin-emrys.co.uk/Pages/Injectors/merddin_and_the_injectors.html#Really
- [30] “Holden and Brooke - Graces Guide.” [Online]. Available: https://www.gracesguide.co.uk/Holden_and_Brooke
- [31] F. Buonomici, M. Carfagni, R. Furferi, L. Governi, A. Lapini, and Y. Volpe, “Reverse engineering modeling methods and tools: a survey,” *Computer-Aided Design and Applications*, vol. 15, no. 3, pp. 443–464, May 2018, publisher: U-turn Press LLC. [Online]. Available: http://www.cad-journal.net/files/vol_15/Vol15No3.html
- [32] Encyclopædia Britannica. (2019) Nicolas-Joseph Cugnot | Facts, Invention, & Steam Car. [Online]. Available: <https://www.britannica.com/biography/Nicolas-Joseph-Cugnot>
- [33] G. Mastinu and M. Ploechl, *Road and Off-Road Vehicle System Dynamics Handbook*. CRC Press, Jan. 2014.
- [34] T. Crump, *A Brief History of the Age of Steam*. Carroll & Graf Publishers, Oct. 2007.
- [35] J. G. Landels, *Engineering in the ancient world*. Berkeley: University Of California Press, 1978.
- [36] O. Batrak, “The Rainhill Trials of Locomotives,” Oct. 2020. [Online]. Available: <https://www.railway.supply/en/the-rainhill-trials-of-locomotives/>
- [37] Kingdom of the Two Sicilies, *Collezione delle leggi e de’ decreti reali del regno delle Due Sicilie*. Stamperia reale., 1836. [Online]. Available: <https://books.google.it/books?id=Y3EuAAAAYAAJ>
- [38] C. Parrini, *La Vita e le Opere di Virginio Bordino*. Firenze: Tipografia della Gazzetta D’Italia, 1881.
- [39] Ministero di agricoltura, industria e commercio, *Descrizione delle macchine e procedimenti per cui vennero accordati attestati di privativa*. G. Marzorati, 1838, vol. V, no. v. 4-6. [Online]. Available: <https://books.google.it/books?id=CxGyAAAAMAAJ>

References

- [40] MAUTO - Museo Nazionale dell'Automobile, "LO SAPEVI CHE...Virginio Bordini," Youtube, Sep. 2023. [Online]. Available: https://www.youtube.com/watch?v=D_pk4q0AIp8
- [41] "La trazione a vapore sulle strade ordinarie," in *Giornale di artiglieria e genio*. Rome: Carlo Voghera, tipografo di S.M., 1875, pp. 294–298.
- [42] E. F. Kranakis, *The French Connection: Giffard's Injector and the Nature of Heat*. The Johns Hopkins University Press, 1982, vol. 23, backup Publisher: Technology and Culture. [Online]. Available: <https://www.jstor.org/stable/3104441?origin=crossref>
- [43] H. Poincaré, "Injecteur Giffard," in *Thermodynamique*, 10th ed., ser. Cours de la Faculté des Sciences de Paris. Paris: Gauthier-Villars, 1908, vol. Cours de physique mathématique, pp. 323–335. [Online]. Available: <https://books.google.it/books?id=jqf9zQEACAAJ>
- [44] S. Kneass, "Early History," in *Practice and Theory of the Injector*, 3rd ed. New York: John Wiley & Sons, 1910, pp. 1–7. [Online]. Available: <https://archive.org/details/practicetheoryof00kneauoft/page/ii/mode/2up>
- [45] C. J. F. de Comberousse, *Discours prononcé sur la tombe de Henri giffard*. Bulletin de la société d'encouragement pour l'industrie nationale, Jul. 1882, vol. 81.
- [46] P. Virat, "Henri-Pierre FLAUD (1817 - 1874), pionnier de l'industrie mécanique à Grenelle," accessed: Jun 03 2025. [Online]. Available: <https://www.paris15histoire.com/flaud-1>
- [47] H. Giffard, *L'injecteur automoteur*, 10th ed. Paris: Mallet-Bachelier, 1861. [Online]. Available: https://books.google.it/books/about/Notice_th%C3%A9orique_et_pratique_sur_l_inje.html?id=ky1WAAAACAAJ&redir_esc=y
- [48] M. Moran, H. Shapiro, B. Munson, and D. DeWitt, *Elementi di Fisica Tecnica per l'ingegneria*, 1st ed. Milan: McGraw-Hill, 2011, table T-3.
- [49] S. Kneass, "Development of the Principle," in *Practice and Theory of the Injector*, 3rd ed. New York: John Wiley & Sons, 1910, pp. 11–12. [Online]. Available: <https://archive.org/details/practicetheoryof00kneauoft/page/ii/mode/2up>
- [50] F. Keppy, *Injectors, their Construction, Care and Management*. Bridgeport, Connecticut: The American Industrial Publishing Co., 1901.
- [51] J. Robinson, "On Giffard's Injector for Feeding Steam Boilers," *Proceedings of the Institution of Mechanical Engineers*, vol. 11, no. 1, pp. 39–51, Jun. 1860, publisher: IMECHE. [Online]. Available: https://doi.org/10.1243/PIME_PROC_1860_011_008_02

- [52] ———, “On some developments of and improvements in Giffard’s injector,” *Journal of the Franklin Institute*, vol. 80, no. 6, pp. 383–387, Dec. 1865. [Online]. Available: <https://www.sciencedirect.com/science/article/pii/0016003265902565>
- [53] L. A. P. Pochet, *Steam Injectors: Their Theory and Use*, 29th ed., ser. Van Nostrand’s science series. New York: D. Van Nostrand Company, 1877, google-Books-ID: 1Es1AAAAMAAJ. [Online]. Available: https://books.google.it/books/about/Steam_Injectors.html?id=1Es1AAAAMAAJ&redir_esc=y
- [54] E. Edwards, “The Injector,” in *Practical Steam Engineer’s Guide in the Design, Construction and Management of American Stationary, Portable and Steam Fire Engines, Steam Pumps, Boilers, Injectors, Governors, Indicators, Pistons and Rings, Safety Valves and Steam Gauges*, 7th ed. Bridgeport, Connecticut: Frederick Keppy, 1891, pp. 233–263.
- [55] W. Stanier, “Injectors and Feed Pumps for Locomotives,” in *Transactions 1908-9*. Swindon Engineering Society, Nov. 1908.
- [56] G. N. Nissenson, *Practical Treatise on Injectors as Feeders of Steam Boilers*. New York: Published by the Author, 1890.
- [57] L. Cei, *Le Caldaie a Vapore con Istruzioni ai Conduttori*, 2nd ed., ser. Manuali HOEPLI. Milan: HOEPLI, 1908.
- [58] ———, *Locomobili e trebbiatrici - Note per gli Ispettori e Istruzioni ai Conduttori*, 4th ed., ser. Manuali HOEPLI. Milano: HOEPLI, 1919.
- [59] G. Anand, “Phenomenological and mathematical modeling of a high-pressure steam driven jet injector,” Ph.D., 1993, iSBN: 9798208681701. [Online]. Available: <https://www.proquest.com/docview/304068132/abstract/4AE2848113854420PQ/1>
- [60] M. A. Grolmes, “Steam–water condensing-injector performance analysis with supersonic inlet vapor and convergent condensing section,” Argonne National Lab., Ill. (USA), Tech. Rep. ANL-7443, May 1968. [Online]. Available: <https://www.osti.gov/biblio/5021859>
- [61] T. Narabayashi, W. Mizumachi, and M. Mori, “Study on two-phase flow dynamics in steam injectors,” *Nuclear Engineering and Design*, vol. 175, no. 1, pp. 147–156, Nov. 1997. [Online]. Available: <https://www.sciencedirect.com/science/article/pii/S0029549397001702>
- [62] N. Deberne, J. F. Leone, A. Duque, and A. Lallemand, “A model for calculation of steam injector performance,” *International Journal of Multiphase Flow*, vol. 25, no. 5, pp. 841–855, Aug. 1999. [Online]. Available: <https://www.sciencedirect.com/science/article/pii/S0301932298000718>

References

- [63] T. Narabayashi, M. Mori, M. Nakamaru, and S. Ohmori, “Study on two-phase flow dynamics in steam injectors: II. High-pressure tests using scale-models,” *Nuclear Engineering and Design*, vol. 200, no. 1, pp. 261–271, Aug. 2000. [Online]. Available: <https://www.sciencedirect.com/science/article/pii/S0029549300002375>
- [64] P. Dumaz, G. Geffraye, V. Kalitvianski, E. Verloo, M. Valisi, P. Méloni, A. Achilli, R. Schilling, M. Malacka, and M. Trela, “The DEEPSSI project, design, testing and modeling of steam injectors,” *Nuclear Engineering and Design*, vol. 235, no. 2, pp. 233–251, Feb. 2005. [Online]. Available: <https://www.sciencedirect.com/science/article/pii/S0029549304003073>
- [65] S. Miwa, H. Endo, T. Moribe, and M. Mori, “Investigation of the supersonic steam injector operation mode,” *Nuclear Engineering and Design*, vol. 334, pp. 57–65, Aug. 2018. [Online]. Available: <https://www.sciencedirect.com/science/article/pii/S0029549318305168>
- [66] J.-j. Yan, S.-f. Shao, J.-p. Liu, and Z. Zhang, “Experiment and analysis on performance of steam-driven jet injector for district-heating system,” *Applied Thermal Engineering*, vol. 25, no. 8, pp. 1153–1167, Jun. 2005. [Online]. Available: <https://www.sciencedirect.com/science/article/pii/S135943110400256X>
- [67] R. Kwidziński, “Condensation heat and mass transfer in steam-water injectors,” *International Journal of Heat and Mass Transfer*, vol. 164, no. 120582, Jan. 2021. [Online]. Available: <https://www.sciencedirect.com/science/article/pii/S0017931020335183>
- [68] H. Zhao, K. Zhang, L. Wang, and J. Han, “Thermodynamic investigation of a booster-assisted ejector refrigeration system,” *Applied Thermal Engineering*, vol. 104, pp. 274–281, Jul. 2016. [Online]. Available: <https://linkinghub.elsevier.com/retrieve/pii/S1359431116307244>
- [69] M. Trela, R. Kwidziński, J. Głuch, and D. Butrymowicz, “Analysis of application of feed-water injector heaters to steam power plants,” *Polish Maritime Research*, vol. 16, no. Special, pp. 64–70, Jun. 2010. [Online]. Available: <https://sciendo.com/article/10.2478/v10012-008-0047-z>
- [70] S. K. Malibashev, “Experimental Investigation of Transparent Models of Steam-Water Injector with a Convergent Nozzle,” *Atomic Energy*, vol. 90, no. 6, pp. 469–474, Jun. 2001, company: Springer Distributor: Springer Institution: Springer Label: Springer Number: 6 Publisher: Kluwer Academic Publishers-Plenum Publishers. [Online]. Available: <https://link-springer-com.ezproxy.biblio.polito.it/article/10.1023/A:1012361125963>
- [71] R. Kwidziński, “Control-volume-based model of the steam-water injector flow,” *Archives of Thermodynamics*, vol. 31, no. 1, pp. 45–59,

- Mar. 2010, place: Warsaw, Poland Publisher: Polish Academy of Sciences. [Online]. Available: <https://www.proquest.com/docview/1321128042/abstract/81146FB1E3C4565PQ/1>
- [72] K. Sato, Y. Abe, A. Kaneko, T. Kanagawa, and M. Mori, “Two-phase flow structure and operating characteristics of supersonic steam injector,” *Mechanical Engineering Journal*, vol. 2, no. 5, pp. 15–00 004, Jul. 2015, publisher: The Japan Society of Mechanical Engineers. [Online]. Available: https://www.jstage.jst.go.jp/article/mej/2/5/2_15-00004/_pdf/-char/en
- [73] H. Ke, Q. Xiao, C. Long, J. Liu, L. Shi, and L. Tang, “A Modified Calculation Method for a Centered Water Nozzle Steam–Water Injector,” *Energies*, vol. 15, no. 9159, Jan. 2022, number: 23 Publisher: Multidisciplinary Digital Publishing Institute. [Online]. Available: <https://www.mdpi.com/1996-1073/15/23/9159>
- [74] Z. Zhang, D. Chong, and J. Yan, “Modeling and experimental investigation on water-driven steam injector for waste heat recovery,” *Applied Thermal Engineering*, vol. 40, pp. 189–197, Jul. 2012, publisher: Elsevier BV. [Online]. Available: <https://linkinghub.elsevier.com/retrieve/pii/S1359431112001020>
- [75] S. Miwa, Y. Xu, T. Hibiki, H. Sakashita, and K. Sawa, “Pressure Elevation of High-Performance Steam-Water Condensing-Injector,” *International Journal of Heat and Mass Transfer*, vol. 170, no. 120971, May 2021. [Online]. Available: <https://www.sciencedirect.com/science/article/pii/S0017931021000740>
- [76] Z. Wang, Q. Zhao, W. Liu, D. Chong, and J. Yan, “Experimental and theoretical studies on the mixing pressure and prediction model of the steam–water two-phase injector,” *International Journal of Heat and Mass Transfer*, vol. 239, p. 126567, Apr. 2025. [Online]. Available: <https://www.sciencedirect.com/science/article/pii/S0017931024013954>
- [77] J. Kaye, E. F. Kurtz Jr., and S. Gouse Jr., “Condensuctor for Deep running Torpedo,” Joseph Kaye and Co., Brookline, Massachusetts, Tech. Rep. N-2, Oct. 1956, not available as unpublished or for private communication.
- [78] S. W. Gouse Jr. and J. H. Leigh, “Heat, mass, and momentum transfer between a high velocity liquid jet and a concentric gas stream in an axisymmetric channel.” Defense Technical Information Center, Fort Belvoir, VA, Tech. Rep. 67, Jan. 1965. [Online]. Available: <http://www.dtic.mil/docs/citations/AD0611063>
- [79] M. Trela, R. Kwidziński, J. Głuch, and D. Butrymowicz, “Analysis of application of feed-water injector heaters to steam power plants,” *Polish*

References

- Maritime Research*, vol. 16, no. Special, pp. 64–70, 2009. [Online]. Available: <https://sciendo.com/article/10.2478/v10012-008-0047-z>
- [80] S. Miwa, H. Endo, T. Moribe, H. Sakashita, M. Mori, and T. Hibiki, “Investigation of the thermal-hydraulic characteristics of supersonic steam injector,” *Applied Thermal Engineering*, vol. 109, pp. 261–271, Oct. 2016. [Online]. Available: <https://www.sciencedirect.com/science/article/pii/S1359431116314235>
- [81] R. Kwidziński, “Experimental and theoretical investigations of two-phase flow in low pressure steam–water injector,” *International Journal of Heat and Mass Transfer*, vol. 144, no. 118618, Dec. 2019. [Online]. Available: <https://www.sciencedirect.com/science/article/pii/S0017931019328005>
- [82] A. C. Kyaw, N. Nagengast, C. Usma-Mansfield, and F. K. Fuss, “A Combined Reverse Engineering and Multi-Criteria Decision-Making Approach for Remanufacturing a Classic Car Part,” *Procedia CIRP*, vol. 119, pp. 222–228, Jan. 2023. [Online]. Available: <https://www.sciencedirect.com/science/article/pii/S2212827123004511>
- [83] B. Sarzyński, L. Śniezek, and K. Grzelak, “Metal Additive Manufacturing (MAM) Applications in Production of Vehicle Parts and Components—A Review,” *Metals*, vol. 14, no. 2, p. 195, Feb. 2024, publisher: MDPI AG. [Online]. Available: <https://www.mdpi.com/2075-4701/14/2/195>
- [84] ISO/ASTM 52900, “Additive manufacturing - General principles - Fundamentals and vocabulary,” 2022.
- [85] A. Hamza, K. Bousnina, I. Dridi, and N. B. Yahia, “Revolutionizing Automotive Design: The Impact of Additive Manufacturing,” *Vehicles*, vol. 7, no. 1, p. 24, Mar. 2025, publisher: MDPI AG. [Online]. Available: <https://www.mdpi.com/2624-8921/7/1/24>
- [86] A. Saboori, A. Aversa, G. Marchese, S. Biamino, M. Lombardi, and P. Fino, “Application of Directed Energy Deposition-Based Additive Manufacturing in Repair,” *Applied Sciences*, vol. 9, no. 16, p. 3316, Jan. 2019, number: 16 Publisher: Multidisciplinary Digital Publishing Institute. [Online]. Available: <https://www.mdpi.com/2076-3417/9/16/3316>
- [87] T. Vaneker, A. Bernard, G. Moroni, I. Gibson, and Y. Zhang, “Design for additive manufacturing: Framework and methodology,” *CIRP Annals*, vol. 69, no. 2, pp. 578–599, Jan. 2020. [Online]. Available: <https://www.sciencedirect.com/science/article/pii/S0007850620301396>
- [88] E. Colombo, “Methods to reverse engineer spare parts,” Master’s thesis, Politecnico di Torino, Turin, May 2019. [Online]. Available: <https://webthesis.biblio.polito.it/12194/>

-
- [89] T. Segreto, C. Alessandra, and D. M. D'Addona, "Assessment of laser-based reverse engineering systems for tangible cultural heritage conservation," *International Journal of Computer Integrated Manufacturing*, vol. 26, no. 9, pp. 857–865, Sep. 2013. [Online]. Available: <https://www-tandfonline-com.ezproxy.biblio.polito.it/doi/full/10.1080/0951192X.2013.799781>
- [90] G. J. Kaisarlis, S. C. Diplaris, and M. M. Sfantsikopoulos, "A Knowledge-Based System for Tolerance Allocation in Reverse Engineering," D. R. Hayhurst, S. Hinduja, J. Atkinson, M. Burdekin, R. G. Hannam, L. Li, and A. W. Labib, Eds. London: Springer, 2000, pp. 527–532.
- [91] Z. Geng and B. Bidanda, "Tolerance estimation and metrology for reverse engineering based remanufacturing systems," *International Journal of Production Research*, vol. 60, no. 9, pp. 2802–2815, Mar. 2021. [Online]. Available: <https://www-tandfonline-com.ezproxy.biblio.polito.it/doi/full/10.1080/00207543.2021.1904158>
- [92] C. S. Frandsen, M. M. Nielsen, A. Chaudhuri, J. Jayaram, and K. Govindan, "In search for classification and selection of spare parts suitable for additive manufacturing: a literature review," *International Journal of Production Research*, vol. 58, no. 4, pp. 970–996, Feb. 2020, publisher: Taylor & Francis. [Online]. Available: <https://doi.org/10.1080/00207543.2019.1605226>
- [93] A. Petruccioli, F. Gherardini, and F. Leali, "Assessment of close-range photogrammetry for the low cost development of 3D models of car bodywork components," *International Journal on Interactive Design and Manufacturing (IJIDeM)*, vol. 16, no. 2, pp. 703–713, Jun. 2022, company: Springer Distributor: Springer Institution: Springer Label: Springer Number: 2 Publisher: Springer Paris. [Online]. Available: <https://link.springer.com/article/10.1007/s12008-022-00865-6>
- [94] D. Thomas, "Costs, benefits, and adoption of additive manufacturing: a supply chain perspective," *The International Journal of Advanced Manufacturing Technology*, vol. 85, no. 5, pp. 1857–1876, Jul. 2016, company: Springer Distributor: Springer Institution: Springer Label: Springer Number: 5 Publisher: Springer London. [Online]. Available: <https://link.springer.com/article/10.1007/s00170-015-7973-6>
- [95] B. Langefeld, P. Schildbach, M. Möhrle, A. Nauth, T. Femmer, and M. Schaukellis, "Taking metal 3D printing to the next level," Nov. 2019. [Online]. Available: <https://www.rolandberger.com/en/Insights/Publications/Additive-manufacturing-Taking-metal-3D-printing-to-the-next-level.html>

References

- [96] B. Langefeld, T. Femmer, M. Schaukellis, M. López, and C. Klatt, “Sustainability in additive manufacturing,” Mar. 2022. [Online]. Available: <https://www.rolandberger.com/en/Insights/Publications/Sustainability-Is-Additive-Manufacturing-a-green-deal.html>
- [97] H. A. Habeeb, D. A. Wahab, A. H. Azman, and M. R. Alkahari, “Design Optimization Method Based on Artificial Intelligence (Hybrid Method) for Repair and Restoration Using Additive Manufacturing Technology,” *Metals*, vol. 13, no. 3, p. 490, Feb. 2023, publisher: MDPI AG. [Online]. Available: <https://www.mdpi.com/2075-4701/13/3/490>
- [98] A. Z. A. Kadir, Y. Yusof, and M. S. Wahab, “Additive manufacturing cost estimation models—a classification review,” *The International Journal of Advanced Manufacturing Technology*, vol. 107, no. 9, pp. 4033–4053, Apr. 2020. [Online]. Available: <https://doi.org/10.1007/s00170-020-05262-5>
- [99] B. Naghshineh, F. Miguel, and H. Carvalho, “Rethinking Additive Manufacturing for Spare Parts Supply Chain Management,” *Research-Technology Management*, vol. 66, no. 4, pp. 38–47, Jul. 2023, publisher: Routledge. [Online]. Available: <https://doi.org/10.1080/08956308.2023.2207970>
- [100] M. Peron, A. M. Coruzzolo, R. Basten, N. Knofius, F. Lolli, and F. Sgarbossa, “Choosing between additive and conventional manufacturing of spare parts: On the impact of failure rate uncertainties and the tools to reduce them,” *International Journal of Production Economics*, vol. 278, p. 109438, Dec. 2024, publisher: Elsevier BV. [Online]. Available: <https://linkinghub.elsevier.com/retrieve/pii/S0925527324002950>
- [101] M. Holmgren, “X Steam, Thermodynamic properties of water and steam,” Aug. 2007. [Online]. Available: <https://it.mathworks.com/matlabcentral/fileexchange/9817-x-steam-thermodynamic-properties-of-water-and-steam>
- [102] IAPWS-IF97, “IAPWS Industrial Formulation 1997 for the Thermodynamic Properties of Water and Steam,” Lucerne, Switzerland, Aug. 2007. [Online]. Available: <https://iapws.org/relguide/IF97-Rev.html>
- [103] “phoenix vltomelx s.” [Online]. Available: <https://www.jwjndt.com/product/phoenix-vtomex-s/>
- [104] “VGSTUDIO MAX.” [Online]. Available: <https://volumegraphics.hexagon.com/en/products/vgstudio-max.html>
- [105] “new: Atos Core.” [Online]. Available: <https://f.nordiskemedier.dk/2uwcu6dmymt16zpa.pdf>

References

- [106] “FORMIGA P 110 Velocis - Qualità dei pezzi eccezionale.” [Online]. Available: <https://www.eos.info/it/soluzioni-polimeriche/stampanti-polimeri/formiga-p-110-velocis>
- [107] angelicachieffi, “File preparation for printing,” Apr. 2018. [Online]. Available: <https://additivemanufacturingapplication.wordpress.com/2018/04/15/file-preparation-for-printing-with-eos-m280/>
- [108] “PA 2200 Performance MDS PA 2200 Performance.” [Online]. Available: <https://www.eos.info/it/soluzioni-polimeriche/materiali-polimerici/schede-tecniche/mds-pa-2200-performance>

Appendix A

H&B

Sirius-"One-Movement"-1890 Injector

This appendix presents a collection of visual and technical images related to the injector produced by the British company Holden & Brooke, historically referred to as the "1890 Injector", the "Sirius Injector" and the "One-movement Injector". According to available sources both online and from books, this model was likely produced by the company from 1890 until approximately the mid-20th century, as proven by the finding of a brochure dated 1958. The content of the appendix is organized in four parts: Section A.1 contains some technical drawings retrieved online, Section A.2 includes commercials and brochures of the injector, Section A.3 provides photographs taken on the available model and Section A.4 reports the results of the CT scan performed.

A.1 Technical drawings

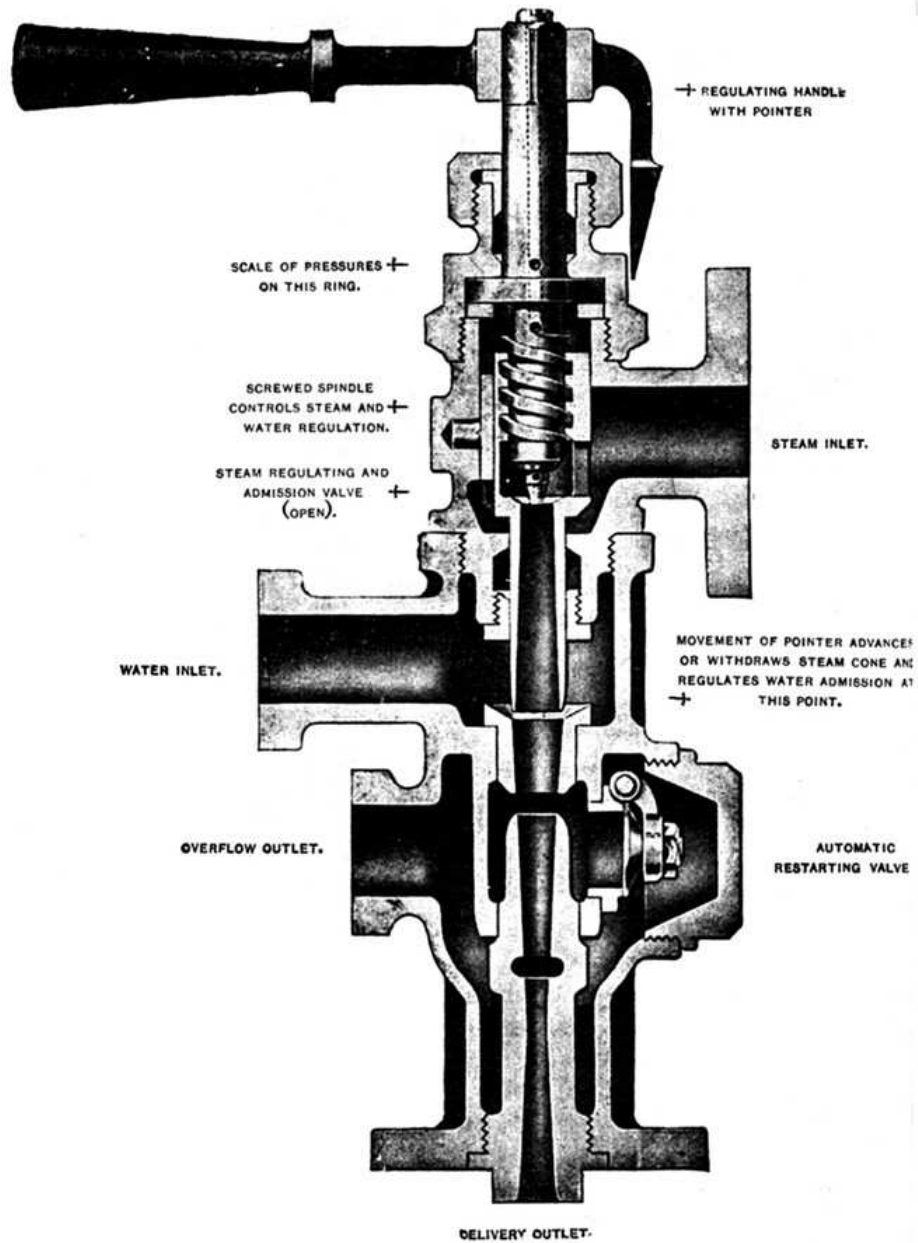
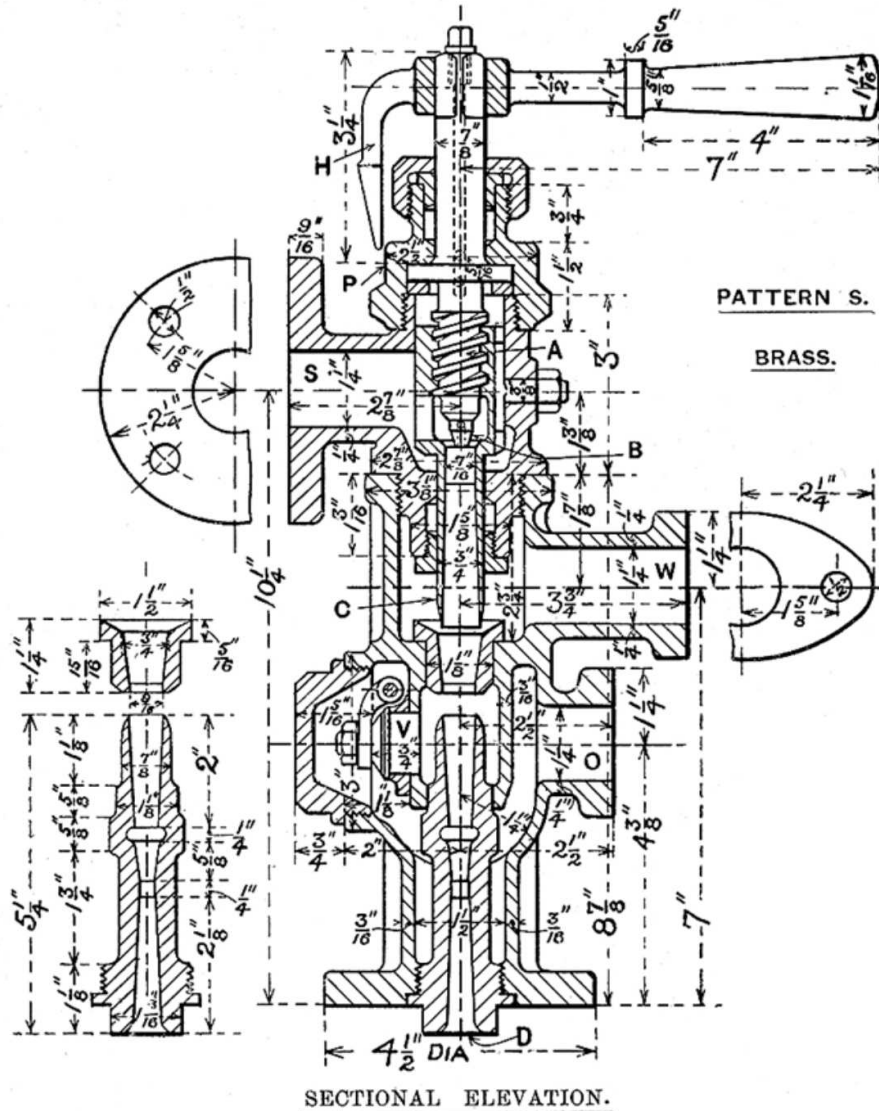


Fig. A.1 Undated technical drawing. [29]

H&B Sirius-"One-Movement"-1890 Injector

— DETAILS OF THE "SIRIUS" INJECTOR. —

(ONE MOVEMENT.)



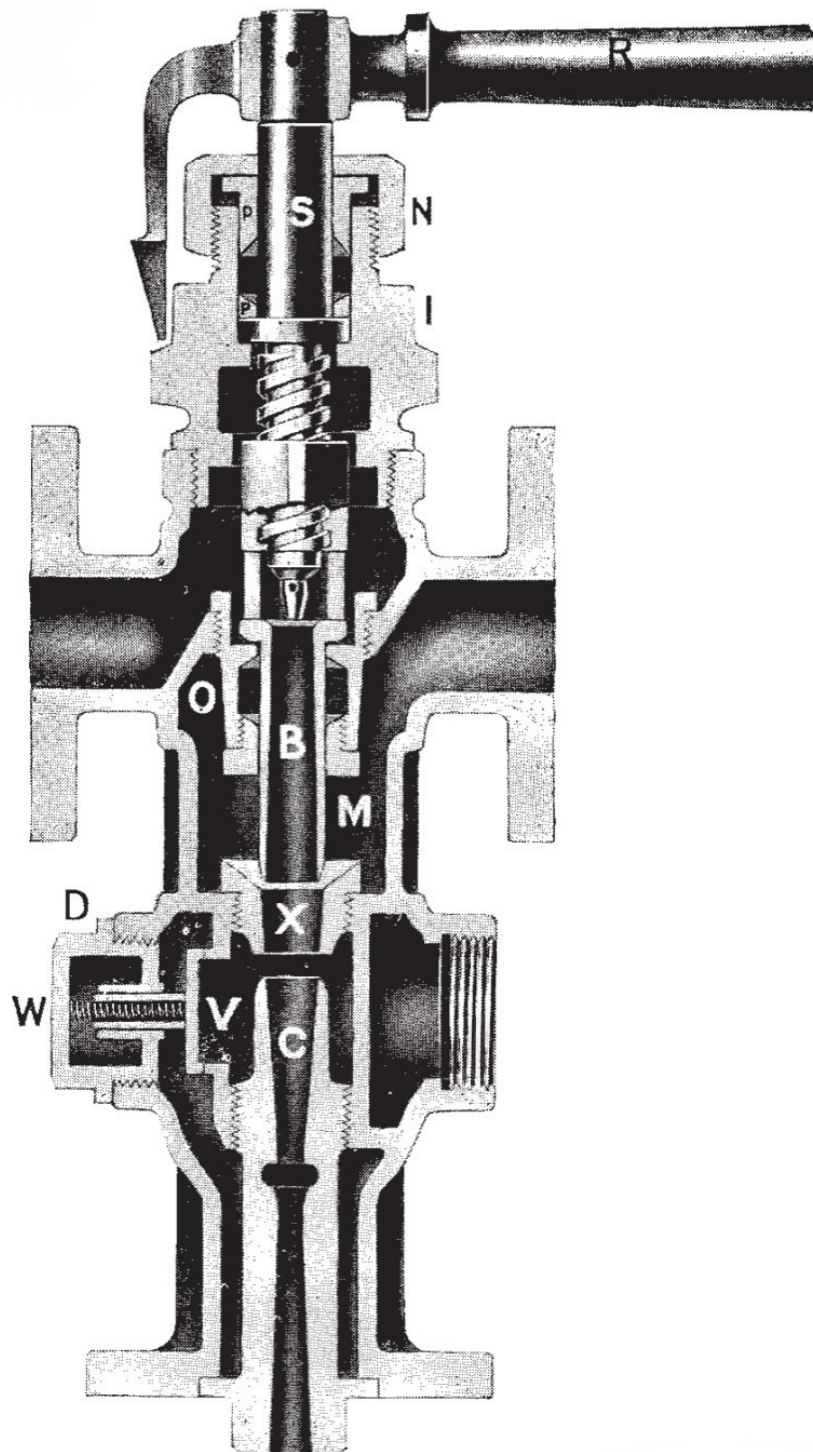


Fig. A.3 1930 technical drawing. [9]

A.2 Commercials

HOLDEN & BROOKE L^{TD.},
Injector Manufacturers.

THE
'1890'

AUTOMATIC, SELF-ACTING
INJECTOR.

Works at any Pressure.
Self-contained Steam Valve.
Entirely Operated and
Regulated by One Move-
ment.
Cannot be Wrongly Worked
or Misunderstood.

By a **partial turn** of the operating handle steam is turned on, and the injector (1) started, (2) regulated for any pressure, and (3) the quantity of feed to boiler varied as **required**.

The "Influx" Automatic, and all other types of Injectors. Also exact duplicates of the original "**Giffard**," "**Atlas**," and other patterns of Injectors made by **Sharp, Stewart & Co.**

EXHAUST STEAM INJECTORS,
TO WORK AGAINST ALL PRESSURES.

ST. SIMON'S WORKS, SALFORD, MANCHESTER.

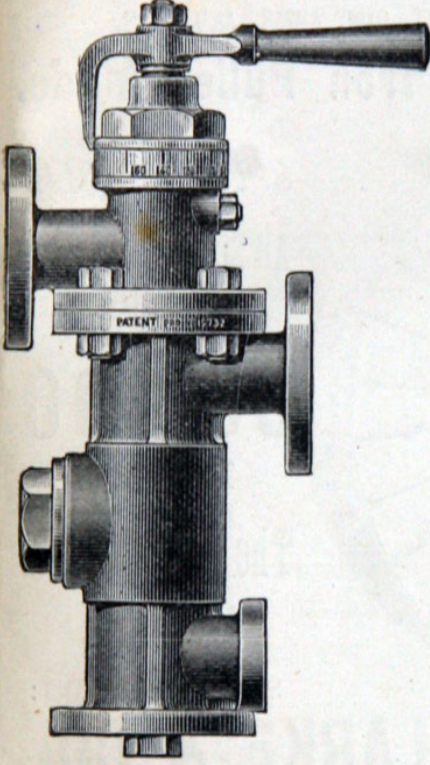
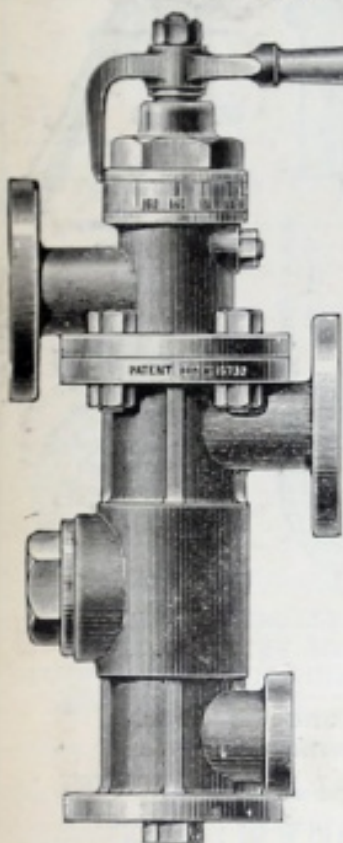


Fig. A.4 1892 commercial. [30]

THE "1890" SELF-ACTING INJECTOR

(BROOKE'S PATENT).



Works at any Pressure.
Water & Steam Regulated
and Injector entirely
operated by one movement.
Cannot be wrongly worked
or misunderstood.
Self-contained Steam Valve.
BY A PARTIAL TURN OF LEVER
Steam is turned on and
the Injector (1) Started ;
(2) Regulated for any Pressure ;
and (3) Quantity of Feed
varied as required.

Steam Pressure.	Highest temp'ture of Feed Water.	Height will Lift.
35lb.	150°	12 to 20 ft.
80 "	135°	
100 "	120°	
150 "	105°	

ALL MAKES OF INJECTORS REPAIRED.

HOLDEN & BROOKE LTD.,
ST. SIMON'S WORKS, SALFORD.

Fig. A.5 1893 commercial. [30]

HOLDEN & BROOKE Ltd.,
SALFORD, MANCHESTER.

The "1890" Self-acting and Self-regulating
INJECTOR



**Cannot possibly be wrongly
worked or misunderstood.**

Works equally well at all pressures
(15lb. to 200lb). Entirely operated by one
movement. Self-contained Steam Valve.
No Water-cock required. High Lifting.

By half a turn of the Lever

Steam is turned on and the Injector (1)
started, (2) regulated for any pressure, and
(3) the quantity of feed varied as required.

TESTIMONIAL.

LONESOME CHEMICAL WORKS,
STREATHAM COMMON,
29th January, 1894.

I have this day ordered another No. 7 "1890" Injector. Those supplied
last year have more than satisfied us; they are working day and night, and
lately (since the severe frost) the two have been drawing through 40ft. of $1\frac{1}{2}$ in.
rubber hose, our suction pipe having burst with frost.

No other type of Injector would have kept us going, for on suddenly start-
ing the No. 6 it draws the hose flat, and then both Injectors fight against one
another for a few seconds for water till the hose recovers itself. Everybody
going along the yard treads on the hose (the boys mostly), when a snort or
howl is the only response, whereas if they were ordinary Injectors it would be
a man's constant job to restart them.

Fig. A.6 1895 commercial. [30]



HOLDEN & BROOKE, L^D.
Engineers,
MANCHESTER.

THE "1890"
SELF-ACTING
INJECTOR

Works equally well at all pressures
(15 to 200 lbs.).

ENTIRELY OPERATED BY ONE
MOVEMENT.

Self-contained Steam-Valve. No regu-
lating cock required.

Works Lifting or Non-lifting.

DELIVERY

By half a turn of the Lever steam is turned on and the Injector
(1) started, (2) regulated for any pressure, and (3) the quantity of feed
varied as required. Cannot be wrongly worked or misunderstood.

Fig. A.7 1896 commercial. [30]

THE SIRIUS' SELF-ACTING INJECTOR
(Brooke's Patent)

SUITS ALL PRESSURES (15 TO 200 LB.)
TAKES HOTTEST FEED WATER.
QUANTITY OF WATER DELIVERED READILY CONTROLLED.
CANNOT BE WRONGLY WORKED OR MISUNDERSTOOD.
ONE MOVEMENT OF ONE HANDLE DOES ALL REGULATING.

Has a self-contained steam valve, and requires no regulating cocks.

By a partial turn (only) of the lever steam is turned on and the Injector (1) started, (2) regulated for any pressure, and (3) the quantity of feed varied as required.



(With either union or flange connections.)


May be fixed above or below the water supply, will lift 10 ft. to 20 ft., and will feed through heaters and economisers.

The quantity of feed can be increased or decreased whilst working by simply moving the pointer slightly to the right or left.

The above advantages are possessed by no other Injector, and wherever trouble has been experienced the SIRIUS may be employed with confidence.

HOLDEN & BROOKE, L.D. WORKS, MANCHESTER.


Fig. A.8 1898 commercial. [30]



"PATTERN S"

THE ORIGINAL
One-Movement
Injector

FOR FEEDING LANCASHIRE
AND SIMILAR TYPE BOILERS



MOST SIZES AVAILABLE FROM STOCK

SIZES : All gunmetal, union connections— $2\frac{1}{2}$ mm. to 5 mm.
All gunmetal, flanged connections— $2\frac{1}{2}$ mm. to 16 mm.
Cast iron body, gunmetal internals, flanged connections—4 mm. to 16 mm.

The "Pattern S" one-movement injector is one of the most reliable and yet one of the simplest injectors on the market today. Simplicity in operation is a vital point to remember when different persons are liable to be operating the injector as no instruction in its operation is necessary. To operate it is merely necessary to turn the handle until steam is admitted and then move the handle round until the position is reached when the injector works "dry", that is with nothing coming out of the overflow. The injector is then at work.

It has self-regulating nozzles which enable it to work always at its highest efficiency whether the pressure is high or low. It deals with hot water, will feed through economisers and is best for those extreme duties which, when certainty of action is called for, are outside the scope of ordinary injectors.

MAY BE FIXED EITHER VERTICALLY OR HORIZONTALLY CAPACITIES OF INJECTORS UP TO SIZE 12 mm. LARGER SIZES ON APPLICATION.

All figures are taken from tests with cold water without suction lift; a suction lift or hot inlet water decreases the capacity; similarly to a greater degree a combination of the two. To obtain best results, work with cold inlet water and low suction lift.

LIFT TABLE*

LIFT AND TEMPERATURE TABLE*

SIZE OF INJECTOR		PRESSURES IN LBS. PER SQUARE INCH															
Nozzles M/M	Pipes inches	25	40	50	60	70	80	90	100	120	140	160	180	200	220	240	250
CAPACITIES IN GALLONS PER HOUR																	
2½	½	76	98	105	111	117	122	125	131	137	141	147	149	150	150	149	147
3	¾	109	140	151	160	168	175	179	188	196	203	212	214	216	216	214	212
3½	1	149	191	206	218	230	238	245	256	268	277	287	291	295	295	291	287
4	1	195	250	270	285	300	312	320	335	350	362	375	380	385	385	380	375
5	1	305	390	420	445	468	486	500	522	548	563	585	592	600	600	572	585
6	1½	438	562	608	640	675	700	720	752	788	822	840	852	865	865	852	840
7	1½	596	765	826	873	919	953	980	1028	1070	1108	1150	1162	1180	1180	1162	1150
8	1½	700	900	1000	1140	1200	1248	1280	1340	1400	1448	1500	1520	1540	1540	1520	1500
9	1½	992	1270	1370	1450	1530	1580	1645	1700	1780	1840	1900	1950	1950	1950	1950	1900
10	2	1220	1560	1690	1780	1870	1950	2000	2100	2180	2260	2340	2380	2400	2400	2380	2340
11	2	1480	1900	2050	2160	2280	2370	2430	2550	2660	2750	2850	2880	2920	2920	2880	2850
12	2	1750	2250	2430	2560	2700	2800	2880	3000	3140	3260	3370	3420	3460	3460	3420	3370

Steam pressure in lbs. per sq. inch ...	25	40	60	80	100	120	140	160	180	200	225	250
Height of lift in feet...	3	15	18	20	20	20	20	20	20	20	20	20

Steam pressure in lbs. per sq. inch ...	25	50	100	150	200	250
Lift in feet...	0 3 0 3 6 10	0 3 6 10	0 3 6 10	0 3 6 10	0 3 6 10	0 3 6 10
Maximum temperature of inlet water "F."	120 115 135 130 120 110	128 123 115 105	117 112 107 100	109 104 100 97	83 80 75 70	

* The above figures are mean figures in that better results are always obtained with the larger sizes than with the smaller.

DECEMBER 1958

LIST 430/58

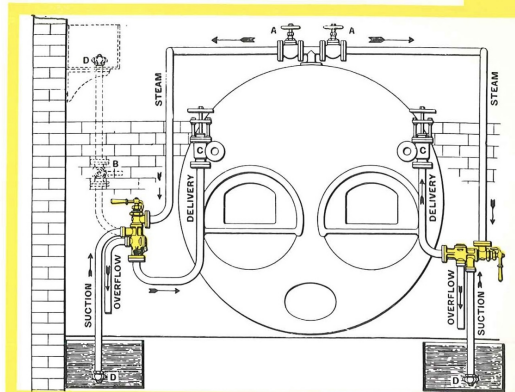
Fig. A.9 1958 brochure (front). [29]

H&B Sirius-"One-Movement"-1890 Injector

INSTALLATION

The illustration shows the correct method of fixing either vertically or horizontally.

- A. Main steam valve.
- B. Water cock (installed only if water supply is overhead).
- C. Feed check and stop valve.
- D. Strainer (the use of a strainer is optional).



MAINTENANCE

The section shows clearly the construction and the method of stripping the injector. The combining nozzle K is renewable and a changeover can be effected with ease.

When sending an injector for repair or ordering spare parts the following working conditions should be stated so that suitable parts may be supplied :-

- (1) Maximum and minimum steam pressure.
- (2) Maximum temperature of inlet water.
- (3) Maximum height of injector above inlet water.

In addition, the progressive number, which is stamped on every instrument, must always be stated when ordering spares.

TESTS AND INSPECTION

Each injector is tested under working conditions before despatch and consequently if a new injector will not work, the fault will be with the local conditions of fixing and working.

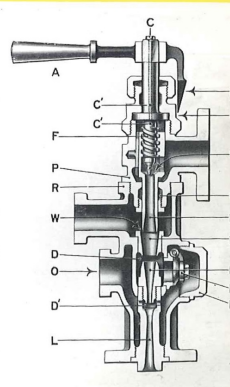
INSTRUCTION BOOKLET

A booklet giving full information on the installation, operation and dismantling of the injector, as well as what to do in case of difficulty, is sent out with each injector.

NEW FEATURES

Improvements in general design and modifications in detail will be embodied for the benefit of clients as and when introduced ; consequently this specification is subject to such alterations without notice.

- A Operating and regulating lever
- B Pointer and pressure index for working position
- C Lubricating hole for spindle
- C' C' Lubricating holes in spindle
- D D' Overflows
- E Steam nozzle
- F Steam spindle
- G Steam nozzle packing
- H Lifting tube
- K Combining nozzle
- L Delivery nozzle and outlet to boiler
- M Overflow valve
- N Overflow cap
- O Overflow outlet
- P Injector body, top
- R Injector body, bottom
- S Steam inlet
- W Water inlet



HOLDEN & BROOKE LTD.

SIRIUS WORKS MANCHESTER 12

Telephone : ARDwick 3883 (9 lines)

Telegrams and Cables : Influx Manchester.

London Office : 66 Victoria Street, S.W.1.

Telephone : VICtoria 7946/7, 1832/3

(Teleprinter Line to Sirius Works)

And at Birmingham, Bristol, York, Glasgow, Belfast, Dublin and throughout the World.

G.X1898

430/899/1258

Fig. A.10 1958 brochure (back). [29]

A.3 Photographs

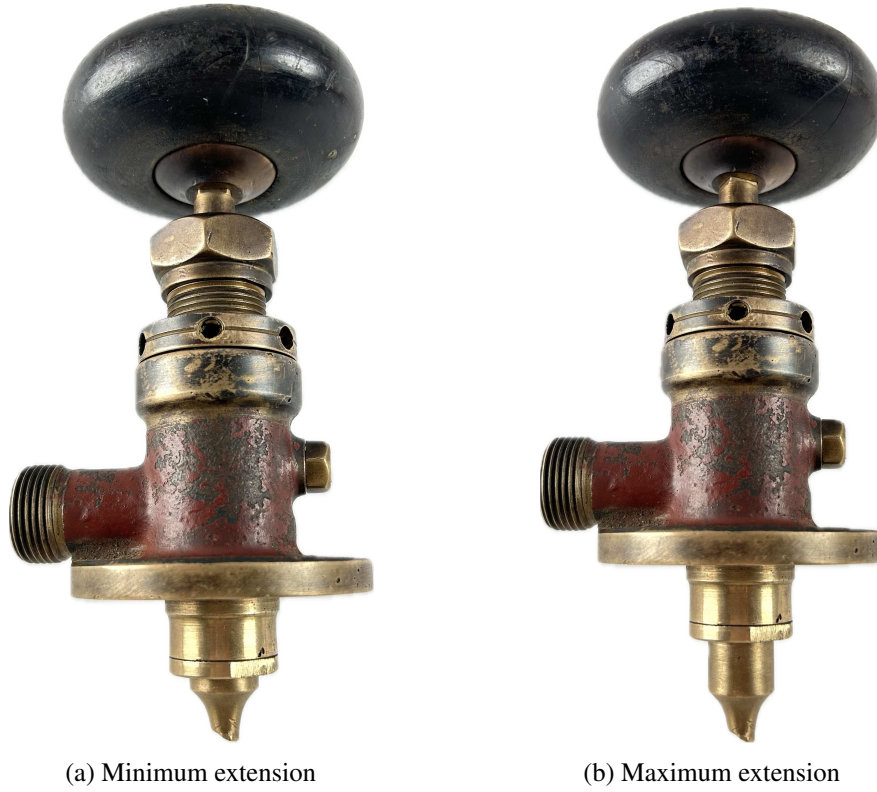


Fig. A.11 Range of extension of the steam nozzle



Fig. A.12 Diffuser outlet

H&B Sirius-"One-Movement"-1890 Injector

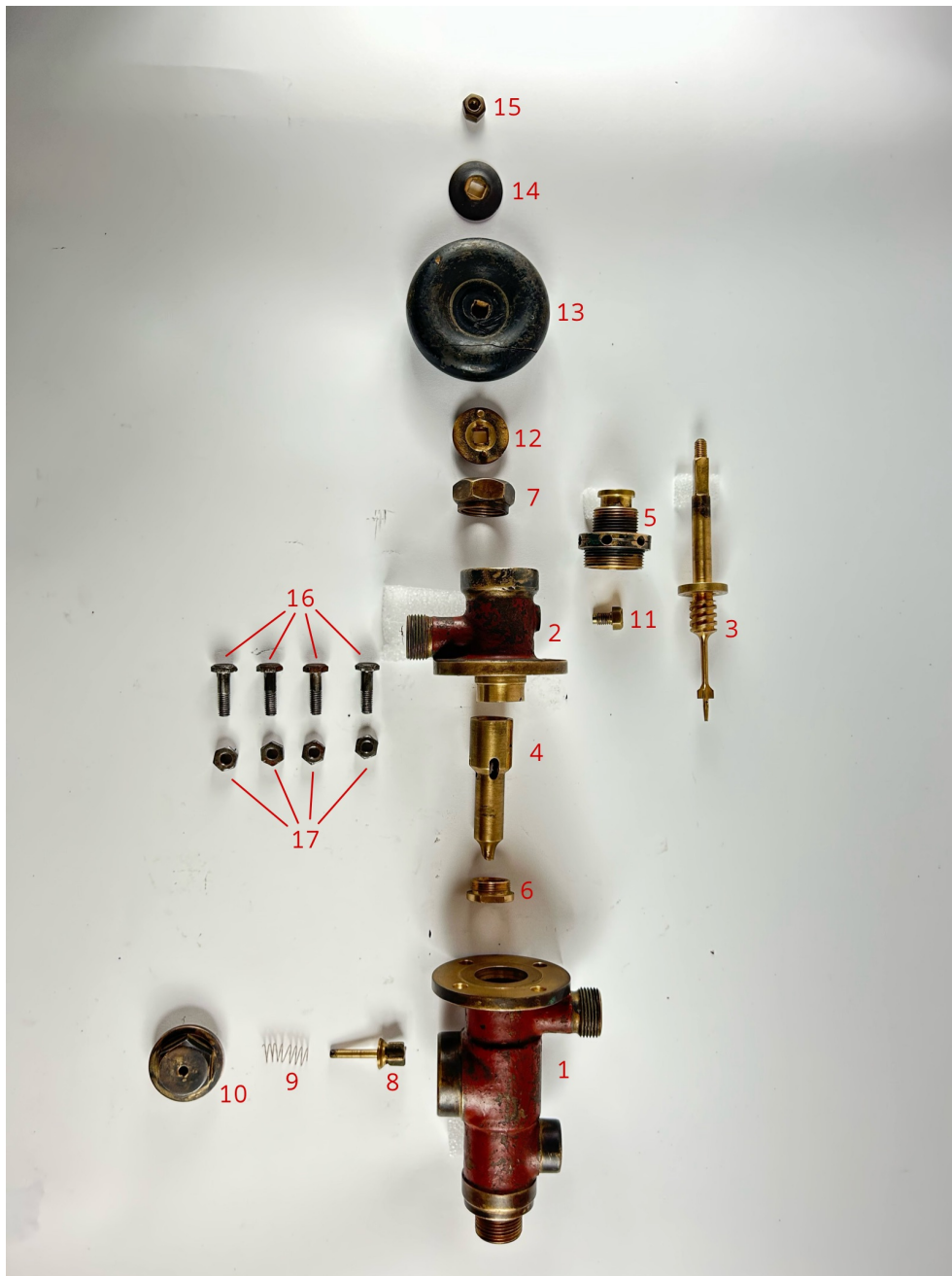


Fig. A.13 Exploded view of the removable parts of the injector . 1. Lower body 2. Upper body 3. Spindle 4. Steam nozzle 5. Upper stuffing box 6. Lower stuffing box 7. Upper stuffing box nut 8. Overflow valve 9. Overflow spring 10. Overflow nut 11. Positioning screw 12. Lower regulating wheel positioner 13. Regulating wheel 14. Upper regulating wheel positioner 15. Regulating wheel nut 16. Flange screws 17. Flange nuts



Fig. A.14 Steam nozzle

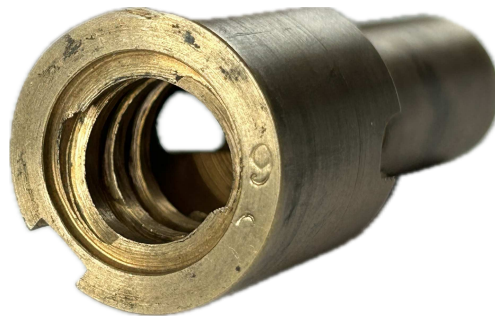


Fig. A.15 Square thread of steam nozzle. *Double start feature.*

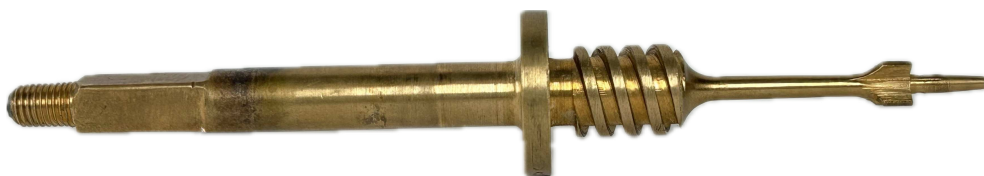


Fig. A.16 Spindle



Fig. A.17 Spindle detail

H&B Sirius-"One-Movement"-1890 Injector

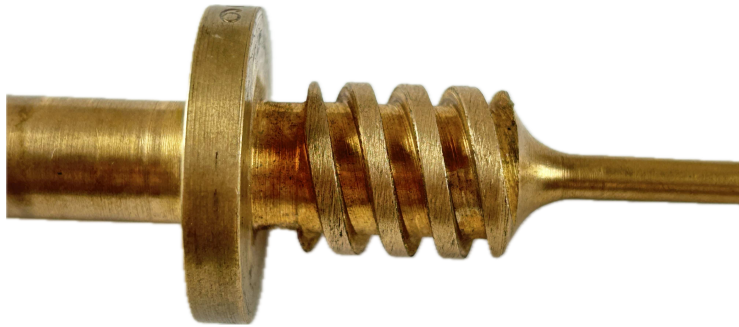


Fig. A.18 Square thread of the spindle. *Double start feature.*



Fig. A.19 Overflow valve



Fig. A.20 Overflow gap



Fig. A.21 Upper stuffing box. *The white spiral is the stuffing.*



Fig. A.22 Mixing chamber inlet

A.4 Tomography scans

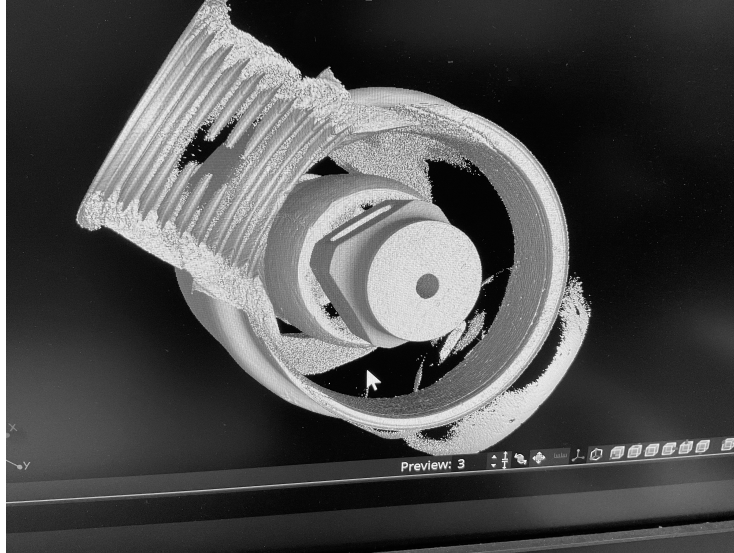


Fig. A.23 Combining nozzle

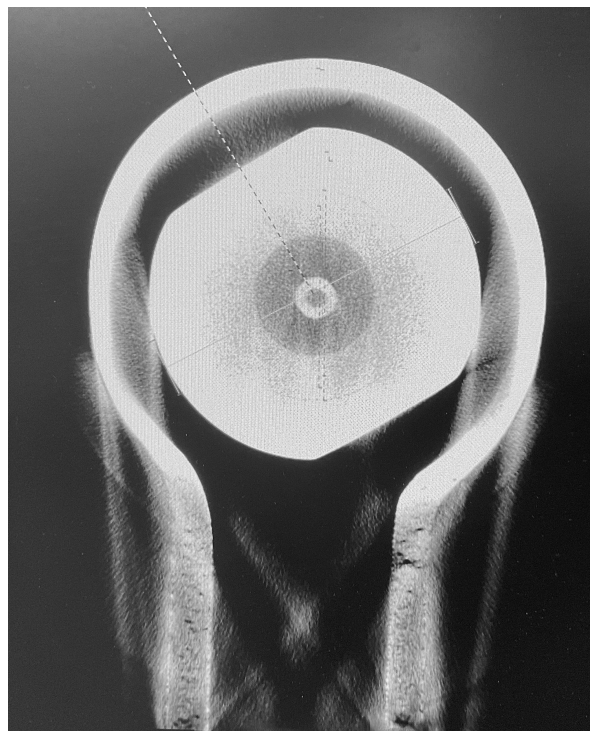
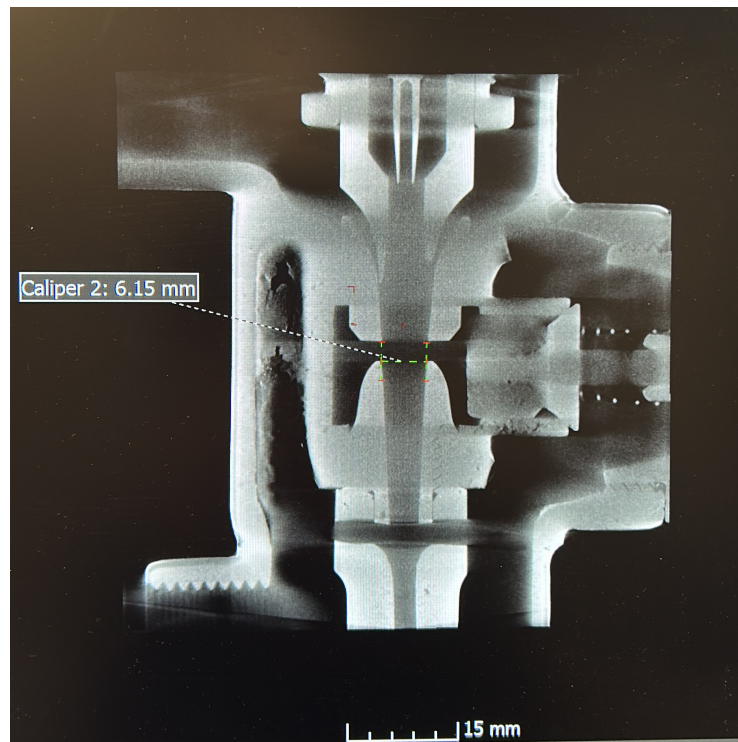
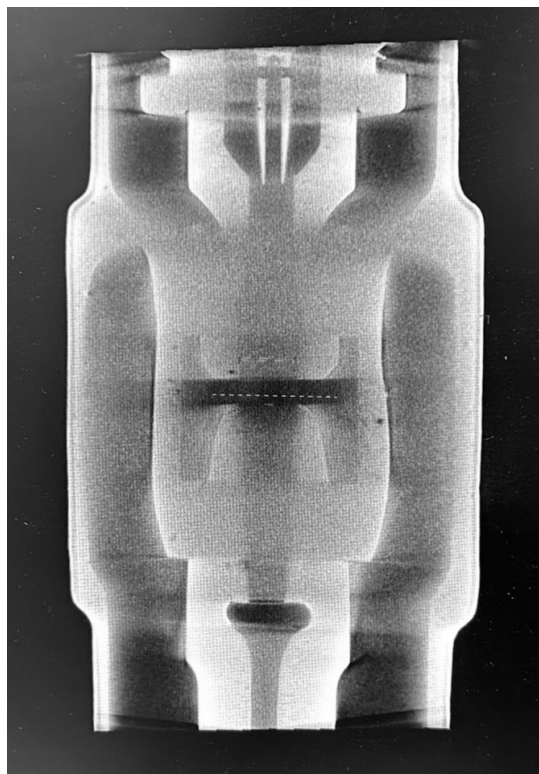


Fig. A.24 Lower stuffing box



(a) Front



(b) Lateral

Fig. A.25 Lower body

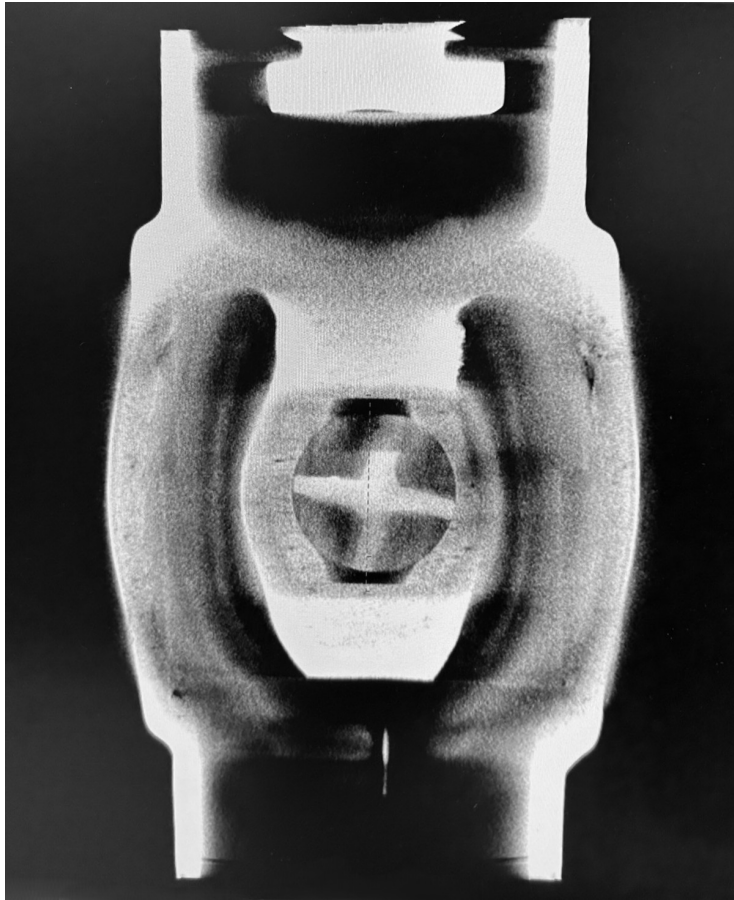


Fig. A.26 Overflow valve

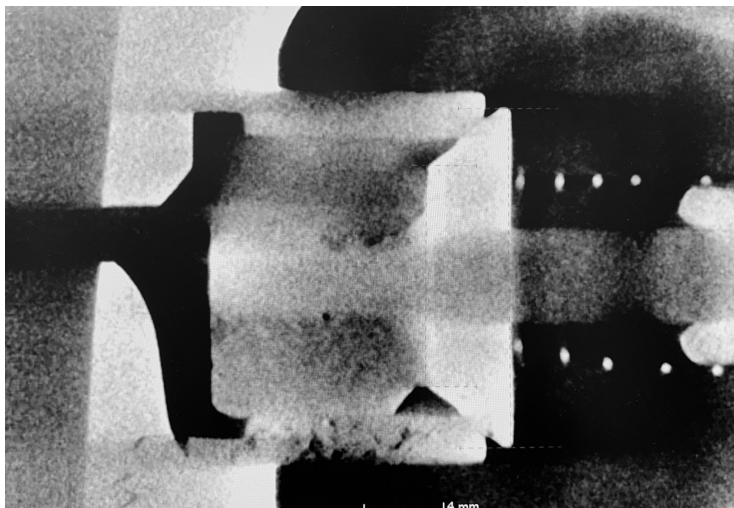


Fig. A.27 Overflow valve detail

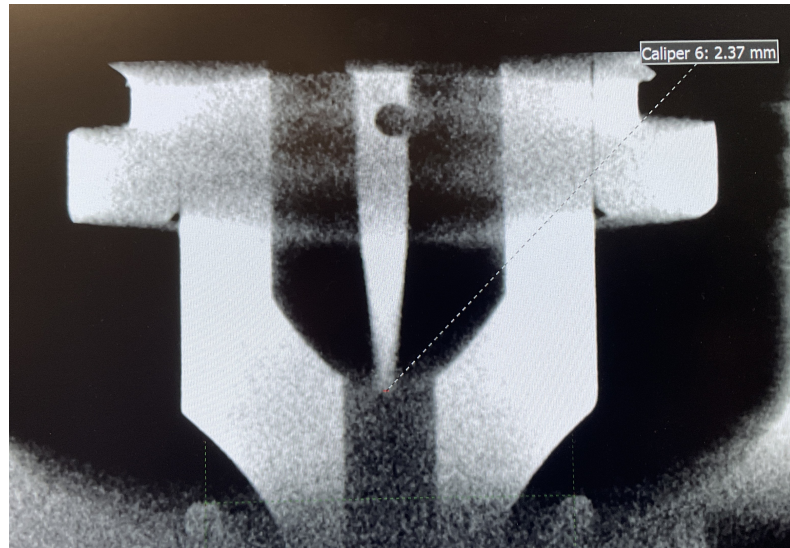


Fig. A.28 Spindle and steam nozzle

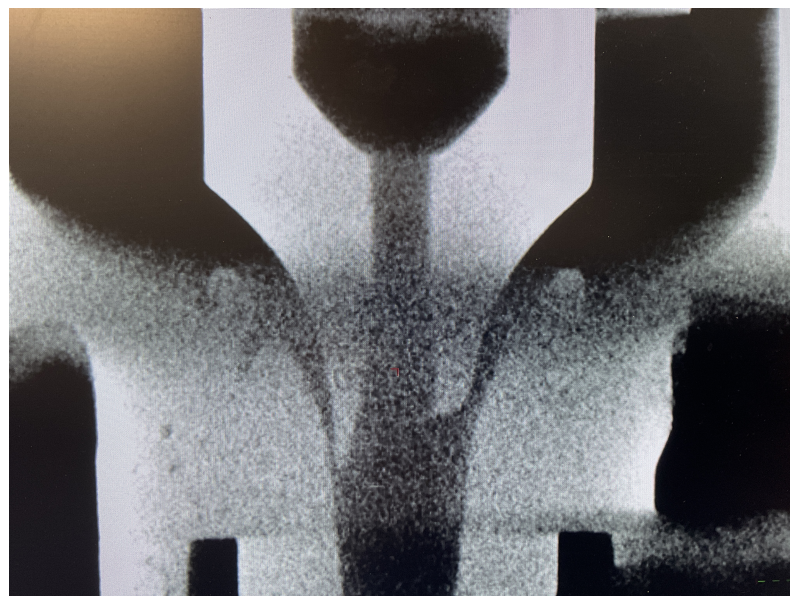


Fig. A.29 Steam nozzle and combining tube

Appendix B

Injector Model MATLAB code

This appendix reports the complete MATLAB code of the analytical model exploited for the analysis of the injectors in this thesis.

```
1 function result = injector_model(data)
2 % injector_model Implement a model for a steam-water
   injector with a
3 % convergent-divergent steam nozzle.
4 %
5 % SECTIONS:
6 % 1 - Inlet of steam nozzle
7 % 2 - Inlet of water nozzle
8 % 3 - Outlet of diffuser
9 % 4 - Throat of steam nozzle
10 % 5 - Outlet of water nozzle
11 % 6 - Outlet of steam nozzle
12 % 7 - Mixing chamber outlet
13 %
14 % ASSUMPTIONS:
15 % 1. The injector operates at critical mode. The flow
   inside the injectors
16 % is a steady, homogeneous and one-dimensional flow.
   -----
17 % 2. At the steam nozzle throat, the flow reaches the
   critical flow
```

```

18 % condition, which means that the sound velocity is
    reached there. -----
19 % 3. The isentropic efficiencies of converging and
    diverging sections of
20 % steam nozzle, eta1 and eta2, are given.
21 % 4. The inlet steam is super-heated and the inlet
    flow velocity is
22 % neglected for both steam and water.
    -----
23 % 5. The heat transfer between the fluid and wall is
    neglected. -----
24 % 6. The gravitational force effect on the flow is
    neglected. -----
25 % 7. The interface of steam and water happens at
    section 5/6, where their
26 % pressure are assumed to be equal.
27 %
28 % BASED ON RESEARCH PAPER:
29 % H. Ma, H. Zhao, L. Wang, Z. Yu, and X. Mao,
    Modeling and investigation
30 % of a steam-water injector, Energy Conversion and
    Management, vol. 151,
31 % no. 0196-8904, pp. 170 178, 2017, doi: https://doi
    .org/10.1016/j.enconman.2017.08.068.
32 %
33 % REFERENCES:
34 % [1] G. Cattadori, L. Galbiati, L. Mazzocchi, and P.
    Vanini, A single-stage
35 % high pressure steam injector for next generation
    reactors: Test results and
36 % analysis, International Journal of Multiphase
    Flow, vol. 21, no. 4,
37 % pp. 591 606, Aug. 1995, doi: 10.1016/0301-9322(94)
    00086-Y.
38 %
39 % AUTHOR:
40 % Leonardo Boscarolo
41

```

Injector Model MATLAB code

```
42 %% Initialization
43 % Data
44 P1 = data.P1;
45 P2 = data.P2;
46 T1 = data.T1;
47 T2 = data.T2;
48 A3 = data.A3;
49 A4 = data.A4;
50 A5 = data.A5;
51 A6 = data.A6;
52 A7 = data.A7;
53
54 % Unfeas
55 unfeasT1 = false; % T1 is lower than Tsat: water
    enters steam nozzle
56 unfeasLift = false; % Lift too high: injector can't
    draw in water
57 unfeasCondensation = false; % Condensation isn't
    completed at the outlet
58 unfeasSupersonic = false; % Supersonic condition not
    reached: backpressure too low
59 unfeasOverflow = false; % Outlet pressure too low:
    overflow
60 unfeasCondition = false; % The injector can't work in
    this condition
61
62 tolerance = 0.1/100; % Tolerance for the iterative
    methods
63 iterationMax = 1000; % Maximum number of iterations
64
65 % Check T1
66 T_sat = XSteam('Tsat_p',P1);
67 if T1 < T_sat
68     unfeasT1 = true; % Water enters into the steam
        nozzle
69 end
70
71
```

```

72 %% 1 - Steam nozzle
73 %%% Convergent section %%%
74 eta1 = 0.9; % [-] Nozzle isentropic efficiency
75 h1 = XSteam('h_pT',P1,T1); % [kJ/kg] Enthalpy of inlet
    steam
76 s1 = XSteam('s_pt',P1,T1); % [kJ/(kg*K)] Entropy of
    inlet steam
77
78 P4min = 0.01; %% CANNOT BE LOWER THAN 0.01
79 P4max = P1;
80 P4average = (P4min+P4max)/2;
81 P4vector = [P4min P4average P4max];
82 delta = [0 1e6 0];
83
84 %%% BISECTION METHOD %%%
85 % To compute iteratively the flow pressure at the
    steam
86 % nozzle throat section. It is assumed that the flow
    reaches the choking
87 % condition
88 iteration = 1;
89 while abs(delta(2)) >= tolerance && iteration <=
    iterationMax
90     P4vector(2) = (P4vector(1)+P4vector(3))/2;
91     P4average = (P4min+P4max)/2;
92     for i=1:length(P4vector)
93         h4_is = XSteam('h_ps',P4vector(i),s1); % [kJ/
            kg] Ideal enthalpy of steam at nozzle
            throat
94         h4 = h1 - eta1*(h1-h4_is); % [kJ/kg] Enthalpy
            of steam at nozzle throat
95         u4 = sqrt(2*(h1-h4)*1000); % [m/s] Speed of
            steam at nozzle throat
96         X4 = XSteam('x_ph',P4vector(i),h4); % [%]
            Vapor fraction
97         if X4 < 1 % wet vapor
98             C4 = XSteam('wV_p',P4vector(i)); % [m/s]
                Speed of sound at nozzle throat

```


Injector Model MATLAB code

```
99         % for the saturated vapor fraction
100     else % dry vapor
101         C4 = XSteam('w_ph',P4vector(i),h4); % [m/s
           ] Speed of sound at nozzle throat
102     end
103     delta(i) = C4-u4;
104 end
105
106 [P4min, P4max]=bisection(delta, P4vector);
107 P4vector = [P4min P4average P4max]; % P4vector is
           updated with the new chosen bounds
108 iteration = iteration + 1;
109
110 end
111
112 % Check if the iteration has been capped
113 if iteration == iterationMax
114     warning('Maximum iterations reached, P4 result may
           not be accurate - P1: '+P1+' bar');
115 end
116
117 P4 = P4vector(2);
118 h4_is = XSteam('h_ps',P4,s1); % [kJ/kg] Ideal enthalpy
           of steam at nozzle throat
119 h4 = h1 - eta1*(h1-h4_is); % [kJ/kg] Enthalpy of steam
           at nozzle throat
120 u4 = sqrt(2*(h1-h4)*1000); % [m/s] Speed of steam at
           nozzle throat
121 X4 = XSteam('x_ph',P4,h4); % [%] Vapor fraction
122 rho4 = XSteam('rho_ph',P4,h4); % [kg/m^3] Total
           density at steam nozzle throat
123 m1_dot = rho4*A4*u4; % [kg/s] Steam mass flow rate
124 s4 = XSteam('s_ph',P4,h4); % [kJ/(kg*K)] Entropy of
           steam at nozzle throat
125 T4 = XSteam('T_ph',P4,h4); % [ C ] Temperature of
           steam at steam nozzle throat
126
127 %%% Divergent section %%%
```

```

128 eta2 = eta1; % [-] Nozzle isentropic efficiency
129
130 P6min = 0.01; %% CANNOT BE LOWER THAN 0.01
131 P6max = P1;
132 P6average = (P6min+P6max)/2;
133 P6vector = [P6min P6average P6max];
134 delta = [0 1e6 0];
135
136 %%% BISECTION METHOD %%%
137 % To compute flow pressure at steam nozzle outlet
138 iteration = 1;
139 while abs(delta(2)) >= tolerance && iteration <=
    iterationMax
140     P6vector(2) = (P6vector(1)+P6vector(3))/2;
141     P6average = (P6min+P6max)/2;
142     for i=1:length(P6vector)
143         h6_is = XSteam('h_ps',P6vector(i),s4); % [kJ/
            kg] Ideal enthalpy of steam at nozzle
            outlet
144         h6 = h4 - eta2*(h4 - h6_is); % [kJ/kg]
            Enthalpy of steam at nozzle outlet
145         u6 = sqrt(2*(h4*1000 + (u4^2)/2 - h6*1000)); %
            [m/s] Speed of steam at nozzle outlet
146         rho6 = m1_dot/(A6*u6); % [kg/m^3]
147         rho6_prime = XSteam('rho_ph',P6vector(i),h6);
            % [kg/m^3]
148         delta(i) = rho6_prime-rho6;
149     end
150
151     [P6min, P6max]=bisection(delta, P6vector);
152     P6vector = [P6min P6average P6max]; % P6vector is
        updated with the new chosen bounds
153     iteration = iteration + 1;
154
155 end
156
157 % Check if the iteration has been capped
158 if iteration == iterationMax

```

Injector Model MATLAB code

```
159     warning('Maximum iterations reached, P6 result may
        not be accurate - P1: '+P1+' bar');
160 end
161
162 P6 = P6vector(2);
163 h6_is = XSteam('h_ps',P6,s4); % [kJ/kg] Ideal enthalpy
        of steam at nozzle outlet
164 h6 = h4 - eta2*(h4 - h6_is); % [kJ/kg] Enthalpy of
        steam at nozzle outlet
165 u6 = sqrt(2*(h4*1000 + (u4^2)/2 - h6*1000)); % [m/s]
        Speed of steam at nozzle outlet
166 rho6 = m1_dot/(A6*u6); % [kg/m^3]
167 X6 = XSteam('x_ph',P6,h6); % [%] Vapor fraction
168 T6 = XSteam('T_ph',P6,h6); % [ C ] Temperature of
        steam at steam nozzle outlet
169
170 % Check that there is enough depression to draw in the
        water, otherwise
171 % this means most probably that the water lift is too
        high.
172 if P6 > P2
173     unfeasLift = true;
174 end
175
176 %% 2 - Suction nozzle
177 P5 = P6; % ASSUMPTION: pressures assumed to be equal
        at the interface
178 T5 = T2; % ASSUMPTION heat exchange between fluid and
        wall is neglected
179 xi1 = 0.9; % [-] Pressure loss coefficient
180 h2 = XSteam('h_pT',P2,T2); % [kJ/kg] Enthalpy of water
        at water nozzle inlet
181 rho2 = XSteam('rho_pT',P2,T2); % [kg/m^3] Density of
        water at the water nozzle inlet
182 rho5 = XSteam('rho_pT',P5,T5); % [kg/m^3] Density of
        water at the water nozzle outlet
183 u5 = sqrt(2 * xi1 * ((P2*10^5)/rho2 - (P5*10^5)/rho5))
        ; % [m/s] Speed of water at water nozzle outlet
```

```

184 h5 = (h2*1000 - (u5^2)/2) / 1000; % [kJ/kg] Enthalpy
      of water at water nozzle outlet
185 X5 = XSteam('x_ph',P5,h5); % [%] Vapor fraction
186 m2_dot = rho5 * A5 * u5; % [kg/s] Water mass flow rate
187
188 %% 3 - Mixing chamber
189 beta = 0.75; % [-] Momentum correction factor
190
191 %%% Find minimum allowable pressure, for which x7
      becomes 0 %%%
192 x7_star = 1;
193 P7_min = 0.01;
194 while x7_star > 0 && P7_min < P1
195     u7 = (beta * (P5*10^5*A5 + P6*10^5*A6 + m1_dot*u6
      + m2_dot*u5) - P7_min*10^5*A7) ...
196         / (m1_dot + m2_dot); % [m/s] Water speed at
      mixing chamber outlet
197     h7 = ((m1_dot*h1*1000 + m2_dot*h2*1000 - (m1_dot+
      m2_dot)*(u7^2)/2) ...
198         / (m1_dot + m2_dot)) /1000; % [kJ/kg] Water
      enthalpy at mixing chamber outlet
199     x7_star = XSteam('x_ph',P7_min,h7);
200     P7_min = P7_min + 0.001;
201 end
202 if P7_min == P1
203     P7_min = 0.01;
204 end
205
206 %%% Find the maximum allowable pressure, where rho7
      then becomes negative %%%
207 rho7_star = 1;
208 P7_max = P1;
209 while rho7_star > 0 && P7_max < 10*P1
210     u7 = (beta * (P5*10^5*A5 + P6*10^5*A6 + m1_dot*u6
      + m2_dot*u5) - P7_max*10^5*A7) ...
211         / (m1_dot + m2_dot); % [m/s] Water speed at
      mixing chamber outlet

```

Injector Model MATLAB code

```
212     h7 = ((m1_dot*h1*1000 + m2_dot*h2*1000 - (m1_dot+
213           m2_dot)*(u7^2)/2) ...
214           / (m1_dot + m2_dot)) /1000; % [kJ/kg] Water
215           enthalpy at mixing chamber outlet
216     rho7_star = (m1_dot+m2_dot)/(A7*u7); % [kg/m^3]
217     P7_max = P7_max + 0.001;
218 end
219 %%% REGULA FALSI %%%
220 % To compute the pressure at the mixing chamber outlet
221 % , since many times
222 % happens that the bisection algorithm doesn't work,
223 % because there are
224 % multiple roots in the interval, in this case it is
225 % used the regula falsi.
226 % It happens also that the extremes of the interval
227 % have the same sign.
228 P7min = P7_min+0.1;
229 P7max = P7_max-0.1;
230 for iteration = 1:iterationMax
231
232     % MIN
233     u7 = (beta * (P5*10^5*A5 + P6*10^5*A6 + m1_dot*u6
234           + m2_dot*u5) - P7min*10^5*A7) / (m1_dot +
235           m2_dot); % [m/s] Water speed at mixing chamber
236           outlet
237     h7 = ((m1_dot*h1*1000 + m2_dot*h2*1000 - (m1_dot+
238           m2_dot)*(u7^2)/2) / (m1_dot + m2_dot)) /1000; %
239           [kJ/kg] Water enthalpy at mixing chamber
240           outlet
241     rho7 = (m1_dot+m2_dot)/(A7*u7); % [kg/m^3]
242     rho7_prime = XSteam('rho_ph',P7min,h7); % [kg/m^3]
243     deltamin = rho7_prime - rho7;
244     % MAX
245     u7 = (beta * (P5*10^5*A5 + P6*10^5*A6 + m1_dot*u6
246           + m2_dot*u5) - P7max*10^5*A7) / (m1_dot +
```

```

236         m2_dot); % [m/s] Water speed at mixing chamber
           outlet
237     h7 = ((m1_dot*h1*1000 + m2_dot*h2*1000 - (m1_dot+
           m2_dot)*(u7^2)/2) / (m1_dot + m2_dot)) /1000; %
           [kJ/kg] Water enthalpy at mixing chamber
           outlet
238     rho7 = (m1_dot+m2_dot)/(A7*u7); % [kg/m^3]
239     rho7_prime = XSteam('rho_ph',P7max,h7); % [kg/m^3]
240     deltamax = rho7_prime - rho7;
241
242     % Compute the next approximation using the false
           position formula
243     P7new = P7max - (deltamax * (P7max - P7min)) / (
           deltamax - deltamin);
244
245     % Check for convergence
246     u7 = (beta * (P5*10^5*A5 + P6*10^5*A6 + m1_dot*u6
           + m2_dot*u5) - P7new*10^5*A7) / (m1_dot +
           m2_dot); % [m/s] Water speed at mixing chamber
           outlet
247     h7 = ((m1_dot*h1*1000 + m2_dot*h2*1000 - (m1_dot+
           m2_dot)*(u7^2)/2) / (m1_dot + m2_dot)) /1000; %
           [kJ/kg] Water enthalpy at mixing chamber
           outlet
248     rho7 = (m1_dot+m2_dot)/(A7*u7); % [kg/m^3]
249     rho7_prime = XSteam('rho_ph',P7new,h7); % [kg/m^3]
250     deltaneu = rho7_prime - rho7;
251     if abs(deltaneu) < tolerance
252         P7 = P7new;
253         break;
254     end
255
256     % Update the interval
257     if deltamin * deltaneu < 0
258         P7max = P7new; % Root is between a and c
259     else
260         P7min = P7new; % Root is between c and b
261     end

```

Injector Model MATLAB code

```
261
262 end
263
264 % If max iterations reached, return best estimate
265 if iteration == iterationMax
266     if abs(deltanew) < 10
267         P7 = P7new;
268         warning('Maximum iterations reached, result
                may not be accurate - P7: '+P7+' bar');
269     elseif abs(deltanew) > 10 || isnan(deltanew)
270         unfeasCondition = true;
271         P7 = NaN;
272     end
273 end
274
275 u7 = (beta * (P5*10^5*A5 + P6*10^5*A6 + m1_dot*u6 +
                m2_dot*u5) - P7*10^5*A7) ...
276     / (m1_dot + m2_dot); % [m/s] Water speed at mixing
                chamber outlet
277 h7 = ((m1_dot*h1*1000 + m2_dot*h2*1000 - (m1_dot+
                m2_dot)*(u7^2)/2) ...
278     / (m1_dot + m2_dot)) /1000; % [kJ/kg] Water
                enthalpy at mixing chamber outlet
279 X7 = XSteam('x_ph',P7,h7); % [%] Vapor fraction
280 T7 = XSteam('T_ph',P7,h7); % [ C ] Temperature of
                water at mixing nozzle outlet
281
282 % Check if steam is completely condensed at the mixing
                chamber outlet
283 if X7 > 0
284     unfeasCondensation = true;
285 end
286
287 %% 4 - Diffuser
288 rho3 = rho7; % ASSUMPTION
289 Cp = 0.65; % Diffuser efficiency - value taken from
                [1]
```

```

290 u3 = (m1_dot + m2_dot)/(A3 * rho3); % [m/s] Water
      speed at diffuser outlet
291 hLoss = (u7^2)/2 * (1 - Cp); % [m] Head loss in the
      diffuser
292 P3 = (rho3 * (((u7^2)/2) + P7*10^5/rho7 - (u3^2)/2 -
      hLoss))/10^5; % [bar] Pressure at diffuser outlet
293 h3 = (((m1_dot*h1*1000 + m2_dot*h2*1000)/(m1_dot +
      m2_dot)) - (u3^2)/2)/1000; % [kJ/kg] Water enthalpy
294 % at diffuser outlet
295 X3 = XSteam('x_ph',P3,h3); % [%] Quality at diffuser
      outlet
296 T3 = XSteam('T_ph',P3,h3); % [ C ] Temperature at
      diffuser outlet
297
298 %% 5 - Performance
299 omega = m2_dot/m1_dot; % [-] Entrainmmnet ratio
300 R = P3/P2; % [-] Compression ratio
301 Phi = P3/P1; % [-] Pressure gain ratio
302 deltaPressure = P3-P1; % [bar] delta pressure at
      boiler inlet
303 Q = (m2_dot+m1_dot)*3600; % [L/h] Water flow into the
      boiler
304
305 % Check that overflow doesn't happen (Overflow: when
      pressure isn't raised
306 % enough to open boiler clack valve)
307 if deltaPressure <= 0
308     unfeasOverflow = true;
309 end
310
311 %% 6 - Result & unfeas
312 % Flow
313 result.m1_dot = m1_dot;
314 result.m2_dot = m2_dot;
315 result.Q = Q;
316 % Pressure
317 result.P4 = P4;
318 result.P5 = P5;

```


Injector Model MATLAB code

```
319 result.P6 = P6;
320 result.P7 = P7;
321 result.P3 = P3;
322 % Quality
323 result.X4 = X4;
324 result.X5 = X5;
325 result.X6 = X6;
326 result.X7 = X7;
327 result.X3 = X3;
328 % Density
329 result.rho4 = rho4;
330 result.rho5 = rho5;
331 result.rho6 = rho6;
332 result.rho7 = rho7;
333 result.rho3 = rho3;
334 % Temperature
335 result.T4 = T4;
336 result.T5 = T5;
337 result.T6 = T6;
338 result.T7 = T7;
339 result.T3 = T3;
340 % Velocity
341 result.u4 = u4;
342 result.u5 = u5;
343 result.u6 = u6;
344 result.u7 = u7;
345 result.u3 = u3;
346 % Entalphy
347 result.h4 = h4;
348 result.h5 = h5;
349 result.h6 = h6;
350 result.h7 = h7;
351 result.h3 = h3;
352 % Performance
353 result.omega = omega;
354 result.R = R;
355 result.Phi = Phi;
356 result.deltaPressure = deltaPressure;
```

```

357 % Unfeas
358 % Check that all velocities are real numbers
359 if isreal(u4) == false || isreal(u6) == false ||
    isreal(u7) == false || isreal(u3) == false ||
    isreal(u5) == false
360     unfeasCondition = true;
361 end
362 result.unfeasSupersonic = unfeasSupersonic;
363 result.unfeasLift = unfeasLift;
364 result.unfeasT1 = unfeasT1;
365 result.unfeasCondensation = unfeasCondensation;
366 result.unfeasOverflow = unfeasOverflow;
367 result.unfeasCondition = unfeasCondition;
368
369
370 %% Bisection Algorithm
371 function [lowerLimit,upperLimit] = bisection(delta,
    vector)
372
373     %Initial control sign
374     if delta(1)*delta(3) >= 0
375         error('The function does not change sign
            inside the range - try changing the initial
            range or invert the delta calculation')
376     end
377
378     % Limit changing
379     if delta(2) < 0 % in case the
        average value is negative, this has to replace
        the lower limit
380         upperLimit = vector(3);
381         lowerLimit = vector(2);
382     elseif delta(2) > 0 % in case the
        average value is positive, this has to replace
        the upper limit
383         lowerLimit = vector(1);
384         upperLimit = vector(2);

```

Injector Model MATLAB code

```
385     elseif delta(2) == 0           % in the very
386         unlikely case that average is perfectly 0
387         return
388     end
389 end
390
391 end
```

Listing B.1 Injector model